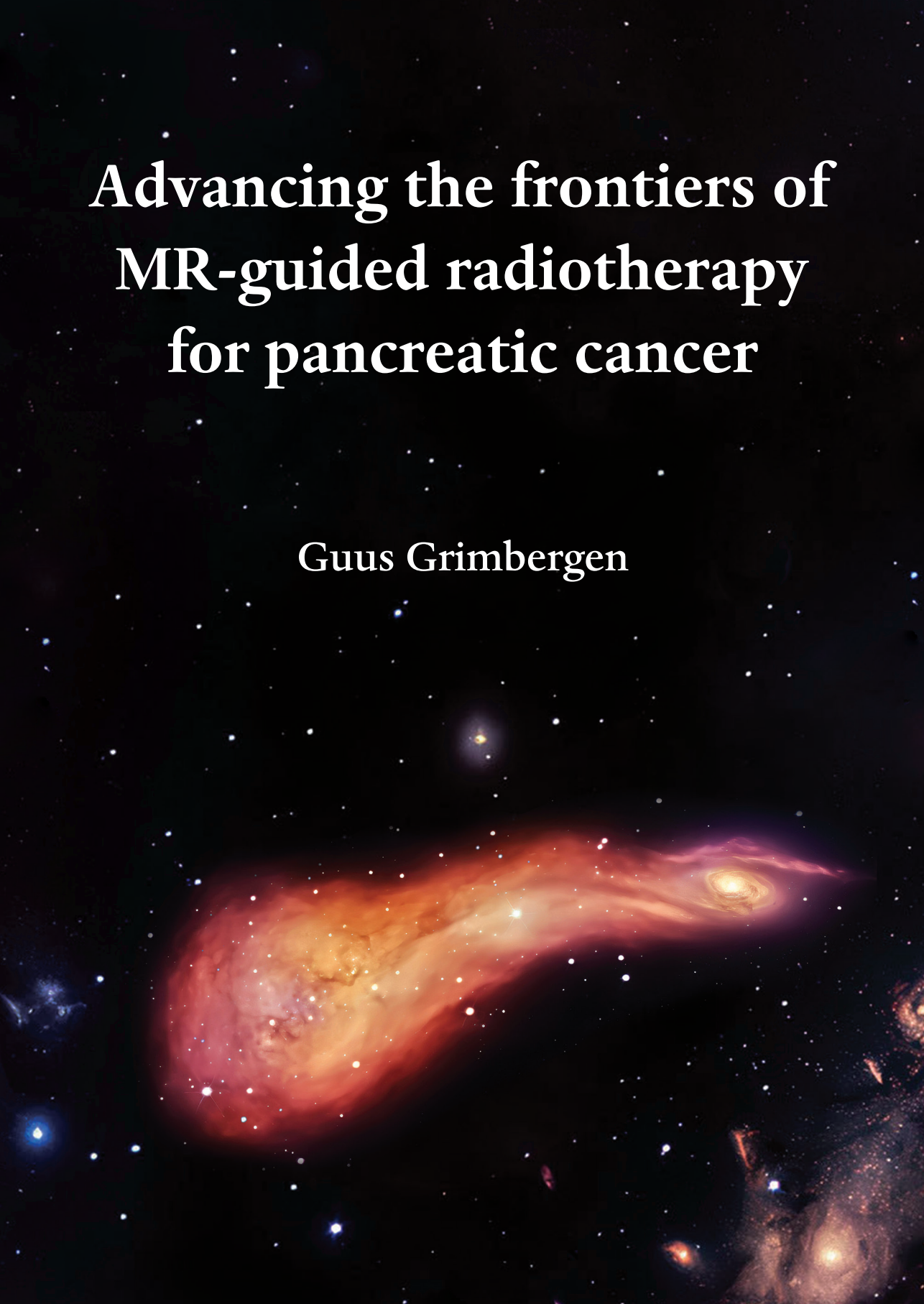


Advancing the frontiers of MR-guided radiotherapy for pancreatic cancer

Guus Grimbergen



Advancing the frontiers of MR-guided radiotherapy for pancreatic cancer

Guus Grimbergen

Cover: *The final frontier.*

The stars, galaxies, and nebulae in this thesis are from the imagination of Midjourney, a generative artificial intelligence platform.

Advancing the frontiers of MR-guided radiotherapy for pancreatic cancer

PhD thesis, Utrecht University, the Netherlands.

© Guus Grimbergen, 2024. All rights reserved. No part of this publication may be reproduced, distributed, or transmitted in any form or by any means without the prior written permission from the author and the publisher holding the copyright of the published articles.

Design and layout: Guus Grimbergen
Typeset in: L^AT_EX 2_ε
Printing: Ridderprint | www.ridderprint.nl
ISBN: 978-90-393-7648-5
DOI: 10.33540/483

The research described in this thesis was supported by the Dutch Cancer Foundation (KWF) under Grant Agreement no. 12665. Financial support for the printing of this thesis was kindly provided by Elekta AB, MIM Software Inc., Modus Medical Devices Inc., and ChipSoft B.V.

Advancing the frontiers of MR-guided radiotherapy for pancreatic cancer

De grenzen verleggen van MRI-geleide radiotherapie voor alvleesklierkanker

(met een samenvatting in het Nederlands)

Proefschrift

ter verkrijging van de graad van doctor aan de Universiteit Utrecht
op gezag van de rector magnificus, prof. dr. H.R.B.M. Kummeling,
ingevolge het besluit van het college voor promoties
in het openbaar te verdedigen op
dinsdag 21 mei 2024 des middags te 4:15 uur

door

Guus Grimbergen

geboren op 27 augustus 1997
te Nieuwegein

Promotoren: Dr. G.J. Meijer
Prof. dr. B.W. Raaymakers
Prof. dr. M.P.W. Intven

Beoordelingscommissie: Dr. M.F. Fast
Prof. dr. M.S. Hoogeman
Prof. dr. ir. J.J.W. Lagendijk
Prof. dr. J.H.W. Leusen
Prof. dr. H.C. van Santvoort

Contents

1. General introduction	9
I Treatment planning	
2. Feasibility of online radial MRI for adaptive radiotherapy of pancreatic tumors	23
3. Treatment planning for MR-guided SBRT of pancreatic tumors on a 1.5 T MR-Linac: a global consensus protocol	37
II Treatment delivery	
4. Intrafraction pancreatic tumor motion patterns during ungated magnetic resonance guided radiotherapy with an abdominal corset	55
5. Dosimetric impact of intrafraction motion under abdominal compression during MR-guided SBRT for (peri-) pancreatic tumors	69
6. Feasibility of delivered dose reconstruction for MR-guided SBRT of pancreatic tumors with fast, real-time 3D cine MRI	85
7. Gating and intrafraction drift correction on a 1.5 T MR-Linac: clinical dosimetric benefits for upper abdominal tumors	99
8. Summary	109
9. General discussion and future outlook	115
Appendix	
Nederlandse samenvatting	133
Bibliography	140
List of publications	157
Dankwoord	161
Curriculum vitae auctoris	167



The background of the page is a deep black space filled with numerous small, bright white stars. On the left side, there is a large, diffuse nebula with a reddish-pink hue. The text is centered in the upper half of the image.

CHAPTER 1

General introduction

1.1. Pancreatic cancer

There is an imperative need to improve treatment options for "the ruthless dictator of all cancers".¹ While life expectancy has substantially improved in most major cancer types over the last decades, the survival rate for pancreatic cancer has barely increased.² Due to the aggressive nature of pancreatic cancer and rapid disease advancement, the vast majority of patients are not eligible for surgical tumor resection.³ It is therefore evident that the greatest need for progress lies in the treatment for inoperable pancreatic cancer.

The main priority for inoperable pancreatic cancer is systemic control with chemotherapy.^{3,4} However, the destructive effects of local tumor progression and the importance of maintaining quality of life in this patient group with very poor life expectancy create the necessity for more targeted approaches, complementary or alternative to chemotherapy. Over the last years, radiotherapy has emerged as the most promising local treatment of inoperable pancreatic cancer.

1.2. Radiotherapy

Radiotherapy refers to any treatment involving ionizing radiation. In oncology, radiotherapy is used as local treatment that induces DNA damage within the tumor cell nuclei, leading to cell death. The central tenet of radiotherapy is to deliver a high radiation dose to malignant tissue, while keeping dose to healthy tissue as low as possible.

Image-guided radiotherapy (IGRT) used to be considered a specific discipline within the field. Today, computed tomography (CT) and magnetic resonance imaging (MRI) form the backbone of radiotherapy treatment planning and delivery. In the weeks before treatment, the patient undergoes a pretreatment session with CT and/or MRI exams, and the visible tumor (known as the gross tumor volume, or GTV), and the organs to be spared (organs at risk, or OAR) are delineated on the scans. Each delineated structure is assigned a dosimetric constraint: for the GTV a minimum dose at which the treatment is considered effective, and for the healthy tissue a maximum dose beneath which treatment can safely be delivered with minimal radiation toxicity. With the CT scan as electron density information, these structures and their boundary conditions are fed into an inverse planning algorithm,^{5,6} which performs particle interaction simulations to calculate the optimal sequence of beam shapes and energies that leads to the desired dose distribution. At the time of treatment, the aim is to replicate this planned dose as closely as possible for every treatment fraction.

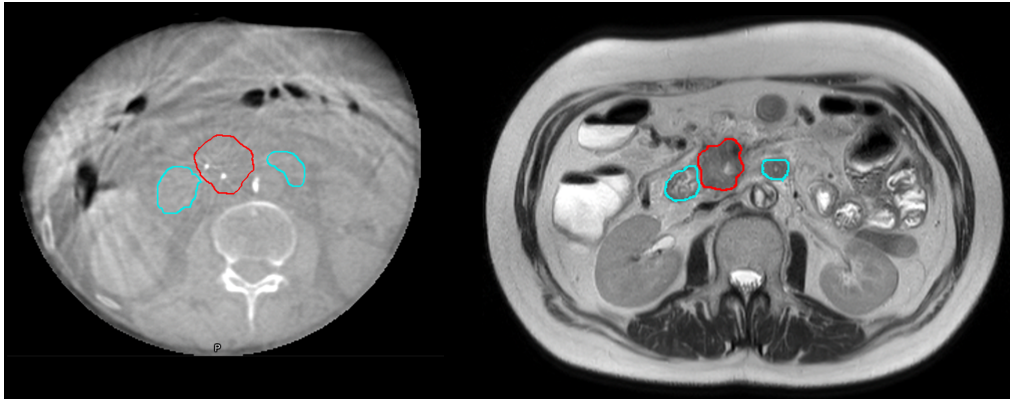


Figure 1.1.: Comparison of a pancreatic tumor on cone-beam CT (left) versus a T_2 -weighted MRI of the same patient (right), along with the contours of the GTV (red) and the duodenum (cyan). The fiducial markers inside the tumor can be seen on the CBCT.

In conventional image-guided radiotherapy, the linear accelerator (linac) units are equipped with a cone-beam CT (CBCT) scanner. This can provide a rudimentary 3D image of the patient at the start of treatment for position verification. Position verification involves correcting any positional differences between the pretreatment plan and the current patient position, by physically shifting the treatment couch or patient itself. It is at this part of the workflow where conventional radiotherapy runs into serious limitations for treatment of pancreatic cancer.

In the upper abdomen, CBCT scans have a severe lack of contrast between healthy and diseased tissue, as well as anatomical landmarks such as bony structures (Fig. 1.1). The tumor position can be approximated with fiducial markers (gold seeds implanted in the tumor), but this still leaves uncertainty in the location of the tumor and organ *boundaries*. Moreover, the positional changes with respect to the pretreatment session can be too complex to be resolved with a simple rigid couch shift.⁷ To compensate for the uncertainty in tumor position and motion, the dose is typically delivered into a large planning target volume (PTV), which is the tumor plus a margin of healthy tissue. In order to limit the dose to this healthy tissue and other OARs (whose position is also uncertain), radiotherapy of pancreatic cancer is conventionally delivered in as many as 30 fractions. Combined, these characteristics lead to an exceptionally conservative treatment that is often considered ineffective for an aggressive disease as pancreatic cancer, which should ideally be prescribed stereotactic body radiotherapy (SBRT), with biologically effective doses (BED_{10}) of 70 to over 100 Gy in order to obtain favorable clinical results.^{8,9} SBRT is a modern radiotherapy



Figure 1.2.: The Elekta Unity, the only commercially available 1.5 T MR-Linac. A 3D rendered cutaway shows the main components: the 1.5 T magnet (yellow), and the 6 MV linac (dark blue) mounted on the rotating gantry (gray). Image adapted from Elekta.

technique which involves high doses delivered in hypofractionated schemes (typically five fractions or less), with treatment plans that have large dose gradients to ensure fast drop off of dose outside the tumor.

1.3. MR-guided radiotherapy

MR-guided radiotherapy is delivering radiotherapy using a hybrid MRI scanner and radiotherapy linac, known as an MR-Linac.¹⁰ The clinical introduction of the low-field MR-Linac (0.35 T) was in 2014,¹¹ and the high-field MR-Linac (1.5 T) in 2017.¹² The work in this thesis will only concern the 1.5 T MR-Linac (Fig. 1.2).

The integration of a 1.5 T MRI scanner in 7 MV linac has opened the way for online adaptive radiotherapy.^{13,14} With the onboard imaging system of the MR-Linac, which has vastly superior soft tissue contrast over CBCT (see Fig. 1.1), the treatment plan can be adapted to a new MRI scan that is made at the start of every treatment fraction. Now, the

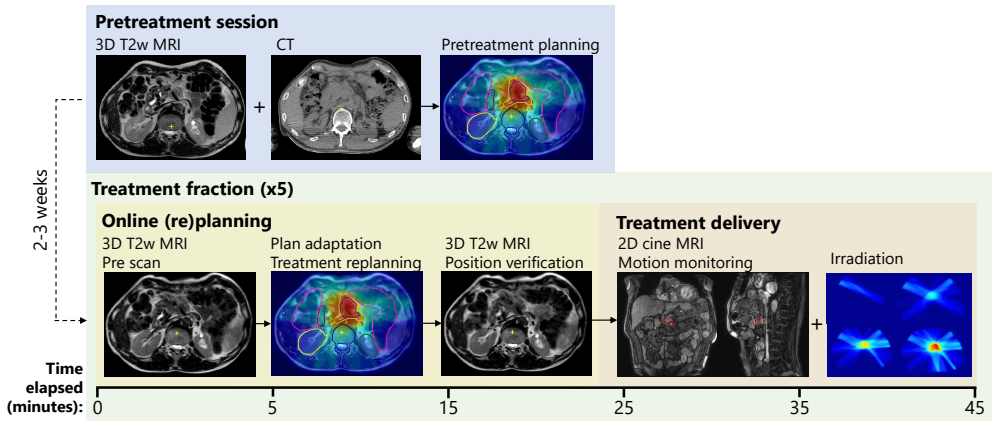


Figure 1.3.: The workflow of online adaptive MR-guided radiotherapy, with the typical MRI sequences and time elapsed for each step in the workflow.

complex anatomical differences with respect to the pretreatment session can be resolved by recontouring the tumor and OARs on the newly acquired MR image. Immediately after, a new dose plan is calculated and delivered while the patient has never left the treatment table. This online adaptive process is repeated every fraction, creating a unique dose plan for each fraction. The online adaptive workflow of the MR-Linac is summarized in Fig. 1.3.

Aside from acquiring imaging for the purpose of online adaptation, MR data can also be acquired *during* treatment delivery. Beam-on imaging is typically performed with fast, time-resolved acquisition schemes to obtain a real-time view of the target area. Typically, balanced gradient echo cine MRI is the scanning technique of choice; both acquisition and reconstruction are fast enough (under 500 ms) to provide images with a both a sufficiently high spatial and temporal resolution, at the cost of a limited field-of-view of one to three intersecting orthogonal 2D planes (Fig. 1.4). This is often deemed sufficient for tumor monitoring during beam-on and any retrospective analyses.

1.4. MR-guided radiotherapy for pancreatic cancer: technical benefits, challenges, and opportunities

Even before the clinical introduction, it was obvious that MR-guidance would lead to a paradigm shift in radiotherapy of pancreatic cancer. Treatment of upper abdominal tumors

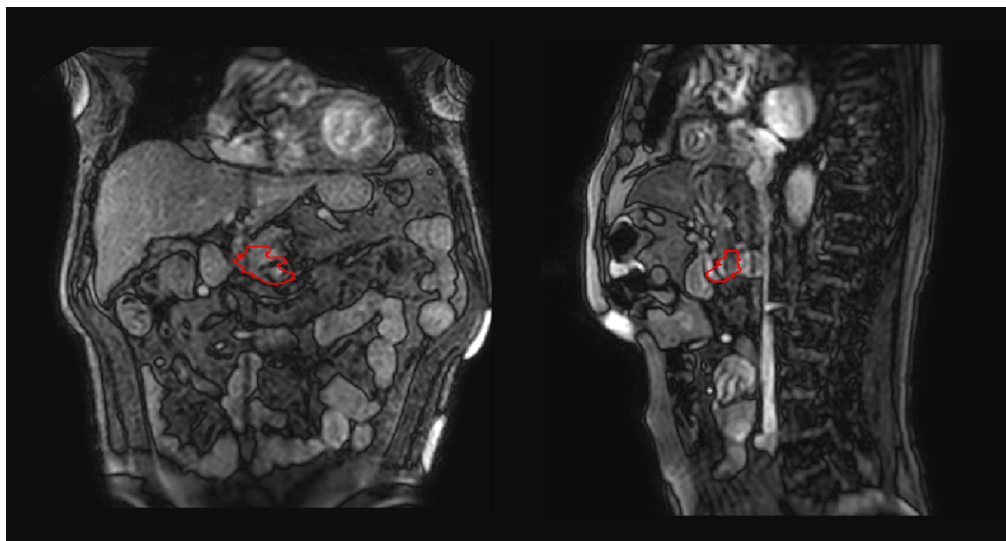


Figure 1.4.: An example of 2D cine MRI that is typically acquired during pancreatic tumor treatment on the MR-Linac, at a rate of 500 ms per dynamic. Here, a single dynamic is shown, consisting of one coronal (left) and sagittal (right) plane. The GTV contour is shown in red.

would benefit the most from the two main promises of the MR-Linac - improved soft tissue visibility and the ability to correct for interfraction motion. Since its inception, hundreds of pancreatic cancer patients have been treated on the MR-Linac worldwide, and the first clinical outcomes are being published. Early results from large cohorts demonstrate that MR-guided SBRT for pancreatic cancer can safely be delivered in high dose regimens, with low acute toxicity rates and no loss of quality of life.¹⁵⁻¹⁹ However, now that MR-guided radiotherapy has been established as a feasible and safe therapy, it has become clear that there are several technical hurdles with regards to treatment planning and delivery that will play increasingly dominant roles as dose is further escalated and PTV margins reduced.^{20,21} This section will further outline these limitations and challenges, and set the scene for the work presented in this thesis.

Interfraction motion management and treatment planning

Pancreatic lesions and surrounding bowel structures have excellent visibility and contrast on T_2 -weighted MRI, and the online adaptive workflow of the MR-Linac negates the problem of interfraction motion, as illustrated in Fig. 1.5. Indeed, the dosimetric benefits of online plan adaptation for pancreatic cancers have been extensively reported.^{7,22,23} At the same time,

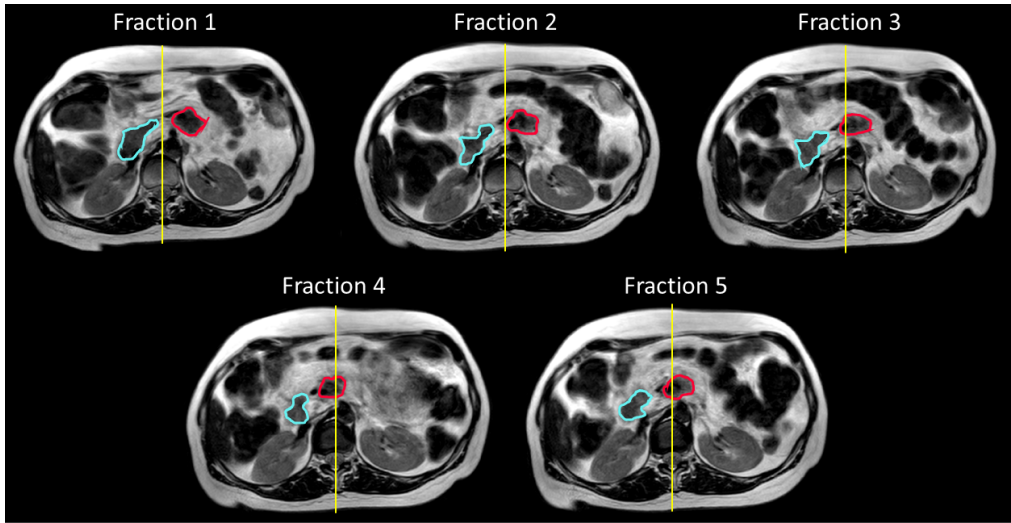


Figure 1.5.: An example of interfraction motion over a five-fraction treatment course on the MR-Linac. The daily acquired MRI scans from the start of each fraction are shown, along with the GTV (red) and duodenum (cyan), as well as their position relative to the midsagittal line (yellow).

manual recontouring of the numerous and complex structures in the upper abdomen is a labor-intensive and time-consuming process. This is the Achilles' heel online plan adaptation for pancreatic tumors, as treatment times on the MR-Linac are substantially longer than in conventional radiotherapy. MR-guided pancreatic treatments can take up to an hour to complete, of which 15-20 minutes is spent updating the GTV and OAR contours.^{14,24-26} This additional time pressure can introduce additional observer uncertainty and might negatively impact the treatment plan quality.

After the contours have been updated, SBRT treatment planning, with its high dose levels and steep gradients, remains a challenge in the upper abdomen as well. Even with online plan adaptation, one cannot avoid the fact that pancreatic tumors are sometimes located directly adjacent to the duodenum or bowels. Because the strict dosimetric constraints of these organs always take priority, cases with unfavorable anatomy will suffer from substantial compromise in tumor coverage. The level of compromise introduces another variable in treatment planning and can lead to situations where two centers may employ the same dosimetric objectives in their protocol, but in the end create two very different treatment plans for patients with unfavorable anatomy.

Intrafraction motion management and treatment delivery

While the online adaptive workflow can mitigate interfraction motion, intrafraction motion remains a concern for ablative treatments with SBRT in the upper abdomen. Early studies on the respiratory motion of pancreatic tumors report large cranio-caudal amplitudes of over 20 mm, and that this motion is also highly unpredictable, with intersubject standard deviations of over 15 mm.^{27,28} At the time, these cautionary tales confirmed the need for large PTV margins, on top of the uncertainties in tumor position and patient setup. However, it is important to realize that the dominant component of abdominal tumor motion is respiratory motion. This motion is mostly periodic, and its effect on treatment delivery is therefore analogous to a Gaussian filter; a static dose plan aimed at a moving target will cause this dose to be "smeared out" over a larger area.^{29,30} Respiratory motion is therefore much less detrimental to treatment delivery than other causes of tumor motion, such as drift. In principle, drift can be regarded as a simple shift of the planned dose, which can lead to larger dosimetric errors than respiratory motion. In the worst case, the tumor has moved from the target position to outside the high dose area, and an organ like the duodenum has taken its place. This could not only render the treatment ineffective, but also risk severe radiation toxicity.

The above situation illustrates that it is much more interesting to express the effect of intrafraction motion in terms of *dose*, instead of only quantifying the motion itself. After all, any intrafraction motion will lead to a nonzero difference between the dose that was originally planned and what was eventually delivered in the patient. We cannot use dosimetric detectors like ionization chambers to measure dose within patients, so the delivered dose must be approximated with dose accumulation. Traditionally, only interfraction imaging was available, so dose accumulation could also only be performed on an interfraction basis. However, the MR-Linac's online motion monitoring capabilities have enabled intrafraction dose accumulation as well.^{31,32} In intrafraction dose accumulation, the motion measured during each treatment delivery is applied as a mathematical transformation to the planned dose matrix, thereby obtaining a new dose map reflecting the dose delivered under the observed motion. This can then be compared to planned dose to assess the dosimetric accuracy of that treatment fraction. It should be noted that dose accumulation, in both interfraction and intrafraction setting, is still an active area of experimental research and as of yet, no clinical decisions are being made based on accumulated dose.

Dose accumulation allows for retrospective treatment evaluation, but motion detrimental to the delivered dose is ideally prevented, or otherwise minimized. Strategies for the manage-

ment of intrafraction motion predate the MR-Linac era, but some can very well be applied in the MR-guided setting. Passive motion management typically involves an abdominal compression belt, which translates respiratory motion from the abdominal region towards the thorax and reduces the amplitude of upper abdominal tumor motion.³³

Active motion management is more sophisticated and usually involves integrated imaging to monitor fiducial tumor markers³⁴ or the tumor itself. In case of the MR-Linac, the abovementioned ability to acquire MR images and irradiate in parallel can be used for this purpose. The measured motion is used in a real-time feedback system coupled to the linac. The two most common types of motion-incorporating beam delivery are gating and tracking. In gating, the beam is turned off if the tumor moves outside a predetermined window, which is typically centered around the exhale position in a free breathing approach, or at inhale combined with breath holds.³⁵ Tracking means that the beam aperture continuously follows the tumor position. Low-field MR-Linac systems have been capable of beam gating based on online cine MRI since 2018.³⁶ A clinical system for the high-field MR-Linac has recently been introduced,³⁷ and will be discussed in this thesis. The technical feasibility of MR-guided beam tracking has been demonstrated in a phantom setting on the high-field MR-Linac.³⁸

1.5. Thesis outline

This thesis addresses the limitations of the current MR-Linac workflow, and describes several technical advances for treatment planning and delivery. The overarching goal of this work is to transform contemporary MR-guided radiotherapy into a next-generation treatment for pancreatic cancer, which extensively capitalizes on the capabilities of the 1.5 T MR-Linac.

The daily acquired MRI scan used for contour adaptation is typically a Cartesian-sampled, 3D T_2w acquisition. The main disadvantage of this sequence is that respiratory motion in the abdomen during acquisition results in substantial image blurring, which can hamper delineation accuracy and speed. In **Chapter 2**, we investigate the use of two alternative, motion-robust MRI sequences with radial sampling schemes as main delineation scan for pancreatic MR-guided radiotherapy.

The complexity of MR-guided SBRT treatment planning for pancreatic cancer has led to a wide variety of treatment planning protocols and strategies used around the world. **Chapter 3** describes a harmonization project within a global consortium of centers that treat

pancreatic cancer on the 1.5 T MR-Linac, and presents the resulting consensus protocol for treatment planning.

Continuous real-time MR imaging alongside beam delivery means that the complete motion patterns of pancreatic tumors during radiotherapy can be characterized with 2D cine MRI. We describe the method to extract and characterize these motion patterns in **Chapter 4**, separated into respiratory and drift components, while using abdominal compression as passive motion management.

Chapter 5 extends the method of the previous chapter by performing time-resolved dose accumulation on the planned dose using the measured motion and linac machine log files. Aside from clinical motion data, this chapter also performs simulations to systematically assess the dosimetric impact of respiratory and drift motion.

The previous two chapters used a standard 2D cine MRI sequence, consisting of interleaved coronal and sagittal planes. **Chapter 6** introduces a novel 3D cine MRI sequence, which is able capture the complete time-resolved volumetric motion information of the upper abdomen at a high temporal resolution. The resulting non-rigid motion fields are used for deformable dose accumulation to once again analyze the delivered dose.

So far, we have focused on analyzing motion and delivered dose for the conventional, ungated delivery, where all tumor motion during beam on needs to be taken into account. In **Chapter 7**, we report the first treatments of MR-guided beam gating and drift correction on the high-field MR-Linac, and we quantify the dosimetric gain of this active motion management system.

The main findings of this thesis are summarized in **Chapter 8**. These findings are discussed within the broader scope of this thesis in **Chapter 9**, where we conclude with some future perspectives on MR-guided radiotherapy for pancreatic cancer.





Part I.

Treatment planning



CHAPTER 2

Feasibility of online radial MRI for adaptive radiotherapy of pancreatic tumors

G Grimbergen
H Eijkelenkamp
JK van Vulpen
S van de Ven
BW Raaymakers
MPW Intven
GJ Meijer

Physics and Imaging in Radiation Oncology (2023), **26**:100434

ABSTRACT

Background and purpose – Online adaptive magnetic resonance (MR)-guided treatment planning for pancreatic tumors on 1.5 T systems typically employs Cartesian 3D T_2w magnetic resonance imaging (MRI). The main disadvantage of this sequence is that respiratory motion results in substantial blurring in the abdomen, which can hamper delineation accuracy. This study investigated the use of two motion-robust radial MRI sequences as main delineation scan for pancreatic MR-guided radiotherapy.

Materials and methods – Twelve patients with pancreatic tumors were imaged with a 3D T_2w scan, a Periodically Rotated Overlapping Parallel Lines with Enhanced Reconstruction (PROPELLER) scan (partially overlapping strips), and a 3D Vane scan (stack-of-stars) on a 1.5 T MR-Linac under abdominal compression. The scans were assessed by three radiation oncologists for their suitability for online adaptive delineation. A quantitative comparison was made for gradient entropy and the effect of motion on apparent target position.

Results – The PROPELLER scans were selected as first preference in 56% of the cases, the 3D T_2w in 42% and the 3D Vane in 3%. PROPELLER scans sometimes contained a large interslice variation which would have compromised delineation. Gradient entropy was significantly higher in 3D T_2w patient scans. The apparent target position was more sensitive to motion amplitude in the PROPELLER scans, but substantial offsets did not occur under 10 mm peak-to-peak.

Conclusion – PROPELLER MRI may be a superior imaging sequence for pancreatic MR-gRT compared to standard Cartesian sequences. The large interslice variation should be mitigated through further sequence optimization before PROPELLER can be adopted for online treatment adaptation.

2.1. Introduction

With the introduction of magnetic resonance linear accelerator (MR-Linac) systems, radiotherapy for upper abdominal tumors can be conducted using an MR-guided online adaptive procedure.^{12,39} During this procedure, treatment plans can be re-adapted to the anatomy at every fraction based on MR imaging, a modality with a vastly superior soft tissue contrast and flexibility compared to computed tomography (CT) imaging of conventional radiotherapy. This introduction of MR-guided radiotherapy (MRgRT) has made high dose, hypofractionated stereotactic body radiotherapy (SBRT) feasible for pancreatic tumors,^{14,15,40–43} which can potentially lead to improved survival.⁹

In MRgRT on a 1.5 T MR-Linac, the imaging sequences typically used for online plan adaptation are based on 3D, Turbo Spin Echo (TSE), Cartesian k -space sampling patterns. These sequences have long been the standard in many routine radiological and radiotherapeutic applications, and therefore trained clinicians are used to the imaging contrast of these scans. Moreover, 3D imaging can be acquired with a high through-plane resolution, which facilitates structure contouring in radiotherapy as there is less structural variation from slice to slice. A substantial downside however, especially in abdominal imaging, is sensitivity to motion, which causes blurring and ghosting artifacts.⁴⁴ This can be a significant concern for MRgRT, as blurred structures may hamper accurate delineation of the tumor and organs at risk (OAR).

In contrast to Cartesian MRI, radial sampling schemes are much less sensitive to motion and might therefore reduce delineation uncertainty in the upper abdomen. Two examples of motion-robust radial MRI sequences are PROPELLER (Periodically Rotated Overlapping Parallel Lines with Enhanced Reconstruction)⁴⁵ and 3D Vane. PROPELLER, also known as MultiVane or BLADE, acquires multiple partially overlapping strips of phase encoding lines (so-called blades), each rotated around the center of k -space. In diagnostic radiology, PROPELLER MRI is a popular sequence for motion-robust T_2 -weighted imaging of the abdomen,^{46–49} but also when there is risk of bulk motion, like in the brain^{50–53} and pediatric imaging.^{54,55} However, the application of PROPELLER in the radiotherapeutic setting has as of yet not been investigated. In 3D Vane, k -space is sampled in a radial stack-of-stars pattern. While this sequence cannot provide T_2w contrast, it can acquire images in 3D fashion, rather than as multiple 2D slices such as PROPELLER. This results in the same high through-plane resolution as in conventional 3D Cartesian sequences.

This study qualitatively and quantitatively investigated the feasibility of employing radial MRI sequences, specifically PROPELLER and 3D Vane, for online contour adaptation during

MR-guided radiotherapy of pancreatic tumors.

2.2. Materials & Methods

2.2.1. Patients material

Twelve consecutive patients that underwent MRgRT for pancreatic tumors between January and June 2022 were included. Patients provided informed consent through the prospective Multi-OutcoMe EvaluationN of radiation Therapy Using the MR-Linac (MOMENTUM) study (NCT04075305). A summary of the patient characteristics is shown in supplementary Table S1.

All patients were treated with a hypofractionated stereotactic body radiotherapy (SBRT) regimen (five fractions of 8 Gy) on an Elekta Unity (Elekta AB, Stockholm, Sweden) MR-Linac, a 7 MV linear accelerator combined with a 1.5 T wide bore MRI scanner. During treatment, abdominal compression was applied with a custom fitted Neofrakt abdominal corset (Spronken Orthopedie NV, Genk, Belgium) to mitigate intrafraction motion.³³

2.2.2. Imaging

For each patient, three imaging sequences were acquired during a MRgRT treatment fraction: a multi-slice 2D (M2D), T_2w PROPELLER scan, a 3D Vane scan and a Cartesian 3D T_2w scan. Imaging was performed using the standard clinical 8-channel receive coil array of the Elekta Unity system. The PROPELLER scan was acquired with a k -space coverage of 318%, as set by the Multivane percentage parameter (500%) in the 1.5T Philips MR system of the MR-Linac used in this study. Echo time (TE) and repetition time (TR) were 130 and 3000 ms. SENSE undersampling with factor 4 was employed to result in a total scan time of three minutes and 30 seconds.

The 3D Vane scan was acquired as a balanced gradient echo stack-of-stars sequence, with Cartesian ordering in the k_z direction. Here, TE and TR were 2.4 and 4.9 ms, and total imaging time was four minutes and 45 seconds. The 3D T_2w scan was a turbo spin echo (TSE) sequence with TE/TR of 124/1300 ms, and total imaging time of four minutes and four seconds. More details on the imaging sequence parameters are given in Table 2.1.

2.2.3. Qualitative analysis

All scans were analyzed by three experts specialized in upper abdominal (MR-guided) radiotherapy: two radiation oncologists (SvdV, 9 years of experience and MPWI, 14 years of

Table 2.1.: Sequence parameters. TSE, turbo spin echo; bTFE, balanced turbo field echo; FOV, field of view; TE, echo time; TR, repetition time; FA, flip angle; BW, bandwidth.

	3D T _{2w}	M2D PROPELLER	3D Vane
Scanning technique	TSE	TSE	bTFE
FOV (mm ³)	451 × 451 × 220	420 × 420 × 210	450 × 450 × 150
Voxel size (mm ²)	0.64 × 0.64	0.58 × 0.58	0.62 × 0.62
Slice thickness (mm)	2.0	3.6	3.0
TE/TR (ms)	124/1300	130/3000	2.4/4.9
FA (°)	90	90	50
Echo train length	100	45	n/a
Readout BW (Hz/pixel)	820	352	718
Total scan time (min:sec)	4:04	3:30	4:45

experience) and one radiation oncology resident (JKvV, 4 years of experience). Per patient, the observers were asked to independently rank the three scans in order of preference for use as main delineation scan in an online adaptive setting. Moreover, each scan was scored on three aspects: 1) in-plane tumor delimitability, i.e. the ability to differentiate and delineate the tumor border; 2) in-plane OAR delimitability, i.e. the ability to differentiate and delineate the borders of the critical OAR (e.g. duodenum, small bowel, stomach); 3) the level of image artifacts in the area in and around the tumor. These aspects were scored on a five-point scale, from 1 (worst) to 5 (best). Concrete examples of criteria for the different scores are in supplementary Table S2.

2.2.4. Quantitative analysis

Gradient entropy is a quasi-objective image quality metric specifically related to motion artifacts.⁵⁶ Entropy is used here in the context of information theory. Gradient entropy postulates that an ideal image consists of areas of uniform gray values, separated by sharp edges. For such an image, the entropy of its gradient image is lower than for an image with blurry edges. Out of 24 metrics, gradient entropy was found to have the highest correlation with expert-based image quality scores.⁵⁶ The gradient entropy H of a 3D image is defined as:

$$H = - \sum_{i,j,k} g_{i,j,k} \log_2(g_{i,j,k}) \quad (2.1)$$

With $g_{i,j,k}$ the voxel values of the normalized gradient magnitude image:

$$g_{i,j,k} = \frac{|m_{i,j,k} * k|}{\sum_{i,j,k} |m_{i,j,k} * k|} + \varepsilon \quad (2.2)$$

With $m_{i,j,k}$ the gray values of the 3D image, k a 3-by-3-by-3 gradient kernel, and $*$ the convolution operator. ε is a small constant to avoid taking the logarithm of 0. Formally, H is expressed in the unit bits. The gradient entropy was calculated for all patient scans.

Aside from delineation uncertainty due to blurring, the asymmetry of a patient's breathing pattern might lead to a change in the tumor's apparent position in the image. For ungated radiotherapy in free breathing, the delineated position of a moving tumor should correspond to the time-weighted average position during the respiratory cycle, also known as the midposition strategy.⁵⁷ Recently, Bertelsen et al. investigated the apparent position of a mobile target for 3D T_2w sequences in a phantom study, under different breathing conditions.⁵⁸ Based on their analysis, we extended this investigation to the PROPELLER and 3D Vane sequences. Motion was simulated using the Quasar MRI 4D motion phantom (Modus Medical Devices, Ontario, Canada), an MRI-compatible phantom containing a mobile cylinder with a 30 mm sphere at the center. Both the sphere and the cylinder were filled with water, and the sphere was doped with $MnCl_2$ for a hypointense contrast with its surroundings. The cylinder was programmed to move with a \cos^6 function, with a period of 5 seconds, and an amplitude of 5 mm, 10 mm or 15 mm. For each amplitude, the function was offset with its average value to ensure the midposition of the target corresponds to its static position. The phantom was placed in the MR-Linac with the direction of motion parallel with the z-axis, i.e. the slice direction of the imaging sequences. As with the other experiments, the sequence parameters were kept identical to the patient acquisitions. For each sequence, the phantom was scanned in static position, and with the phantom in motion with the three different amplitudes. The target was automatically segmented in a single coronal slice of each image by k-means clustering with three clusters. As the target was always roughly in the center of the image, the cluster of the central voxel was assigned as the target segmentation, resulting in a binary mask of the target. To obtain a mask shape more reminiscent of human contouring, rough edges of the mask were smoothed by means of Gaussian filtering ($\sigma = 2$) and rebinarizing. The z-component of the mask's center of mass (COM) was extracted and compared to the static configuration, to quantify the offset of the target position as a result of motion.

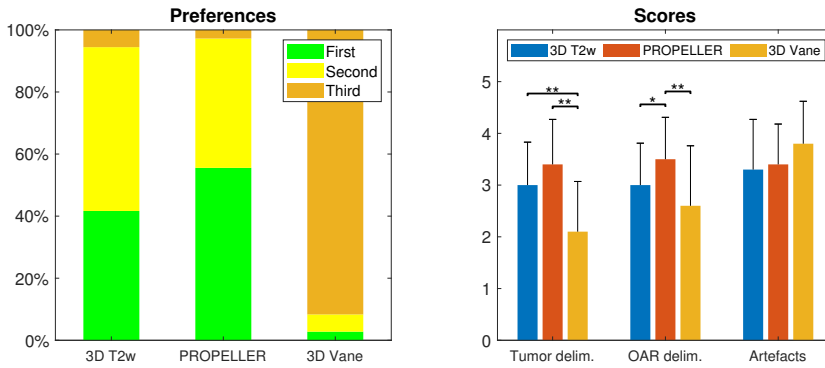


Figure 2.1.: The qualitative analysis results. a) The proportions of first, second and third preferences given out by the observers for each scan over all patients. b) The average scores for tumor/OAR delimitability and artifacts for each sequence. Significance markers indicate p -values below 0.05 (*) and 0.001 (**).

2.2.5. Statistical analysis

Descriptive statistics were performed for the results of COM offset and observer preference. Differences between the gradient entropy and observer scores for tumor delimitability, OAR delimitability and artifacts were determined using the one-way analysis of variance (ANOVA) test and Tukey post hoc test ($p < 0.05$) in Statistical Package for Social Sciences (SPSS) version 25 (IBM, Armonk, NY).

2.3. Results

2.3.1. Qualitative analysis

Over the three observers, the 3D T_{2w} was in (rounded to the nearest percentage) 42% of the cases selected as the first preference, PROPELLER in 56%, and 3D Vane in 3% (Fig. 2.1a). In general, the PROPELLER images had sharper edges and improved visual definition of OARs (Fig. 2.2).

It was noted that in some PROPELLER scans, there was a large interslice variability in respiratory phase, causing structures to vary in position between slices. In two patients, the observers noted that this variability was so severe that it would have critically impeded the delineation process. This was the most commonly cited reason why the 3D T_{2w} scan was preferred above the PROPELLER scan, even if the PROPELLER scan was still of superior in-plane quality. Remarkable was that this interslice variability effect seemed very pronounced in some patients, but barely present in others (Fig. 2.3). The 3D Vane was indicated to

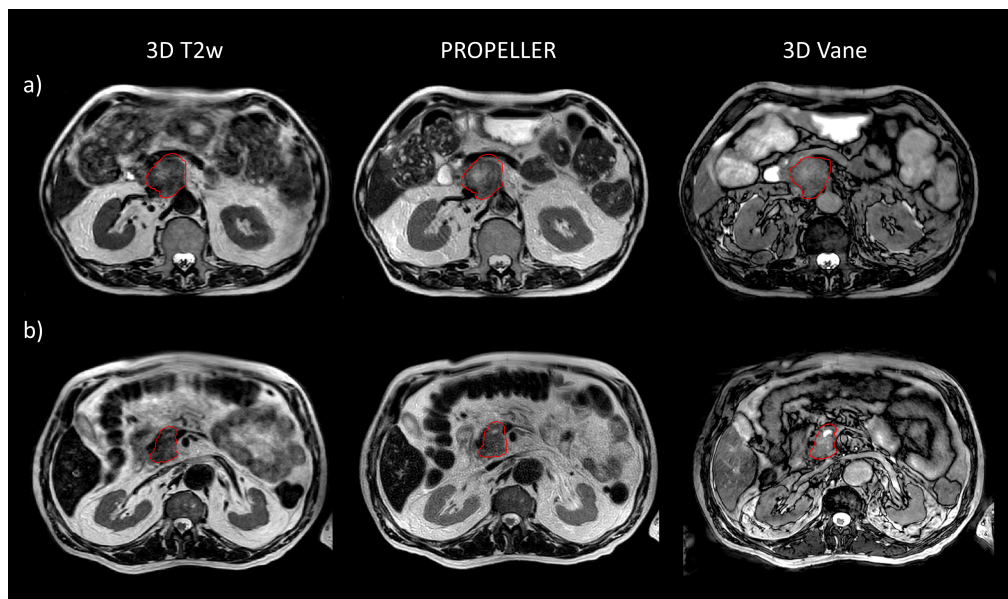


Figure 2.2.: Two example cases of 3D T_2w , PROPELLER, and 3D Vane scans. The GTV contour is shown in red. a) A case where there was good agreement between the observers on the preference of the PROPELLER over the 3D T_2w scan; b) A case where there was no clear agreement over the preference between PROPELLER and 3D T_2w . The 3D Vane scan was selected as least preferred in both cases.

be least preferred in 92% of the cases, with the most commonly cited reasons being the unconventional contrast of this sequence, and no contrast between tumor and healthy tissue. The mean (SD) scores (higher is better) for tumor delimitability, OAR delimitability, and artifacts were: 3D T_2w : 3.0 (0.8), 3.0 (0.8), 3.3 (1.0); PROPELLER: 3.4 (0.9), 3.5 (0.8), 3.4 (0.8); 3D Vane: 2.1 (1.0), 2.6 (1.2), 3.8 (0.8) (Fig. 2.1b). Tumor delimitability scores were significantly higher in both the 3D T_2w scans and the PROPELLER scans compared to the 3D Vane scans (both $p < 0.001$), but PROPELLER was not scored significantly higher than 3D T_2w ($p = 0.122$). OAR delimitability was scored significantly higher in the PROPELLER scans than in the 3D T_2w scans ($p = 0.050$) and in the 3D Vane scans ($p < 0.001$). The observers noted that the scoring for tumor and OAR delimitability was often highly correlated, as both scores reflect the ability to distinct tumor from OARs.

2.3.2. Quantitative analysis

The mean (SD) gradient entropy in bits for each sequence was: 3D T_2w : 23.7 (0.3); PROPELLER: 22.9 (0.3); 3D Vane: 22.6 (0.3). Again, a lower gradient entropy signifies an image with sharper boundaries between structures. The gradient entropy in the 3D T_2w

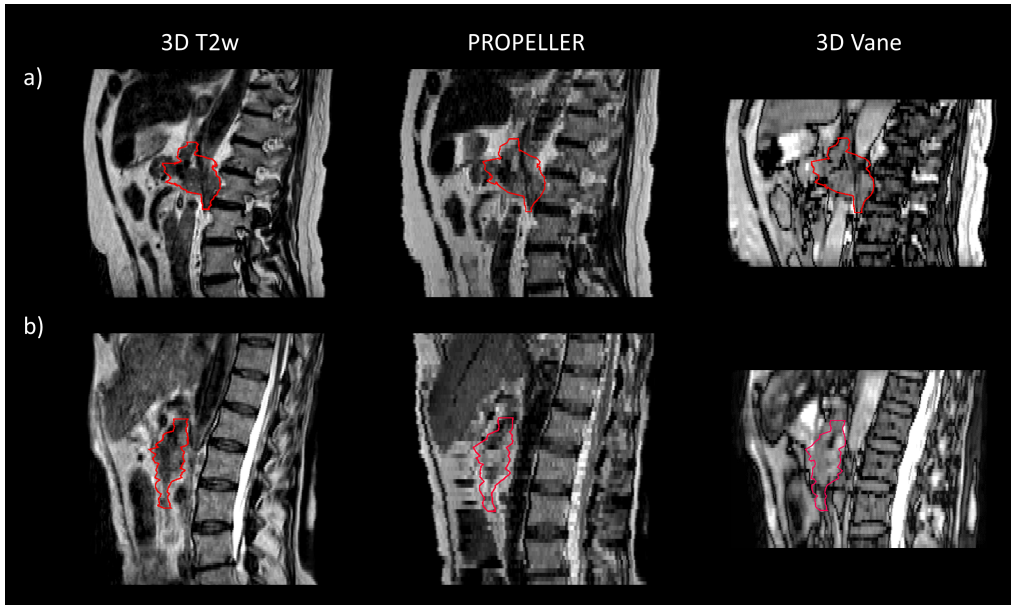


Figure 2.3.: Two example cases of 3D T_2w , PROPELLER, and 3D Vane scans in the sagittal plane, where the interslice variability of the PROPELLER scans is demonstrated. The GTV contour is shown in red. a) A case with low interslice variability in the PROPELLER scans; b) A case with high interslice variability.

scans was significantly higher than in the other two sequences (both $p < 0.001$).

The center of mass offsets, relative to the midposition, are given in Fig. 2.4 as a function of motion amplitude. The acquired images, target segmentations and COM positions are given in supplementary Fig. S1. In all sequences, the center of mass of the segmented target showed a trend towards the exhale position as the motion amplitude increased past 10 mm. At 5 mm amplitude, there was no noticeable difference with a static scans. At 10 and 15 mm, the target offset was larger in the PROPELLER scan than in the 3D sequences. The amount of motion blurring also increased in the 3D sequences with larger amplitudes, but in the PROPELLER scans a discrete copy of the target appeared at approximately the inhale level.

2.4. Discussion

This study investigated the use of two motion-robust, radial MRI sequences, PROPELLER and 3D Vane, as primary delineation scan during online adaptive MR-guided radiotherapy of pancreatic tumors. In both the qualitative and quantitative sense, the PROPELLER images

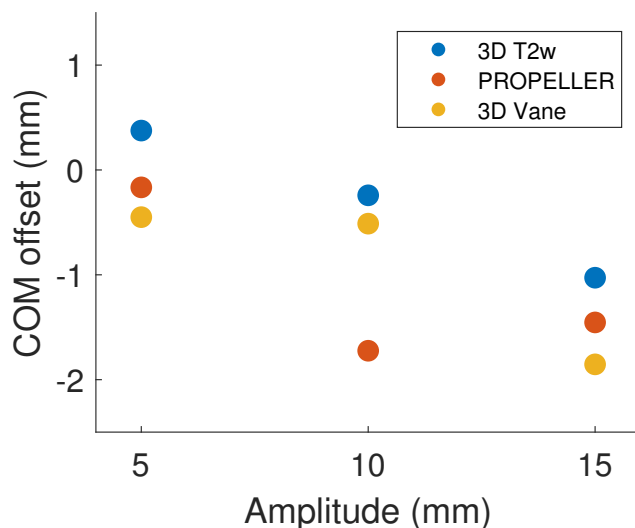


Figure 2.4.: The target segmentations' center of mass offset with respect to the midposition, as a function of phantom motion amplitude, for the four different scans. A positive value is towards inhale, a negative value is towards exhale.

were at least on par with the conventionally used 3D T_2w scans. The PROPELLER scans presented with substantially less motion blur, but could suffer from more interslice variation compared to the 3D T_2w scans. While the 3D Vane scans were unequivocally deemed not suitable as main delineation scan, the unconventional contrast might still aid delineation as auxiliary imaging, comparable to diffusion weighted imaging.

Since the advent of MRgRT, 3D Cartesian sequences have been standard delineation scans for daily treatment delineation and adaptation on 1.5 T systems, because of their high geometric fidelity, hardware compatibility, and predictable image artifacts. One should realize, however, that one of the main goals of MRgRT has always been increasing target definition accuracy, in order to safely increase target dose. In the MRgRT workflow, the uncertainty in delineation plays an increasingly important role as other geometrical errors from inter- and intrafraction motion get reduced. Due to the online adaptive setting, there is an additional time pressure for the physician to recognize and delineate the tumor and OARs. A large part of on-table time during MRgRT is taken up by contouring, especially in the upper abdomen where tumor morphology can be complex and with a large number of OARs to delineate; centers commonly report around 15 minutes for contouring.^{14,24–26} Image quality therefore plays a crucial part in the workflow. Moreover, going by the lack of publications on this

subject, we believe that the MRgRT community should explore more deeply the versatile toolbox that MRI can offer to improve visual image quality. Further investigation should also focus on the influence of image quality on interobserver delineation variability, ideally while simulating the online adaptive setting. Because this is not trivial to reliably achieve with multiple observers, assessing contouring performance was considered beyond the scope of this study.

The large interslice variability in the PROPELLER scans that was present in some patients (Fig. 2.3) could be expected in a multi-2D scan, where each slice is acquired with an independent excitation and readout. This variability is probably amplified by the relatively large slice thickness compared to the 3D sequences. In this study, intrafraction motion (a probable cause of interslice variability) was already mitigated using abdominal compression to reduce tumor motion during irradiation. However, in patients where the interslice variability was especially noticeable, the observers unilaterally preferred the 3D T_2w over the PROPELLER scans. This suggests that additional measures might have to be taken to further mitigate this variability. One solution would be to acquire PROPELLER images with respiratory triggering, causing each slice to be acquired in the exhale state, but this would also introduce a positional offset in the delineations which, again, should ideally be positioned at midposition. Future real-time motion monitoring solutions during beam-on might correct for positional bias, by translating the contours based on motion measured in cine MRI. However, a triggered sequence will also prolong acquisition time. Therefore, a more viable solution might be optimizing sequence parameters like slice acquisition order and TSE shot length, in order to reduce the probability that slices are acquired in different respiratory phases.

Regarding the quantitative analysis, the gradient entropy measurements confirm that PROPELLER MRI produces images with sharper edges compared to 3D T_2w MRI. Interestingly, the 3D Vane images had the lowest gradient entropy of all four sequences. This could be due to the characteristic phase cancellation artifact at tissue boundaries where voxels contain an equal amount of water and fat.^{59,60} This artifact, inherent to gradient echo sequences, results in a dark outline between different tissues, and thus a very sharp and local gradient in voxel intensity. In clinical practice, this might improve delineation accuracy in places where tissue boundaries are less visible in the primary T_2w scan. This property, and also considering the fact that 3D Vane was scored highest in terms of artifacts (Fig. 2.1), suggests that even though it is deemed unsuitable as primary delineation scan, 3D Vane may still have a substantial clinical value in aiding the delineation process as auxiliary imaging.

The findings of the phantom COM measurements echo the results from Bertelsen et al.,⁵⁸ that a target's apparent position shifts from the time-averaged position towards the median position as motion amplitude increases (Fig. 2.4). The results in our study suggest that this effect is more pronounced in the PROPELLER scans than in the 3D sequences. However, it should be noted that the larger slice thickness creates an uncertainty in the exact COM position, so the difference in the effect on motion in 2D and 3D sequences might not be significant. In any case, these results emphasize the importance of mitigating respiratory motion when treating pancreatic lesions, not only for dosimetric considerations but also for image quality and positional accuracy. Abdominal compression, as applied in this study, can be a simple but effective method to achieve this: we have previously reported typical intrafraction tumor respiratory amplitudes between 5 to 10 mm peak-to-peak in similar cohorts when using the same abdominal compression strategy as in this study.^{33,61}

There are some technical hurdles that need to be addressed when clinically implementing PROPELLER MRI in daily MRgRT. The most important consideration here is geometric fidelity. In the current clinical systems, correction for nonlinearity of the spatial encoding gradients is only performed in 2D (in-plane) for multislice 2D scans, while 3D scans are fully corrected. This means that in reality, PROPELLER slices are warped in the through-plane direction at further distances from the isocenter (>10 cm).⁵⁹ These geometric inaccuracies could lead to systematic, nontrivial dose errors if left uncorrected.⁶² This is one of the main reasons that 3D sequences were chosen as the standard scans for MR-guided radiotherapy. However, a geometric comparison between the 3D and PROPELLER sequences was purposefully omitted in this study, because a 3D correction for multislice 2D scans is currently only a software limitation. Gradient nonlinearities can be fully characterized using spherical harmonics coefficients, which enable retrospective 3D correction of both multislice 2D and 3D images. This has been performed before on the Unity MR-Linac,⁶² and we expect that this will become available in the standard clinical environment in the future.

To conclude, PROPELLER MRI may be a superior imaging sequence for MRgRT of pancreatic tumors. The PROPELLER sequence produces noticeably sharper in-plane images compared to the standard 3D T_2w MRIs. This improved image quality might facilitate and thereby accelerate the online treatment adaptation process, while also reducing delineation uncertainty. However, further sequence optimization before clinical implementation is warranted, to prevent large interslice variation and ensure geometric fidelity.

Supplementary materials





CHAPTER 3

Treatment planning for MR-guided SBRT of pancreatic tumors on a 1.5 T MR-Linac: a global consensus protocol

G Grimbergen
H Eijkelenkamp
LMW Snoeren
R Bahij
U Bernchou
E van der Bijl
HD Heerkens
S Binda
SSW Ng
C Bouchart

Z Paquier
K Brown
R Khor
R Chuter
L Freear
A Dunlop
RA Mitchell
BA Erickson
WA Hall
P Godoy Sripes

N Tyagi
J de Leon
C Tran
S Oh
P Renz
A Shessel
E Taylor
MPW Intven
GJ Meijer

Submitted

ABSTRACT

Background and purpose – Treatment planning for MR-guided stereotactic body radiotherapy (SBRT) for pancreatic tumors can be challenging, and as such there is a wide variation of protocols and practices around the world. This study aimed to harmonize treatment planning by developing a consensus planning protocol for five-fraction MR-guided pancreas SBRT on a 1.5 T MR-Linac.

Materials and methods – A worldwide consortium was founded of thirteen centers that were treating or were planning to treat pancreatic tumors on a 1.5 T MR-Linac. A planning exercise was conducted in which centers were asked to create treatment plans for two cases of locally advanced pancreatic cancer with different anatomical complexities. The formation of a consensus protocol consisted of three phases. Each phase was followed by a consensus meeting where the instructions for the next phase were determined based on the results of the previous phase. After three phases, a consensus protocol was reached.

Results – In the benchmarking phase (phase I), substantial variation between the five-fraction SBRT protocols became apparent (for example, the gross tumor volume (GTV) $D_{99\%}$ ranged between 36.8 – 53.7 Gy for case 1, 22.6 – 35.5 Gy for case 2). The next phase involved planning according to the same basic dosimetric objectives, constraints, and planning margins (phase II), which led to a large degree of harmonization (GTV $D_{99\%}$ range: 47.9 - 53.6 Gy for case 1, 33.9 - 36.6 Gy for case 2). The final consensus protocol was formulated in a template for the treatment planning system, and this template was used for treatment planning in phase III. This not only resulted in further dosimetric harmonization (GTV $D_{99\%}$ range: 48.2 - 50.9 Gy for case 1, 33.5 - 36.0 Gy for case 2) but also in less variation of estimated treatment delivery times/monitor units.

Conclusion – A global consensus protocol has been developed for treatment planning for MR-guided pancreatic SBRT on a 1.5 T MR-Linac. Aside from harmonizing the large variation in the current clinical practice, this protocol can provide a starting point or road map for centers that are planning to treat pancreatic tumors on 1.5 T MR-Linac systems.

3.1. Introduction

MR-guided stereotactic body radiotherapy (SBRT) has been established as a novel and promising therapy for pancreatic tumors. Early clinical outcomes demonstrated that stereotactic treatment with prescribed doses of up to 50 Gy in five fractions (equivalent to a biologically effective dose for $\alpha/\beta = 10$ (BED₁₀) of 100 Gy) can safely be delivered while maintaining low acute toxicity rates.^{15,17,18,40,43,63}

These high dose levels in a complex anatomical region make SBRT treatment planning for pancreatic tumors a complex task. There are currently notable differences between documented institutional protocols with regards to prescribed dose, organ at risk (OAR) constraints and safety margins, see Table 3.1.^{14–17,25,41,42,64–68} However, even if these descriptions are identical in two institutions, there can still be nontrivial differences in treatment plans due to the fact that target coverage is sometimes compromised in favor of the strict dosimetric constraints of abutting radiosensitive digestive, biliary, and vascular structures.^{22,69} This means that additional clinical and technical variables influence the dose distribution outside the usual dosimetric considerations. Moreover, there is a wide range of expertise levels in centers that treat pancreatic tumors with MR-guided SBRT, mainly due to the dispersed and still ongoing adoption of MR-Linac systems around the world. This lack of a consensus planning protocol increases the risk of suboptimal treatment delivery and may hinder proper evaluation of the added value of MR-guided SBRT in these patient groups.

To address this issue, a consortium of centers with a 1.5 T MR-Linac was founded, with the aim to create a harmonized treatment planning protocol for five-fraction MR-guided SBRT for pancreatic cancer. The consortium comprised thirteen centers across North America, Europe, and Australia that are treating or planning to treat pancreatic cancer with MR-guided SBRT, with considerable differences in relevant experience. This work reports the outcome of this collaboration, which is a consensus protocol for treatment planning for pancreatic tumors on the 1.5 T MR-Linac.

3.2. Materials & Methods

3.2.1. Planning and evaluation process

To reach a consensus, an iterative planning exercise was designed in which each center was asked to create a clinically acceptable treatment plan for two example cases, according to a set of instructions that became more prescriptive in each phase. Treatment planning was

Table 3.1.: Existing treatment planning protocols for MR-guided SBRT for pancreatic cancer, as reported in various studies. Prescribed dose is given as # fractions × fraction dose. OAR, organ at risk; GTV, gross tumor volume; PTV, planning target volume; dd, duodenum; st, stomach; sb, small bowel; c, colon.

	Prescribed dose (Gy)	OAR constraints ¹	GTV-PTV margin (mm)
Bohoudi et al. ⁴¹	5x8 Gy	$D_{1cc} < 33$ Gy; $D_{20cc} < 25$ Gy	3 mm
Chuong et al. ⁶⁷	5x10 Gy	$D_{0.03cc} < 40$ Gy; $D_{0.5cc} < 35$ Gy (dd, st, sb) $D_{0.03cc} < 43$ Gy; $D_{0.5cc} < 38$ Gy (c)	3 mm
Daamen et al. ¹⁴	5x8 Gy	$D_{0.5cc} < 35$ Gy; $D_{10cc} < 25$ Gy (dd, st, sb) $D_{0.5cc} < 32$ Gy (c)	3 mm
Hassanzadeh et al. ¹⁶	5x10 Gy	$D_{0.5cc} < 36$ Gy	5 mm
Henke et al. ⁶⁴	5x10 Gy	$D_{0.5cc} < 35$ Gy (dd, c) $D_{0.5cc} < 33$ Gy (st) $D_{0.5cc} < 30$ Gy (sb)	5 mm
Koay et al. ⁶⁵	5x10 Gy	$D_{0.5cc} < 40$ Gy; $D_{1cc} < 35$ Gy; $D_{2cc} < 30$ Gy	5 mm
Parikh et al. ¹⁷	5x10 Gy	$D_{0.5cc} < 33$ Gy	3 mm
Placidi et al. ⁴²	5x6-8 Gy	Not reported	3 mm
Rudra et al. ¹⁵	5x10 Gy	Multiple (multi-center)	3 mm
Stanescu et al. ²⁵	5x6-8 Gy	Not reported	5 mm
Tyagi et al. ⁶⁶	5x10 Gy	$D_{0.035cc} < 33$ Gy; $D_{5cc} < 25$ Gy (dd, st, sb) $D_{0.035cc} < 33$ Gy; $D_{5cc} < 30$ Gy (c)	5 mm
Yoon et al. ⁶⁸	Multiple	$D_{0.5cc} < 35$ Gy	5 mm

¹ Confined to the reported constraints for duodenum (dd), stomach (st), small bowel (sb) and colon (c)

performed in Monaco v5.51.10/v5.51.11, the treatment planning software (TPS) of the 1.5 T MR-Linac (Elekta Unity, Elekta AB, Sweden). The centers performed treatment planning independently, and were not able to view each other's results during planning.

The central element for reaching a consensus was the joint evaluation and discussion that followed each planning exercise, in which the instructions for the next phase were determined. These evaluation sessions were attended by physicists, clinicians, and radiotherapy technologists (RTTs) from each center. These discussions were centered around the results from previous studies, clinical experiences, and current protocols of individual centers. This iterative plan – evaluate cycle was repeated until a consensus protocol was reached.

After the first phase, the estimated delivery times of the treatment plans were also taken into consideration during the discussions. As surrogate for estimated delivery time, the number of monitor units (MUs) reported by the TPS was used. Due to the slightly different calibration setups used between centers, the reported MUs were normalized to the standard reference setup of 1 MU = 1 cGy measured at source-axis distance (SAD) of 143.5 cm, in 10 cm of water, with a field size of 10x10 cm².

After consensus was reached, harmonization was also evaluated statistically by performing Bartlett's test for homogeneity of variances between critical dose-volume histogram (DVH) parameters calculated in the treatment plans of the final phase and treatment plans of the initial phase. A statistically significant difference in variance was defined as $p < 0.05$.

3.2.2. Case data

All participating centers were sent the same two anonymized data sets, reflecting two cases of locally advanced pancreatic cancer. Case 1 was a 62-year-old male with at least 10 mm distance between the tumor and the nearest luminal organs. This case was therefore considered to be favorable for radiotherapy planning (Fig. 3.1a). Case 2 was a 71-year-old female with the tumor abutting both the duodenum and small bowel along a considerable surface area, making this case less favorable (Fig. 3.1b).

Each data set consisted of a mid-ventilation CT (corresponding to the 20% phase of a 4DCT) and a structure set containing the gross tumor volume (GTV) and OARs. Treatment planning was performed on the CT scan to bypass differences in electron density conversion protocols. Centers were not allowed to edit existing OAR and target contours in the structure set, but were in phases I and II allowed to create custom planning target volume (PTV) and other margin structures (e.g. planning organ at risk volumes (PRVs)) and delineate additional OARs. To aid in this, auxiliary imaging was provided in the form of the complete 4DCT, arterial and portal phase contrast-enhanced CTs and a 3D T_2 -weighted MRI.

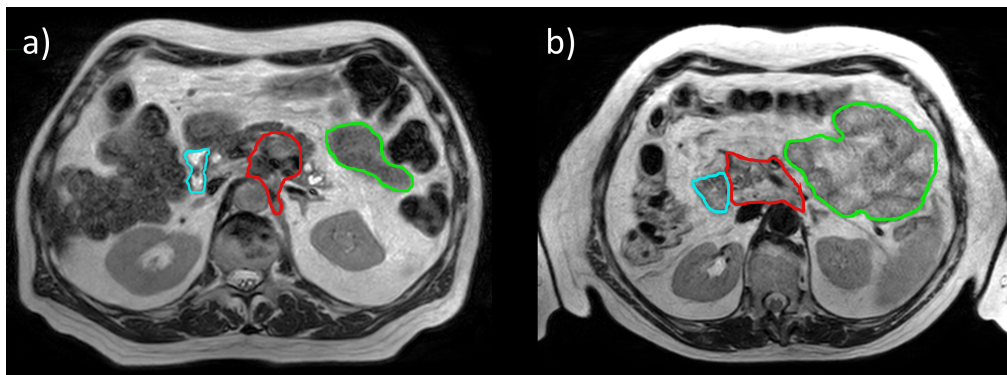


Figure 3.1.: 3D T_2w MRI data of case 1 (a) and case 2 (b), on which the planning contours are projected (red = GTV, cyan = duodenum, green = small bowel). Note that not all contours are shown and that treatment planning itself was performed on a CT dataset.

3.3. Results

After three phases of planning and evaluation, a consensus protocol was reached within the consortium. The instructions for the three planning phases were as follows:

Phase I: Create a treatment plan according to the native five-fraction SBRT protocol of each center. This included the local dose prescription, OAR constraints, PTV/PRV margins, beam configuration, et cetera.

Phase II: Create a treatment plan adhering to the same consensus-based dose prescription, DVH constraints/objectives for the GTV, PTV, and most critical OARs, and PTV margin.

Phase III: Create a treatment plan using the same consensus-based template for the TPS. The TPS template not only contained the exact DVH constraints and objectives, but also dictated the specific cost function(s) for each planning structure, beam configuration, and sequencing parameters such as maximum amount of segments and minimum segment area. Treatment planning optimization was only allowed by modifying a fixed set of parameters of the preset cost functions. Modification of the structures, margins, and DVH constraints was not allowed.

The dosimetric results from the three planning phases are summarized in Fig. 3.2 and Fig. 3.3,

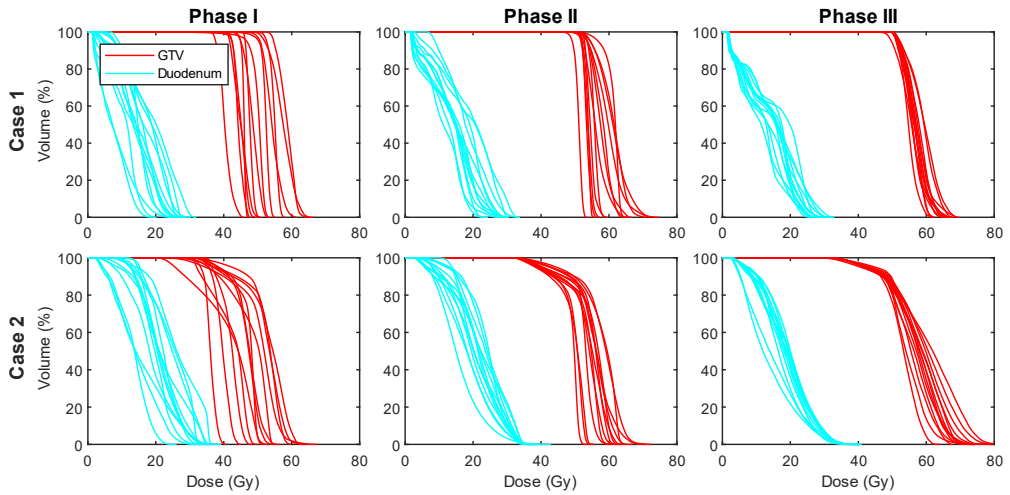


Figure 3.2.: Dose-volume histograms (DVHs) of the GTV (red) and duodenum (cyan) from all thirteen centers. The DVHs are extracted from the treatment plans of case 1 (top row) and case 2 (bottom row), as created in phases I-III (columns).

where Fig. 3.2 contains the individual DVHs of the GTV and duodenum from all centers, and Fig. 3.3 contains boxplots of DVH parameters of the GTV ($D_{99\%}$, $D_{90\%}$, $D_{50\%}$, $D_{1\%}$), duodenum, small bowel, and stomach (all $D_{0.5cc}$). The individual dose distributions from all centers are shown in Fig. 3.4 for phase I, and supplementary Figs. S1 and S2 for phases II and III.

The sections below contain a detailed description of the instructions, outcomes, and discussion of each phase.

3.3.1. Phase I

There was a considerable variation in the baseline practice among the consortium members, see Fig. 3.4 for all individual dose plans for case 1 and case 2. The main difference between the treatment protocols was the prescribed dose for the five-fraction protocol. The prescriptions were 5x7 Gy ($n=1$), 5x8 Gy ($n=6$), 5x9 Gy ($n=4$), and 5x10 Gy ($n=5$). For case 1, all centers were able to reach an acceptable level of target coverage as per the center-specific protocol, with the median (range) GTV $D_{99\%} = 44.0$ Gy (36.8 – 53.7 Gy). This proved more challenging for case 2 due to the unfavorable anatomy, with the median (range) GTV $D_{99\%} = 33.1$ Gy (22.6 – 35.5 Gy). In this case, the loss in target coverage to adhere

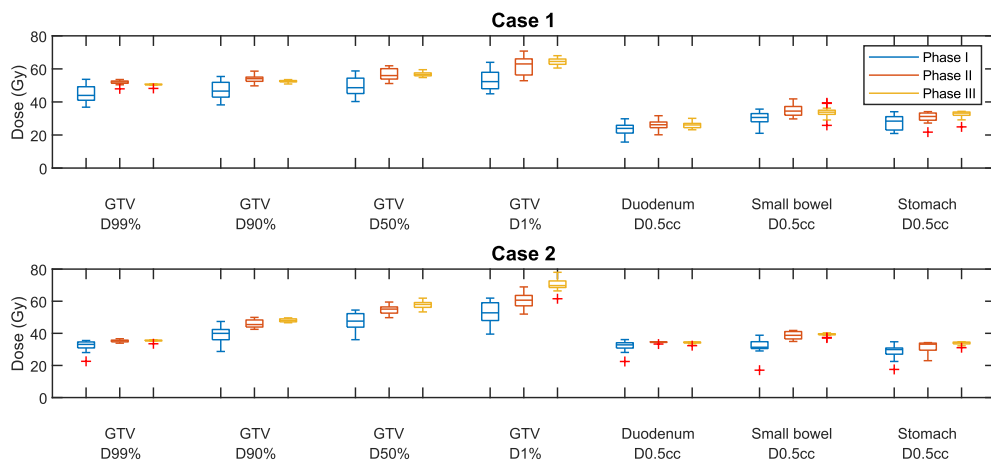


Figure 3.3.: Boxplots of the distribution of the most critical DVH parameters of the GTV, duodenum, small bowel and stomach, in phases I-III. The whiskers of the boxplot extend to the minimum and maximum of the values not considered outliers (values further than 1.5 times the interquartile range from the box). The outliers are indicated by the red plus signs.

to the duodenum and small bowel constraint was also different between centers. As an illustration of the variance in OAR doses, the median (range) duodenum $D_{0.5cc}$ was 24.0 Gy (15.7 - 29.8 Gy) for case 1, and 32.8 Gy (22.5 - 36.1 Gy) for case 2. Most centers created a dose gradient within the GTV boundaries. Differences in gradient steepness and its distance to the nearest OAR boundaries demonstrated different levels of conservative planning, and one center scaled down the prescribed tumor dose for case 2 from 5x8 Gy to 5x6 Gy. Further differences were visible in dose homogeneity and conformity within the GTV (judged qualitatively), and high dose spillage outside the GTV into unspecified tissue.

Outside the dosimetric characteristics, the main noteworthy differences between protocols were the number of beams (range 8 - 19), PTV margins (range 3-5 mm), the exact definition of PTV objective criterion (in terms of minimum dose to minimum volume), and the use and size of planning organ at risk volume (PRV) and/or subtractive PTVs, meaning the PTV is locally shrunk to maintain a certain minimum distance to the nearest OAR. However, agreement was found on the use of abdominal compression, which was used by almost every center for passive mitigation of respiratory motion.

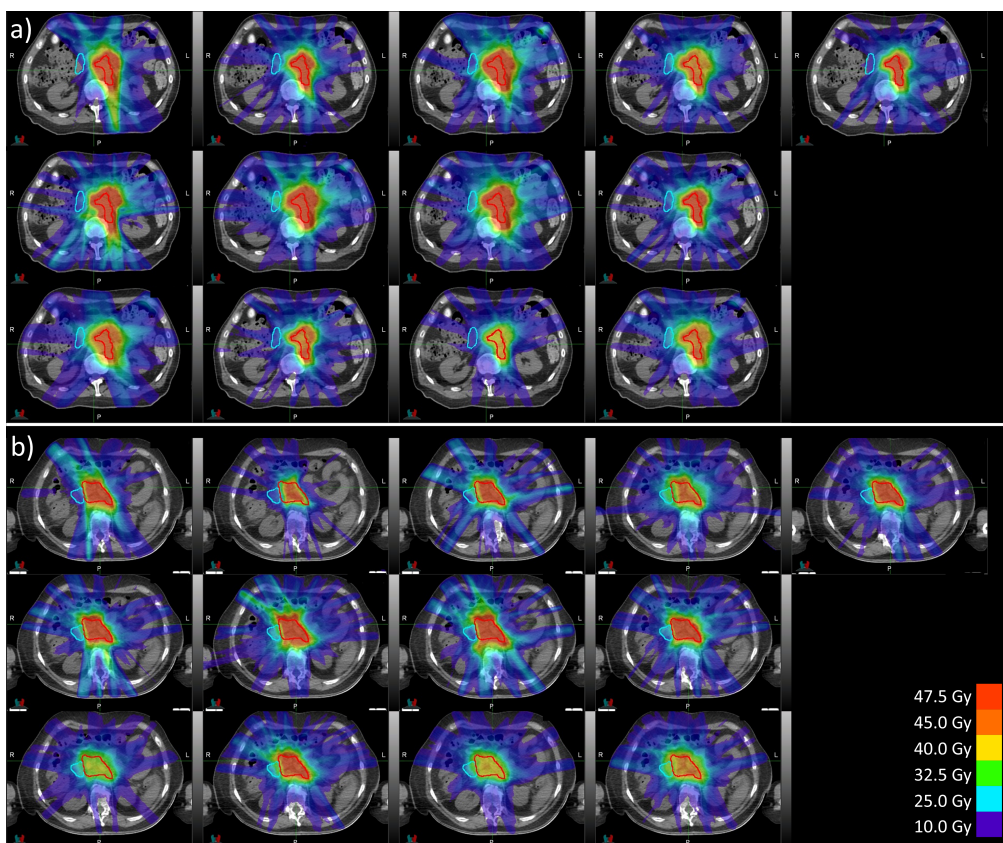


Figure 3.4.: The dose distributions for a) case 1 and b) case 2 from all thirteen centers in phase I (variation in baseline practice). Red = GTV, cyan = duodenum.

3.3.2. Phase II

Considering the results from phase I, the consortium agreed on a basic set of goals and constraints to use for planning in phase II. It was decided to set a prescription dose of 5×10 Gy (GTV $V_{100\%} > 99\%$), motivated by this dose level already being the standard in five centers and the favorable clinical outcomes reported in earlier studies.^{15,17} Consensus was also found in the OAR constraints for the critical luminal organs, with $D_{0.5cc} < 35$ Gy for the duodenum, stomach, and colon, and $D_{1cc} < 40$ Gy for the small bowel. The more permissive constraint for the small bowel was motivated by the higher organ motility compared to e.g. the duodenum, and therefore a larger probability that the dose hot spot in the small bowel is in a different location from day to day. At tumor dose levels beyond 50 Gy, a constraint for the aorta, inferior vena cava, superior mesenteric artery, and celiac trunk of

$D_{0.1cc}$ | 53 Gy was agreed upon. Furthermore, a GTV to PTV margin of 2 mm was chosen, anticipating the upcoming implementation of active motion management functionalities (gating and baseline drift correction) on the high-field MR-Linac.³⁷ PRVs were abandoned too for this reason, also motivated by the online adaptive treatment, and improved healthy tissue visibility compared to conventional (cone-beam CT-guided) radiotherapy. Finally, there was agreement to maximize the integral dose to the GTV within the above constraints.

The above instructions resulted in a substantial harmonization of treatment plans, with the median (range) GTV $D_{99\%} = 52.1$ Gy (47.9 - 53.6 Gy) for case 1, and 35.4 Gy (33.9 - 36.6 Gy) for case 2 (Fig. 3.3). All OAR constraints were respected; the median (range) duodenum $D_{0.5cc}$ was 26.2 Gy (20.1 - 31.7 Gy) for case 1, and 34.6 Gy (33.3 - 34.8 Gy) for case 2. The instruction to maximize the integral dose (without setting limits to the maximum dose) resulted in a much steeper dose gradient within the GTV, although deviations between plans became apparent in the median dose ($D_{50\%}$ range 51.1 - 61.9 Gy for case 1, 49.8 - 59.5 Gy for case 2) and maximum dose ($D_{1\%}$ range 52.8 - 70.8 Gy for case 1, 52.0 - 68.9 Gy for case 2).

As a surrogate for treatment delivery time, the number of MUs for each plan was also evaluated for each treatment plan. Here, a considerable variation between centers was apparent, with the median (range) MUs were 2755 (1646 - 4057) for case 1, and 3578 (2146 - 4873) for case 2.

3.3.3. Phase III

Following the harmonization of the most critical DVH parameters in phase II, the consortium adopted those planning constraints as part of the consensus protocol. One exception was the small bowel constraint of $D_{1cc} < 40$ Gy, which multiple centers deemed too permissive compared to existing protocols and literature. As such, the constraint was changed to $D_{0.5cc} < 40$ Gy.

For phase III, a TPS template was created in which the agreed upon DVH parameters were set as planning constraints. The remaining technical settings within the template (cost functions, beam setup, sequencing parameters) were a selection of the most frequently used settings by the centers in the consortium, weighted by center experience. The template was distributed as a file set which centers were able to import into the TPS for phase III.

All centers were able to successfully create treatment plans using the consensus template. All but three centers deemed the resulting treatment plan clinically acceptable, with three

centers citing that the abandoning of PRV would not be acceptable for current clinical use. Moreover, one of these centers cited an unacceptably high maximum dose within the GTV compared to their current practice. The DVHs (Fig. 3.2) and DVH parameters (Fig. 3.3) showed further harmonization of the treatment plans, with the median (range) GTV $D_{99\%} = 50.5$ Gy (48.2 - 50.9 Gy) for case 1, and 35.6 Gy (33.5 - 36.0 Gy) for case 2. There was also a decreased spread in the median dose ($D_{50\%}$ range 54.8 - 59.5 Gy for case 1, 53.3 - 61.9 Gy for case 2). Although the maximum dose was overall increased, the spread did not become smaller compared to phase II ($D_{1\%}$ range 60.5 - 68.0 Gy for case 1, 61.5 - 78.0 Gy for case 2). For the duodenum $D_{0.5cc}$, the median (range) was 26.1 Gy (23.2 - 30.1 Gy) for case 1, and 34.5 Gy (32.3 - 34.6 Gy) for case 2. A statistical comparison between the DVH parameter variance of phase III showed a significantly reduced variation compared to phase I ($p < 0.05$) in all GTV parameters for case 1, and all GTV parameters except $D_{1\%}$ and OAR $D_{0.5cc}$ for case 2. The detailed results of the statistical analysis are given in supplementary Table S1. The range in estimated MU count needed to deliver the treatments was also modestly decreased compared to phase II, with the median (range) MUs being 2398 (1979 - 2973) for case 1 and 3543 (3049 - 4551) for case 2. Finally, there was also harmonization observed in the isodose volumes (not confined to dose within a specific tissue or structure) of the treatment plans (see supplementary Fig. S3).

The final consensus protocol is summarized in Table 3.2. A detailed description of the technical parameters of the final consensus template is given in supplementary Table S2. The files to import the template directly in Monaco are available online through the following public download link: <https://surfdrive.surf.nl/files/index.php/s/XxArrdkTk2sW4ru>.

3.4. Discussion

Current clinical practices for MR-guided pancreas SBRT vary considerably between centers around the world. A consensus planning protocol has been developed for treating pancreatic tumors with MR-guided SBRT, reflecting a worldwide collaboration between thirteen 1.5 T MR-Linac users. Apart from the consensus protocol presented here, the discussions were considered especially fruitful across the whole consortium. The collective sharing, comparing, and benchmarking of treatment plans, protocols, and clinical experience was an exceptionally educational process for improving plan quality. With this work, we share these insights with the MRgRT community and provide a road map or guide for centers that are starting out with this complex treatment modality. As we found after phase II that treatments can largely

Table 3.2.: Consensus protocol for five-fraction MR-guided SBRT for pancreas. Target objectives are subject to concession if OAR constraints cannot be met. There is no specific maximum dose limit to the GTV.

Parameter	Value
Prescription dose (#fractions × dose)	5×10 Gy
GTV	$V_{100\%} > 99\%$
PTV	$V_{95\%} > 95\%$
Duodenum, colon, stomach	$D_{0.5cc} < 35$ Gy
Small bowel	$D_{0.5cc} < 40$ Gy
Biliary duct	$D_{0.1cc} < 50$ Gy
Large vessels (aorta, inferior vena cava)	$D_{0.1cc} < 53$ Gy
Superior mesenteric artery	$D_{0.1cc} < 53$ Gy
Celiac trunk	$D_{0.1cc} < 53$ Gy
Kidneys	$D_{\text{mean}} < 10$ Gy; $D_{67\%} < 16.8$ Gy
Spinal cord	$D_{0.1cc} < 28$ Gy
GTV-PTV margin	2 mm with active motion management
Number of beams	9 - 14
Number of segments	As low as reasonably possible (lower limit = 45)
Passive motion management	Abdominal compression
Arms position	Arms down

be harmonized when using the same set of DVH constraints, this consensus protocol can easily be adopted by any MR-Linac center. We have made the consensus template available for download. Centers may choose to adopt the complete template or parts thereof, or simply investigate outside clinical practice for educational purposes.

There were two main recurring points of debate, i.e. the attempt to maximize the dose to the GTV without considering any constraints here and the omission of PRVs. On these points, the final consensus was less outspoken than for the other aspects of the protocol, with three centers citing these omissions the reason they would not consider the resulting treatment plans clinically acceptable. It should be noted that two of these centers added the nuance that active motion management should at least be implemented before they would consider planning without PRVs. Indeed, recent efforts with the newly developed gating

system for the 1.5 T MR-Linac have shown promising results in terms of congruence of the delivered and planned dose within the upper abdomen,³⁷ which might change the future perspective on the general need for PRVs.

Furthermore, constraints like $D_{0.1cc} < 120\%$ for the PTV were part of conventional protocols to both force a homogeneous dose distribution and limit high dose to healthy tissue within the PTV. However, MR-guided radiotherapy has led to substantially smaller safety margins, decreasing the amount of healthy tissue within the high dose region. In combination with online motion management, and again anticipating active motion management, multiple centers within the consortium abandoned these constraints (the same argument can be made for the abandonment of PRVs). Moreover, the planning exercises in this study showed that an unbounded maximum dose can increase the mean tumor dose in cases where complete target coverage cannot be achieved. This might have a radiobiological advantage. On the other hand, increasing the maximum dose might lead to more MUs needed for the treatment plan. This was reflected in the relatively large range of MUs for case 2 after phase III (3049 - 4551), probably due to the large spread of GTV $D_{1\%}$ for this case (61.5 - 78.0 Gy), which was not reduced compared to phase II.

In this study, target and OAR delineations were already provided. Although all centers noted that their delineation protocol is based on the SABR guidelines,⁷⁰ it is known that delineations of pancreatic tumors and surrounding OARs is subject to nontrivial interobserver variation.^{71,72} This might contribute to further treatment plan differentiation in clinical practice. However, for the scope of this study, delineations were kept the same to make differences in planning strategy more clearer between centers. This allowed us to come to a consensus in pure terms of treatment planning protocol only. Further harmonization of treatment should be focused on reducing interobserver variation, by creating consensus protocols for e.g. delineation guidelines and online imaging for treatment adaptation. The iterative plan - evaluation framework from this study could be very well be applied for these purposes as well.

The comparison between MUs in phases II and III lead to the valuable information that even if two plans are dosimetrically very similar, the estimated delivery time can still be very different. In the extreme case of our results (the case 1 MU range of 1979 - 2973), a treatment plan from one center could take more than twice as long to deliver in another center (assuming the same dose rate), which the latter center might find unacceptably long. Sequencing parameters which influence the number of MUs for a plan are often not exhaustively evaluated when centers design their treatment protocol, but we found that there is substantial room for optimization without loss of plan quality. Because these settings

are embedded in the TPS template, phase III ensured harmonized plan sequencing and therefore the resulting MU range was smaller than in phase II. We should emphasize that with phase III, the primary goal regarding delivery time was once again harmonization, and not necessarily achieving the *shortest* delivery time possible. This study only involved two example cases with different levels of dosimetric complexity, which is still the dominant factor in the amount of MUs. We therefore cannot guarantee that using the consensus template will lead to generalized optimal treatment times when adopted into clinical practice, but it will at least mitigate inter-user variability in radiation delivery time. The robustness of the template in an online setting can be evaluated in subsequent studies as the reference plan only serves as a starting point for daily plan adaptation.

The OAR constraints in the final consensus protocol were based on collective experience, and the lack of trial-based evidence for clinical safety might be an objection against adoption of these constraints. However, there is a growing body of literature on clinical outcomes after MR-guided SBRT for pancreas. The recent SMART trial used the same 5x10 Gy dose prescription as our protocol, with very similar, albeit slightly more conservative constraints for the GI organs (duodenum, small bowel, stomach, and colon $D_{0.5cc} < 33$ Gy) and reported no acute grade ≥ 3 toxicities that the authors deemed definitely related to treatment.¹⁷ Moreover, the constraints in our protocol are below those identified in two dosimetric feasibility studies for dose escalated pancreas SBRT.^{65,73} We therefore consider these OAR constraints to be safe for adoption into clinical practice. The consensus protocol is subject to future refinement as the number of patients being treated on the 1.5 T MR-Linac increases globally and long-term outcomes data become available. Since most centers within this consortium are part of the prospective Multi-OutcoMe EvaluatioN of radiation Therapy Using the MR-linac (MOMENTUM) study (NCT04075305),⁷⁴ future clinical outcomes from a large cohort can be easily collected from centers that decide to adopt this protocol.

3.5. Conclusion

A worldwide consortium of thirteen centers found a wide variation in treatment planning protocols for pancreatic tumors with MR-guided SBRT on a 1.5 T MR-Linac. After multiple rounds of internal discussions where protocols and treatment plans were compared, the consortium has developed a collective consensus protocol for MR-guided pancreas SBRT. Treatments can already be largely harmonized when the same basic set of DVH constraints and objectives is used. Further harmonization of both treatment planning and delivery is

possible with the consensus TPS template, which is now available for download for all 1.5 T MR-Linac users.

Supplementary materials



Part II.

Treatment delivery



CHAPTER 4

Intrafraction pancreatic tumor motion patterns during ungated magnetic resonance guided radiotherapy with an abdominal corset

G Grimbergen
H Eijkelenkamp
HD Heerkens
BW Raaymakers
MPW Intven
GJ Meijer

Physics and Imaging in Radiation Oncology (2022), 21:1-5

ABSTRACT

Background and purpose – Stereotactic body radiotherapy (SBRT) has been shown to be a promising therapy for unresectable pancreatic tumors. However, intrafraction motion, caused by respiratory motion and organ drift, is one of the main concerns for efficient dose delivery in ungated upper abdominal radiotherapy. The aim of this study was to analyze the intrafraction gross tumor volume (GTV) motion in a clinical cohort.

Materials and methods – We included 13 patients that underwent online adaptive magnetic resonance (MR)-guided SBRT for malignancies in the pancreatic region (5×8 Gy). An abdominal corset was fitted in order to reduce the abdominal respiratory motion. Coronal and sagittal cine MRIs of the tumor region were made at 2 Hz during the entire beam-on time of each fraction. We used deformable image registration to obtain GTV motion profiles in all three directions, which were subsequently high-pass and low-pass filtered to isolate the motion caused by respiratory motion and baseline drift, respectively.

Results – The mean (SD) respiratory amplitudes were 4.2 (1.9) mm cranio-caudal (CC), 2.3 (1.1) mm ventral-dorsal (AP) and 1.4 (0.6) mm left-right (LR), with low variability within patients. The mean (SD) maximum baseline drifts were 1.2 (1.1) mm CC, 0.5 (0.4) mm AP and 0.5 (0.3) mm LR. The mean (SD) minimum baseline drifts were -0.7 (0.5) mm CC, -0.6 (0.5) mm AP and -0.5 (0.4) mm LR.

Conclusion – Overall tumor motion during treatment was small and interfractionally stable. These findings show that high-precision ungated MR-guided SBRT is feasible with an abdominal corset.

4.1. Introduction

Pancreatic cancer is one of the most aggressive cancer types, with a median overall survival rate of typically around 19 months. For non-metastatic unresectable tumors or isolated local recurrences, prognosis is around 14-15 months.^{75,76} Stereotactic body radiotherapy (SBRT) has been shown to be a promising therapy for these tumor types.^{40,77-79} The main challenge in SBRT in the upper abdomen is avoiding the many radiosensitive gastro-intestinal organs, such as the duodenum, small bowel, colon, stomach or post-resection anastomoses, which often lie in close proximity to the gross tumor volume (GTV). The introduction of magnetic resonance guided radiotherapy (MRgRT) allows for online plan adaptation based on magnetic resonance imaging (MRI) visualized anatomy at each fraction. The superior soft tissue contrast of MRI, together with the capability for replanning at each fraction, enables the delivery of higher biological effective doses in a lower number of fractions.^{41,42} However, intrafraction motion remains of concern for ablative treatments with SBRT. Early studies on respiratory intrafraction motion have found GTV motion to be large with average cranio-caudal motion amplitudes of over 20 mm, and highly variable with standard deviations of over 15 mm.^{27,28} Consequently, research has mainly been focused on gating schemes^{16,80} or development of motion surrogate models.^{81,82} Alternatively, the use of abdominal compression techniques during treatment, e.g. with an abdominal corset, can reduce the respiratory motion in the abdominal area, thereby significantly reducing the residual cranio-caudal motion in the upper abdominal structures.³³

Besides respiratory motion, dosimetric inaccuracies can also be caused by gastro-intestinal (GI) organs slowly drifting away from the planning position during treatment, for example due to bowel peristalsis or muscle relaxation or tensioning. Previous research on abdominal organ drifts during treatment has reported relatively small deviations of 1-4 mm from the baseline.^{83,84} However, this type of motion is often assumed to be non-periodic and linear causing a dose shift and may therefore be more of concern than periodic respiratory motion, which only results in a blurring of the dose.

The aim of this study was to retrospectively analyze and characterize respiration and drift motion patterns of pancreatic tumors in our currently treated patient population, across a clinical cohort of 13 patients that underwent MRgRT.

4.2. Materials & Methods

4.2.1. Patients

Thirteen patients with malignancies in the pancreatic region underwent online adaptive MR-guided SBRT between February 2020 and September 2020. The cohort included seven male and six female patients, with a median age of 64 years (range 40-76 years). Consecutive informed consent was provided for registry in the prospective Multi-OutcoMe Evaluation of radiation Therapy Using the MR-linac (MOMENTUM) study (NCT04075305), which has been approved by the institutional review board (IRB) of the University Medical Center Utrecht.

A summary of the patient and treatment characteristics is given in Table 4.1. Detailed characteristics for the individual patients are given in supplementary Table A.

4.2.2. Image acquisition and treatment protocol

Before treatment, each patient was provided with a polyurethane Neofrakt abdominal corset (Spronken Orthopedie NV, Genk, Belgium).³³ This is a custom fitted corset that was molded to the patient's lumbar spine, directly after their first consult with the attending radiation oncologist. The molding takes around 20 min. Two to three weeks prior to the start of treatment, each patient underwent a planning and simulation session. First, the patient underwent computed tomography (CT) scanning on a Philips Brilliance big bore CT scanner (Philips BV, Best, the Netherlands), during which the corset was applied and fastened with Velcro straps. The tightness of the straps was marked with a pen to ensure reproducibility. Immediately afterwards, the patient was scanned on a 1.5 T Philips Ingenia MRI scanner (Philips BV, Best, the Netherlands). During this session, a 3D T_2 -weighted (T_2w) scan (FOV: 451 × 451 × 220 mm, voxel size: 0.64 × 0.64 × 2.00 mm, TE/TR: 124/1300 ms, FA: 90°) was acquired, as well as gadolinium-enhanced coronal (FOV: 450 × 450 mm, voxel size: 2.01 × 2.01 × 7.00 mm, TE/TR: 1.31/2.62 ms, FA: 50°) and sagittal (FOV: 320 × 320 mm, voxel size: 1.43 × 1.43 × 7.00 mm, TE/TR: 1.43/2.86 ms, FA: 50°) bFFE cine MRs during one minute at 2 Hz.

Treatment was carried out on the Elekta Unity (Elekta AB, Stockholm, Sweden) magnetic resonance linear accelerator (MR-Linac), a 7 MV linear accelerator combined with a 1.5 T wide bore MRI. The SBRT treatment itself consisted of five fractions of 8 Gy, given every other weekday. The protocol for each fraction was as follows. First, the patient was positioned on the MR-Linac table on a custom fitted vacuum cushion, and secured with

Table 4.1.: Patient and treatment characteristics.

	<i>n</i> = 13 (%)
Sex	
Male	7 (54)
Female	6 (46)
Age (years)	
median (IQR)	64 (53 – 69)
range	40 – 76
Tumor volume (cm³)	
GTV	
median (IQR)	26 (15 – 62)
range	13 – 108
PTV	
median (IQR)	49 (34 – 105)
range	25 – 159
Diagnosis	
Pancreatic adenocarcinoma	
Locally advanced	4 (31)
Locally recurrent	4 (31)
Cholangiocarcinoma	
Locally recurrent	4 (31)
Adrenocortical carcinoma	
Locally recurrent	1 (8)
Prior treatment	
Surgery	9
Time prior to SBRT (months)	
median (IQR)	15 (12 – 19)
range	9 – 25

the abdominal corset. Next, a 3D T_2w scan was acquired. The GTV and organs at risk (OAR) were contoured on this scan by the attending radiation oncologist. We employed an isotropic GTV to planning target volume (PTV) margin of 3 mm. During contouring, a position verification (PV) 3D T_2w scan was made, to ensure no large position shifts had occurred. After contouring, a 9–14 beam intensity-modulated radiotherapy (IMRT) plan was generated and the treatment delivery was started after approval by the physician. During the entire beam-on time, interleaved coronal and sagittal (FOV: 426 × 426 mm, voxel size: 1.06 × 1.06 × 7.00 mm, TE/TR: 1.37/2.73 ms, FA: 40°) bFFE Cine MRs were acquired at 2 Hz. The planes were centered on the GTV. Ultimately, once irradiation had been completed, a final 3D T_2w post scan was made to evaluate the 3D anatomy of the patient at the end of the treatment session. An illustration of the treatment workflow is given in Fig. 4.1.

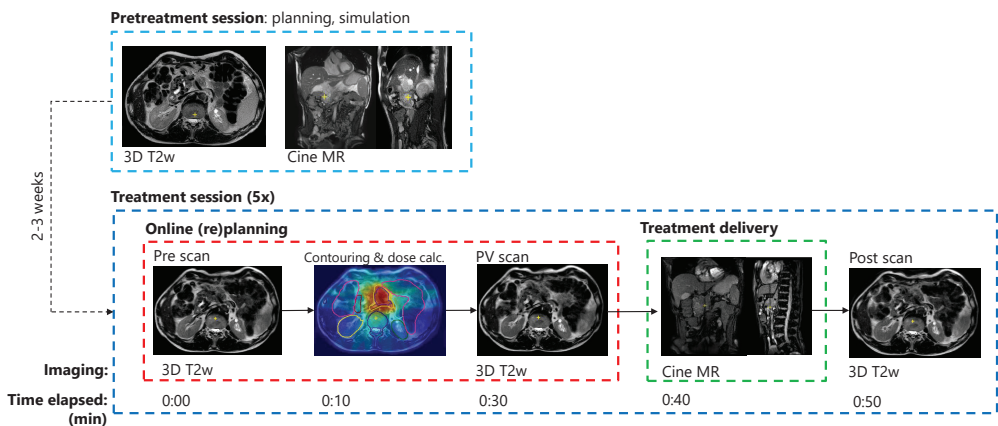


Figure 4.1.: The workflow of the treatment protocol, with the average time elapsed in minutes at each step of the online adaptive workflow.

4.2.3. Motion analysis

The continuous interleaved sagittal and coronal cine MRIs during the entire beam-on time allowed for the extraction of high-temporal resolution 3D motion profiles of the GTV from start to end of treatment.

All computations were performed in Matlab 2019a (Mathworks Inc., Natick, MA, USA). As non-rigid registration algorithm, we employed the GPU implementation of EVOlution.⁸⁵ The dynamics within a set of cine MRIs were deformably registered to the 10th dynamic of that set. The 10th dynamic was chosen to ensure sufficient contrast has been manifested for successful image registration. Then, the GTV contour, as delineated on the pre 3D MRI, was propagated onto the coronal and sagittal planes of the 10th dynamic. In case of the planning cine MRIs, for which no direct delineation of that day was available, the contour of the first fraction was used. The contour was manually translated to match the tumor position in the image, and converted to a binary mask. From there, the deformation vector fields (DVF) from the image registration were used to warp the GTV masks from the 10th dynamic to all other dynamics, creating a tumor delineation that moved along with the anatomy in 2D + time in both the sagittal and coronal plane. We subsequently tracked the displacement of the GTV centroid over time to obtain the motion profiles. The displacement position was normalized to the average position of the first 30 s, which served as the reference starting

position of the GTV during treatment. Cranio-caudal motion profiles were obtained from both the coronal and sagittal cine MRIs, denoted as CC_C and CC_S respectively. Left-right (LR) motion was obtained from the coronal plane and anterior-posterior (AP) motion from the sagittal plane.

Since the motion profiles contain signals from both respiratory and drift motion, both had to be isolated to ensure reliable results. To analyze the respiratory motion, the raw motion profiles were high-pass filtered with an elliptic infinite impulse response (IIR) filter. Visual inspection of the average power spectrum of all motion profiles showed that the respiratory frequency components were between 0.10 and 0.25 Hz (see supplementary material Fig. B). From this, a cutoff frequency of 0.05 Hz was chosen for the high-pass filter, which should be high enough to remove all low-frequency motion due to drift, but low enough to avoid attenuation of the respiratory signal. The drift motion was obtained by low-pass filtering the raw signal with a moving average filter with a sliding window of 50 samples, or 25 seconds. The duration of cine MRIs from the simulation session was deemed too short to reliably extract data on baseline drift, and only respiratory motion was analyzed for these sets.

In all four displacement directions, we calculated the respiratory amplitude M_{resp} as the difference between the maximum and minimum value in the high-pass filtered signal, excluding the top and bottom 5 percentiles to reduce sensitivity to outliers. The baseline drift extrema $M_{\text{drift,min}}$ and $M_{\text{drift,max}}$ are calculated as the minimum and maximum values in the low-pass filtered signal, respectively.

Since motion in the cranio-caudal direction was measured in both the coronal and sagittal plane, we performed Bland-Altman analysis to assess the agreement between the two methods of measurement for cranio-caudal respiration amplitude and minimum and maximum baseline drift.

4.3. Results

4.3.1. Motion analysis

An example of the respiratory and drift motion decoupled from a raw CC_C motion profile is given in Fig. 4.2. The two frequency components were clearly visible in the raw motion signal. The low-pass filtered respiratory motion had a stable equilibrium around the baseline, with a peak-to-peak amplitude equal to the unfiltered signal. The high-pass filtered drift motion lacked any high frequency oscillations and follows the average position of the raw motion profile. These findings indicate a successful filtering strategy.

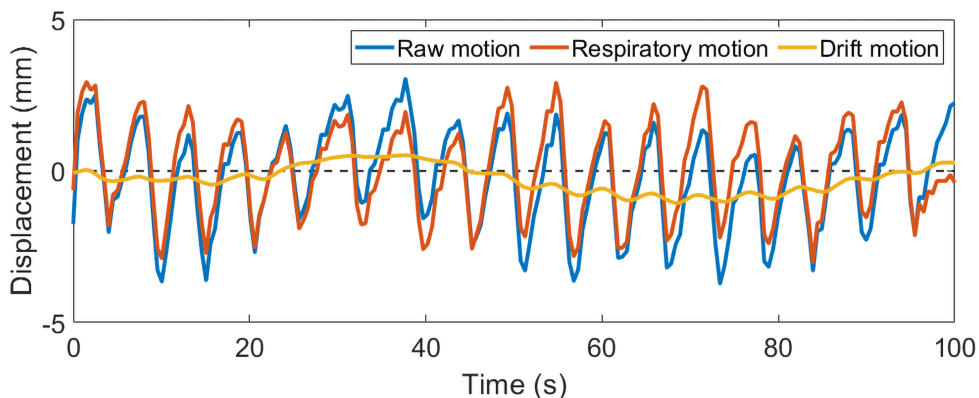


Figure 4.2.: The first 100 seconds of an exemplary CC_C motion signal that has been both high-pass and low-pass filtered to obtain the isolated respiratory and drift motion. Note that the respiratory signal has a stable equilibrium around $y = 0$, while its amplitude remains equal to the raw signal.

Respiratory motion

The mean (SD) respiratory amplitudes over all patients were 4.2 (1.9) mm CC_C , 3.9 (1.7) mm CC_S , 2.3 (1.1) mm AP and 1.4 (0.6) mm LR (see Table 4.2). Overall, there was a good agreement between the CC values extracted from the coronal and sagittal cine MRIs. Bland-Altman analysis on the measurement differences between CC_C and CC_S yielded a 95% CI of -1.68 – 2.29 mm. The mean difference was 0.3 mm, indicating slightly higher amplitude for the coronal cine MRIs (supplementary material Fig. C).

There was a large similarity of the respiration amplitude within individual patients for the different fractions. For patients 01, 04, 06, 09 and 11, we observed that the respiratory amplitude during the planning session was higher than during to the treatment fractions for either the sagittal and/or coronal Cine MRI assessment.

Table 4.2.: Mean and SD of the respiratory amplitudes and minimum and maximum baseline drifts over all patients and fractions.

	M_{resp}	$M_{\text{drift,min}}$	$M_{\text{drift,max}}$
	mean (SD) - mm	mean (SD) - mm	mean (SD) - mm
CC_C	4.2 (1.9)	-0.7 (0.5)	1.2 (1.1)
CC_S	3.9 (1.7)	-0.7 (0.5)	1.2 (1.0)
AP	2.3 (1.1)	-0.6 (0.5)	0.5 (0.4)
LR	1.4 (0.6)	-0.5 (0.4)	0.5 (0.3)

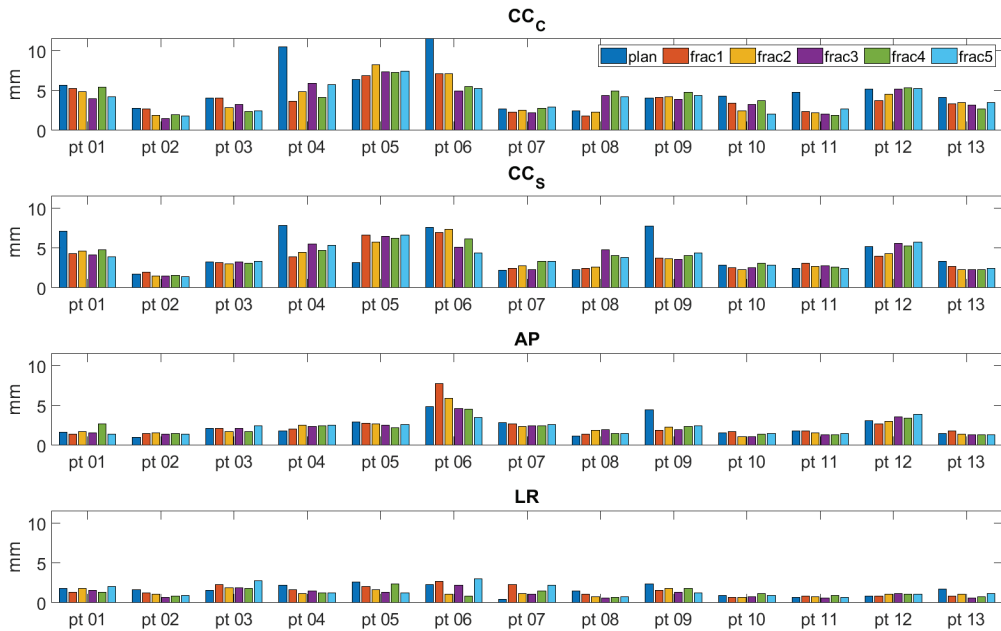


Figure 4.3.: The peak-to-peak respiratory amplitudes, excluding the top and bottom 5th percentiles, for all patients and all fractions.

There was a large similarity of the respiration amplitude within individual patients for the different fractions. For patients 01, 04, 06, 09 and 11, we observed that the respiratory amplitude during the planning session was higher than during to the treatment fractions for either the sagittal and/or coronal cine MRI assessment.

Baseline drift

The mean (SD) minimum baseline drifts over all patients and fractions were -0.7 (0.5) mm CC_C , -0.7 (0.5) mm CC_S , -0.6 (0.5) mm AP and -0.5 (0.4) mm LR . The mean (SD) maximum baseline drifts were 1.2 (1.1) mm CC_C , 1.2 (1.0) mm CC_S , 0.5 (0.4) mm AP and 0.5 (0.3) mm LR . The minimum and maximum baseline drifts for all individual fractions are plotted in Fig. 4.4. The displacements were generally the largest in cranio-caudal direction. There was again a good agreement between CC_C and CC_S for most patients: for $M_{\text{drift},\text{min}}$, the 95% CI of the $CC_C - CC_S$ differences was $-0.61 - 0.54$ mm and for $M_{\text{drift},\text{min}}$, this was $-0.60 - 0.75$ mm. In both cases, there was a negligible bias of -0.03 mm and 0.07 mm, respectively (supplementary material Fig. C).

Overall, the values were smaller than the respiratory amplitudes. The patients with the

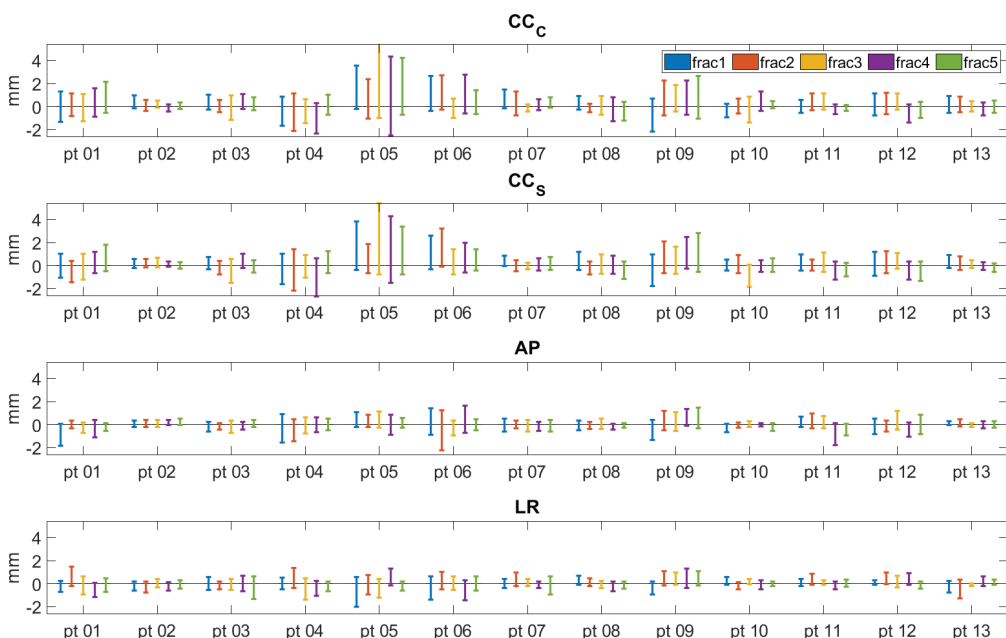


Figure 4.4.: The maximum and minimum baseline drifts for all patients and all fractions. In each bar, the top point indicates the maximum drift value and the bottom point indicates the minimum value.

largest differences between $M_{\text{drift,min}}$ and $M_{\text{drift,max}}$, patients 04, 05, 06 and 09 were characterized by a systematic unidirectional drift. In most of these patients where there was a systematic drift observed, the tumor moved in the cranial direction. For patients with smaller drifts, the absolute values for $M_{\text{drift,min}}$ and $M_{\text{drift,max}}$ were approximately similar and generally within 2 mm.

4.4. Discussion

This study provided an analysis of pancreatic tumor motion during online MR-guided SBRT for patients wearing an abdominal corset. In our cohort, respiratory amplitudes were small and stable within patients. Drift motions were small as well, with no large GTV displacements observed during the treatments. Wearing of the corset was tolerated well, and none of the patients reported pain or other discomfort that urged loosening the corset.

Based on the van Herk margin recipe,^{29,30} the observed intrafraction motion would require margins of 1.95 mm *CC*, 1.10 mm *AP*, and 0.60 mm *LR* to obtain adequate dose coverage (supplementary material D). This is well below the 3 mm isotropic PTV margins used in this

study. Moreover, these margins were less than 1.0 mm larger compared to the margins in a complete static configuration. This substantiates our hypothesis that additional motion mitigation techniques (e.g. gating or tracking) are of limited value when using an abdominal corset.

The respiratory displacements observed in this study are substantially smaller than early literature, with mean cranio-caudal amplitudes of under 5 mm.^{27,28} We believe this can mainly be attributed to the use of the abdominal corset. Remarkably, the original study on this corset from Heerkens et al. also found higher motion amplitudes than in this study, even with the corset employed (6.0 mm CC_C , 5.6 mm CC_S , 2.6 mm AP and 2.2 mm LR).³³ It should be noted that Heerkens et al. analyzed the amplitudes of the raw motion profiles without decoupling respiration and drift, resulting in larger values. Secondly, the authors excluded the top and bottom 2.5% of the values, while our study excluded the top and bottom 5%. Thirdly, both our study and Heerkens et al. included a small number of patients: 13 and 10 patients respectively. The differences in results could be an effect due to these small cohort sizes. Finally, Heerkens et al. analyzed mainly locally advanced tumors. Our patient cohort included mainly recurrent carcinomas, often restricted by fibrotic tissue, which can further inhibit tumor mobility. However, due to our small population size and imbalance of recurrent and advanced carcinomas within our cohort, we can provide no conclusive evidence for a connection between tumor mobility versus site and stage. A larger and more balanced patient population might lead to more insights into this differentiation. One of our main findings was that within patients, there was little interfractional variability of respiratory amplitudes. Given that each patient appears to possess a characteristic amplitude, this could lead to an expansion of the online adaptive workflow. As an example, PTV margins can be tailored to the respiration amplitude of the patient.

For patients 01, 04, 06, 09 and 11, we observed that the respiratory amplitude during the planning session was higher than during the treatment fractions for either the sagittal and/or coronal cine MRI assessment. Additionally, we also noted larger differences between the values for CC_C and CC_S in these cases. These discrepancies might have several causes, but the most likely explanation is that the corset could have been fastened less tightly during the planning sessions than during treatment. The setting of the straps with which the corset was fastened was marked during the CT planning session. However, it might have occurred that during the subsequent MRI session immediately afterwards, the corset was not fastened all the way to the marks. While corset tightness is not as clinically relevant during the planning session as during treatment, it would have been a proper procedure to ensure equal compression during all sessions. Nonetheless, it further supports our theory that a properly

tightened corset, while also mitigating motion in general, would lead to less variability in motion amplitudes within patients.

The more prominent differences between the CC_C and CC_S amplitude assessments could well be associated to possible misalignments of sagittal and coronal planes on the planning cine MRIs, as these planes were aligned by the radiographers in the absence of the GTV definition. Depending on GTV shape, through plane motion in the 2D cine MRIs could also have led to an over- or underestimation of CC_C and CC_S amplitudes.

Motion assessments due to slow organ drift revealed only small extrema with respect to the baseline. Moreover, drift did not occur in a linear fashion, where the average GTV position would slowly deviate away from the baseline, but rather inhibited its own periodic motion. Any large deviations often resolved back towards initial position, and in eight out of thirteen patients the values in Fig. 4.4 show approximately equally large drifts in all three directions. This corresponds to the findings of Cusumano et al.,⁸³ which reported no large drifts in the pancreas subgroup of their multi-site cohort.

The use of orthogonal 2D planes poses some limitations. First, the planes were centered on the GTV, and as a result, most of the surrounding OARs fell out of plane and could not reliably be tracked. The intrafraction motion of the many radiosensitive OARs is valuable information for determining whether the treatment was delivered safely. Upon visual basis it was determined that in close proximity to the GTV, the surrounding tissue moved quasi-rigidly along with the GTV. Volumetric imaging would have provided the necessary information to track the OARs as well, but this is much slower than 2D cine MRI. Second, we defined the GTV motion as the displacement of its center of mass over time, not accounting for deformations internally or at the boundary. However, visual inspection of the cine MRIs again yielded that the tumor itself did not appear to deform significantly from physiological motion. Therefore, we believe that the position of its center of mass was adequate to provide an accurate motion profile.

In conclusion, ungated, high-precision MR-guided SBRT for pancreatic tumors is feasible for patients that wear an abdominal corset, potentially allowing dose escalation strategies. Motion mitigation using corsets could well be a simple and attractive alternative for more complex gating and tracking approaches when treating abdominal lesions.

Supplementary materials





CHAPTER 5

Dosimetric impact of intrafraction motion under abdominal compression during MR-guided SBRT for (peri-) pancreatic tumors

G Grimbergen
H Eijkelenkamp
HD Heerkens
BW Raaymakers
MPW Intven
GJ Meijer

Physics in Medicine & Biology (2022), **67**(18):185016

ABSTRACT

Background and purpose – Intrafraction motion is a major concern for the safety and effectiveness of high dose stereotactic body radiotherapy (SBRT) in the upper abdomen. In this study, the impact of the intrafraction motion on the delivered dose was assessed in a patient group that underwent MR-guided radiotherapy for upper abdominal malignancies with an abdominal corset.

Materials and methods – Fast online 2D cine MRI was used to extract tumor motion during beam-on time. These tumor motion profiles were combined with linac log files to reconstruct the delivered dose in 89 fractions of MR-guided SBRT in twenty patients. Aside the measured tumor motion, motion profiles were also simulated for a wide range of respiratory amplitudes and drifts, and their subsequent dosimetric impact was calculated in every fraction.

Results – The average (SD) $D_{99\%}$ of the gross tumor volume (GTV), relative to the planned $D_{99\%}$, was 0.98 (0.03). The average (SD) relative $D_{0.5cc}$ of the duodenum, small bowel and stomach was 0.99 (0.03), 1.00 (0.03), and 0.97 (0.05), respectively. No correlation of respiratory amplitude with dosimetric impact was observed. Fractions with larger baseline drifts generally led to a larger uncertainty of dosimetric impact on the GTV and organs at risk (OAR). The simulations yielded that the delivered dose is highly dependent on the direction of on baseline drift. Especially in anatomies where the OARs are closely abutting the GTV, even modest *LR* or *AP* drifts can lead to substantial deviations from the planned dose.

Conclusion – The vast majority of the fractions was only modestly impacted by intrafraction motion, increasing our confidence that MR-guided SBRT with abdominal compression can be safely executed for patients with abdominal tumors, without the use of gating or tracking strategies.

5.1. Introduction

Stereotactic body radiotherapy (SBRT) has been shown to be an effective therapy for unresectable pancreatic carcinomas,^{15,40,63,77,78} potentially increasing life expectancy in a patient population with a generally poor prognosis. Mr-guided radiotherapy (MRgRT) enables online visualization of anatomy changes for a tailored treatment to the anatomy of the day, and has made high dose radiotherapy for upper abdominal malignancies feasible.⁴² An important concern with MR-guided online adaptive SBRT in the upper abdomen is intrafraction motion. This is not only because of the large variability and unpredictability of tumor motion in the upper abdomen,^{27,28} but also because beam-on times are generally prolonged on MR-guided systems due to their limited linac dose rate compared to conventional systems. Active motion management methods, like using internal targets for gating^{86,87} or tracking,^{88,89} or gating on deep inspiration breath holds,⁹⁰ can significantly improve target coverage. The downside of methods using internal targets is the invasive placement of internal markers, and gating generally prolongs treatment.^{80,91} Moreover, these methods might not be readily available on all systems. Passive motion mitigation through abdominal compression has shown to be a simpler, more accessible alternative for both pancreatic tumors^{33,61,66,92-95} as well as liver tumors.⁹⁶⁻⁹⁹ For pancreatic tumors, abdominal compression with an abdominal corset can significantly reduce cranio-caudal tumor motion during treatment to around 5 mm.^{33,92-95} This results in respiratory intrafraction tumor motion that is small and stable between treatment fractions.⁶¹ However, because of the close proximity of upper abdominal tumors to abutting organs at risk (OAR), the exact impact of the residual intrafraction motion on the delivered dose remains of concern.

In this study, the impact of the residual intrafraction motion, after abdominal compression, on the delivered dose was assessed in a group of patients that underwent MRgRT for upper abdominal malignancies. Aside from analyzing in-vivo motion, a wide range of motion scenarios was simulated in every fraction in order to systematically assess the impact of respiratory amplitude and drift on tumor coverage and OAR dose.

5.2. Materials & Methods

5.2.1. Patients overview and treatment protocol

Twenty patients were included that underwent online adaptive MR-guided SBRT for upper abdominal malignancies between January 2021 and September 2021. Consecutive informed consent was provided for registry in the prospective Multi-OutcoMe Evaluation of radiation Therapy Using the MR-linac (MOMENTUM) study (NCT04075305). A summary of the patient characteristics is given in Table 5.1.

All patients were treated with a hypofractionated stereotactic regimen (5x8 Gy) on a Elekta Unity (Elekta AB, Stockholm, Sweden) magnetic resonance linear accelerator (MR-Linac), a 7 MV linear accelerator combined with a 1.5 T wide bore MRI scanner. The treatment protocol was as follows: for each fraction, patients were positioned on a custom fitted vacuum cushion, and secured with a custom fitted Neofrakt abdominal corset (Spronken Orthopedie NV, Genk, Belgium).³³ This corset is fastened with Velcro straps. For the first fraction, the tightness of the straps was marked with a pen to ensure reproducibility in abdominal compression for the remaining fractions. The treatment was conducted in an online adaptive fashion,¹⁴ where every treatment session began with a 3D T_2 -weighted (T_2w) pre MRI (FOV: $451 \times 451 \times 220$ mm, voxel size: $0.64 \times 0.64 \times 2.00$ mm, TE/TR: 124/1300 ms, FA: 90°) to visualize the anatomy. The gross tumor volume and OAR contours were adapted to this scan by the attending radiation oncologist. An isotropic GTV to planning target volume (PTV) margin of 3 mm was used. Our institutional planning objectives and constraints are shown in supplementary Table A. After contouring, a 9-14 beam step-and-shoot intensity modulated radiotherapy (IMRT) plan was generated, and the treatment delivery was started after approval by the physician. During treatment delivery, interleaved coronal and sagittal T_2/T_1 -weighted bFFE cine MRIs were acquired, centered on the GTV. Both slices were acquired at a frequency of 2.8 Hz for the entire beam-on time. A detailed overview of the cine MRI sequence parameters is given in supplementary Table B.

5.2.2. Intrafraction motion measurement

Deformable image registration (DIR) with EVOlution⁸⁵ ($\alpha = 0.35$, patch size = 5×5) was used to warp every dynamic of the cine MRI set to a reference dynamic. The resulting 2D deformation vector fields were used to warp the GTV annotation to the dynamics, resulting in a contour that moved along with the anatomy in 2D + time in both the sagittal and coronal plane. The displacement of its center of mass in the CC , LR (respectively the y and x components of the contour centroid in the coronal plane), and AP (the x component

Table 5.1.: Patient characteristics.

	<i>n</i> = 20 (%)
Sex	
Male	11 (55)
Female	9 (45)
Age (years)	
median (IQR)	71 (63 – 75)
range	49 – 84
Tumor volume (cm³)	
GTV	
median (IQR)	46 (12 – 77)
range	3 – 157
PTV	
median (IQR)	79 (24 – 115)
range	8 – 231
Tumor location	
Pancreas	15 (75)
Peripancreatic	5 (25)
Tumor type	
Pancreatic primary tumor	4 (15)
Pancreatic isolated local recurrence	6 (30)
Non-pancreatic isolated recurrence	5 (25)
Non-pancreatic oligometastasis	4 (20)
Unknown	1 (5)

in the sagittal plane) direction was tracked over time, resulting in motion profiles of the tumor centroid with a high temporal resolution of 2.8 Hz (supplementary video 1). These motion profiles were used for the dose accumulation described in the following section. In order to test the validity of the estimated tumor motion, an additional study was conducted to compare the motion profiles from EVOlution to the motion profiles extracted with optical flow¹⁰⁰ and Elastix,¹⁰¹ two commonly used methods for DIR. A high degree of agreement between EVOlution, optical flow and Elastix was found, with the mean differences in center of mass position under one millimeter. Details and results of this study can be found in supplementary data C.

The intrafraction motion of a fraction was characterized by the respiratory amplitude and maximum baseline drift. These were quantified by applying a high-pass and low-pass filter to isolate the motion caused by respiration and baseline drift, respectively. The high-pass filter was an elliptic infinite impulse response (IIR) filter with a cutoff frequency of 0.05 Hz, and the low-pass filter was a moving average filter with a sliding window of 25 seconds. The respiratory amplitude was calculated as the difference between the 5th and 95th percentile of the respiratory motion profile, and the maximum baseline drift as the largest signed value in the drift motion profile. Finally, the magnitude of the respiratory amplitude and drift was calculated as the respective vector length (2-norm) over the individual values for *CC*, *AP*, and *LR*, that is: $\|\text{resp}\|_2 = \sqrt{\text{resp}_{CC}^2 + \text{resp}_{AP}^2 + \text{resp}_{LR}^2}$, and $\|\text{drift}\|_2 = \sqrt{\text{drift}_{CC}^2 + \text{drift}_{AP}^2 + \text{drift}_{LR}^2}$.

5.2.3. Delivered dose reconstruction

The reconstruction of the delivered dose was based on Kontaxis et al.¹⁰² For each fraction, the corresponding log file was saved from the machine. These log files include the current state of the linac, e.g. gantry angle, multi-leaf collimator (MLC) positions, and beam energy, logged at an interval of 40 ms. Each log file was split into partial log files of 360 ms, containing a single linac state. The splits were made on the absolute acquisition times of the cine MRI dynamics. Then, each partial log file was combined with a pseudo-CT volume, generated from a bulk density assignment of the pre MRI, to calculate a partial dose plan with GPUMCD.¹⁰³ All dose calculations were run on a dedicated workstation equipped with an NVIDIA GeForce Titan X GPU. An isocenter shift was applied to each partial dose plan based on the displacement measured in the cine MRI dynamic that corresponds to the same time point as the partial dose plan. In other words, a displacement was only applied to the part of the treatment that was delivered at the same time as when the displacement occurred in the body. Finally, all translated partial dose plans were summed to obtain the delivered dose plan.

The method of dose reconstruction is illustrated in Fig. 5.1.

5.2.4. Motion simulation

Aside from the motion as measured in the imaging data, we simulated intrafraction motion profiles with a wide range of motion amplitudes and drift magnitudes. The rationale for this exercise is that by doing so, we could break down the dosimetric outcome for each

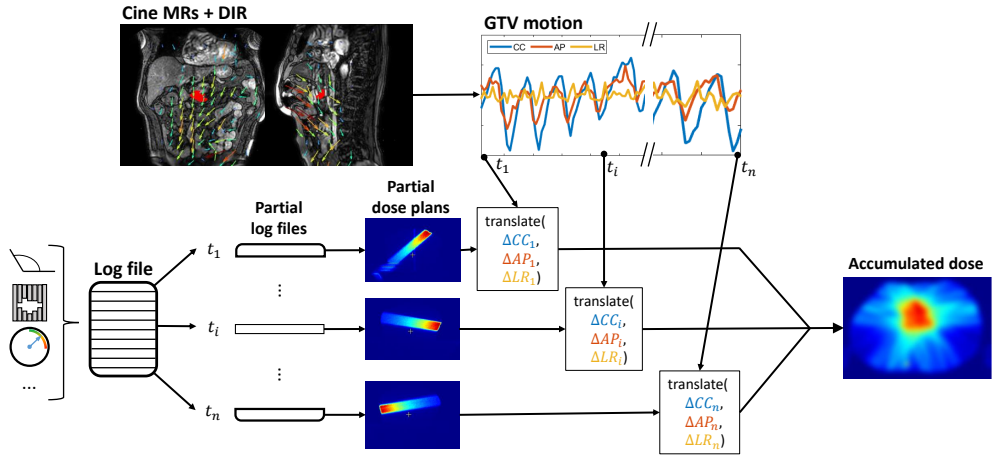


Figure 5.1.: The workflow of the dose reconstruction method. The coronal and sagittal cine MRIs, along with their respective GTV contour projections (red), are deformably registered along time. This results in a 3D GTV motion profile. The linac machine log file is split into partial log files based on the cine MRI acquisition timestamps, and each partial log file is reconstructed into a partial dose plan. Every dose plan is then translated according to the 3D displacement measured at its corresponding time point in the motion profile. The translated dose plans are summed to obtain the accumulated dose.

clinical motion profile to the individual origins. And reversely, we could assess the pattern of the impact of the periodic respiratory motion separately from the motion drift in anterior, posterior, cranial, caudal, left and right directions. To mathematically model intrafraction motion, we adopted a commonly used equation, which assumes respiratory motion follows an asymmetric cosine pattern in 1D and was first coined by Lujan et al. (1999):¹⁰⁴

$$z(t) = z_0 - r \cos^{2n}\left(\frac{\pi t}{\tau}\right) \quad (5.1)$$

with z_0 the position at exhale, r the respiratory peak-to-peak amplitude, τ the respiratory period and n a parameter to set the asymmetry of the motion profile: a larger value for n leads to a longer time spend in exhale position and steeper motion profiles during a respiratory cycle. The starting phase ϕ is excluded in Eq. (5.1). Visually, we determined that $\tau = 5$ s and $n = 3$ best fit the general shape of the motion profiles from our measured data. Furthermore, we set z_0 to the average position of the first 30 seconds, similar to how the mid-ventilation position was defined in the measured motion profiles. Equation (5.1) was extended from 1D to the three principal directions of motion: cranio-caudal (CC), anterior-posterior (AP) and left-right (LR). An additional component was added to Eq. (5.1) to simulate a linear drift over the course of the motion profile, with total magnitude d . The value of r was set as the

respiratory amplitude in the CC direction, and the respiratory amplitudes in the AP and LR directions were set to $r/2$. Because of the relation between r and z_0 , that essentially means that the LR and AP motion profiles are half that of the CC motion, outside of the drift term.

Overall, the model for the 3D motion vector $\mathbf{z}(t) = [z_{CC}(t) \ z_{AP}(t) \ z_{LR}(t)]^T$ was described with the following equations:

$$z_{CC}(t) = z_0 - r \cos^6\left(\frac{\pi t}{5}\right) + d \frac{t}{T} \quad (5.2)$$

$$z_{AP}(t) = \frac{1}{2} \left(z_0 - r \cos^6\left(\frac{\pi t}{5}\right) \right) + d \frac{t}{T} \quad (5.3)$$

$$z_{LR}(t) = \frac{1}{2} \left(z_0 - r \cos^6\left(\frac{\pi t}{5}\right) \right) + d \frac{t}{T} \quad (5.4)$$

where T represents the total duration of the simulation motion, which was set to the duration of the measured motion profile of the fraction in question. Equations (5.2) to (5.4) were sampled at the frequency of the measured motion (2.8 Hz). In each simulation, drift was implemented in one direction only: if d was set to a nonzero value in the one direction, d was set to zero in the other directions. The model parameters r and d were set to $r \in \{0, 5, \dots, 20\}$ mm and $d \in \{-5, 0, 5\}$ mm. Negative values indicate drift in the caudal/anterior/right direction, and positive values indicate drift in the cranial/posterior/left direction. The instance $(r, d) = (0, 0)$ was excluded, since this is equal to the planned dose. In sum, this yielded 34 different motion simulations. For every fraction, the delivered dose was reconstructed for all 34 simulated motion patterns, in the same manner as the dose was reconstructed for the measured motion of that fraction (as described in Section 5.2.3).

5.2.5. Evaluation

The impact of the measured and simulated intrafraction motion was dosimetrically evaluated by comparing the planned to the delivered dose based on key dose-volume histogram (DVH) parameters in the GTV and multiple OARs. The OARs of interest were the duodenum, stomach and small bowel. For the GTV, we evaluated ratios of the $D_{99\%}$, i.e. the minimum dose to 99% of the volume. For the OARs, we evaluated the ratios of the $D_{0.5cc}$, i.e. the minimum dose in 0.5 cm³ of the volume. The ratios were calculated as the delivered dose divided by the planned dose. For example: a fraction with a relative $D_{99\%} < 1$ means the delivered $D_{99\%}$ of the GTV was lower than the planned $D_{99\%}$. Only OARs were included for dose evaluation if they were within a 2.5 cm isotropic margin of the GTV, because the dose level outside this margin was too low to be dosimetrically relevant.

5.3. Results

The patient cohort of this study consisted of eleven male and nine female patients, with a median age of 71 years (range 49 — 76 years). All twenty patients received full treatment of five fractions. In eleven fractions, the linac log files were written as multiple separate files due to treatment interruptions. Because linac data was missing in between these files, these fractions were disregarded from this study, resulting in a total of 89 evaluable fractions. Average beam-on time was 11.3 minutes, and the log file of each fraction was split into an average of 1808 linac states. The dose calculations to compute partial dose plans out of the linac states took 8.4 hours per fraction on average. Application of the isocenter shifts, obtained from a motion profile, to these partial dose plans took 6 minutes on average. A full simulation run for the artificial motion data, in which 34 motion profiles were processed, took 3.4 hours per fraction.

Delivered dose to the GTV was evaluated in all 89 fractions. The dose to the duodenum was evaluated in 38 fractions, the dose to the small bowel in 80 fractions, and the dose to the stomach in 58 fractions.

5.3.1. Impact of measured motion

The average (SD) relative $D_{99\%}$ of the GTV was 0.98 (0.03) (Fig. 5.2). In more than 85% of the fractions (77/89), the delivered $D_{99\%}$ of the GTV was more than 95% of the planned $D_{99\%}$. For only two fractions, the delivered $D_{99\%}$ of the GTV was lower than 90% of the planned $D_{99\%}$. Subanalysis revealed that the dose distributions for some patients were more prone to deterioration with the respect to planned target coverage than other, see supplementary Figure D.

The average (SD) relative $D_{0.5cc}$ of the duodenum, small bowel, and stomach was 0.99 (0.03), 1.00 (0.03), and 0.97 (0.05), respectively. All hot spots of the delivered dose to the OARs remained below 110% of the planned $D_{0.5cc}$.

Overall, it was observed that fractions with larger respiratory amplitudes generally also inhibit larger drifts. For these fractions, the variability of dosimetric impact on both the GTV and OARs was larger than in fractions where smaller motion had been measured. This can be seen in Fig. 5.2, as the relative DVH parameter values fan out with larger respiratory amplitude and drift, while still centered around 1.00.

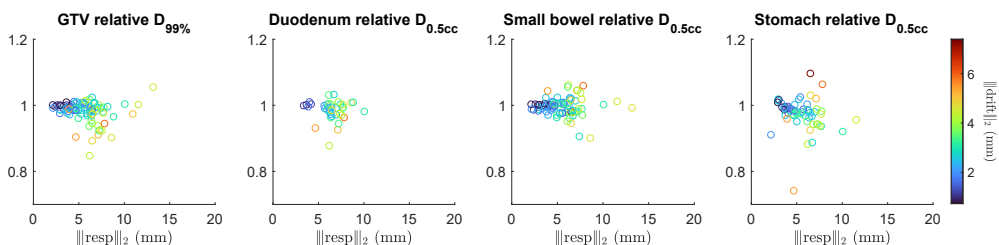


Figure 5.2.: The relative DVH parameters in the GTV and OARs of the measured intrafraction motion. Each point represents a fraction, accumulated with the motion measured during that fraction, and characterized by the magnitudes of the respiratory amplitude(x-axis value) and drift of that fraction (point color).

5.3.2. Impact of simulated motion

The GTV $D_{99\%}$ was very robust to respiratory amplitudes up to 10 mm (Fig. 5.3). For drifts, asymmetric patterns were observed for the different directions. Drifts in the anterior and right direction induced a decreased tumor coverage, while drifts in the cranial, caudal, posterior and left direction hardly impacted delivered dose.

For the OARs, the dose decline as a function of respiratory amplitude increased was less steep than for the GTV. On average, each OAR was only influenced by a drift in a single direction. This was *LR* drift for the duodenum, *AP* drift for the small bowel and *CC* drift for the stomach. The stomach had a much more pronounced relation to drift, albeit with larger uncertainties. With a respiratory amplitude of under 10 mm, a caudal drift of 5 mm led to the delivered $D_{0.5cc}$ of the stomach to be over 110% of the planned $D_{0.5cc}$ on average. Vice versa, a cranial drift of 5 mm caused the delivered $D_{0.5cc}$ to drop to 90% of the planned $D_{0.5cc}$. The 5 mm *LR* drifts in the duodenum and *AP* drifts in the small bowel only caused deviations of no more than 5% above or below the planned $D_{0.5cc}$.

5.4. Discussion

We have calculated the delivered dose for upper abdominal tumors based on the intrafraction motion. In our workflow, the coupling of cine MR-derived motion data to log file-derived treatment delivery data allows for high frequency, time-resolved dose accumulation that includes all motion measured from beam-on to beam-off.

Typically small differences were observed between the planned $D_{99\%}$ and the actually delivered $D_{99\%}$ for the GTV. Interestingly, no correlation was observed between the respiratory amplitude of the measured intrafraction motion, and the impact on both the delivered

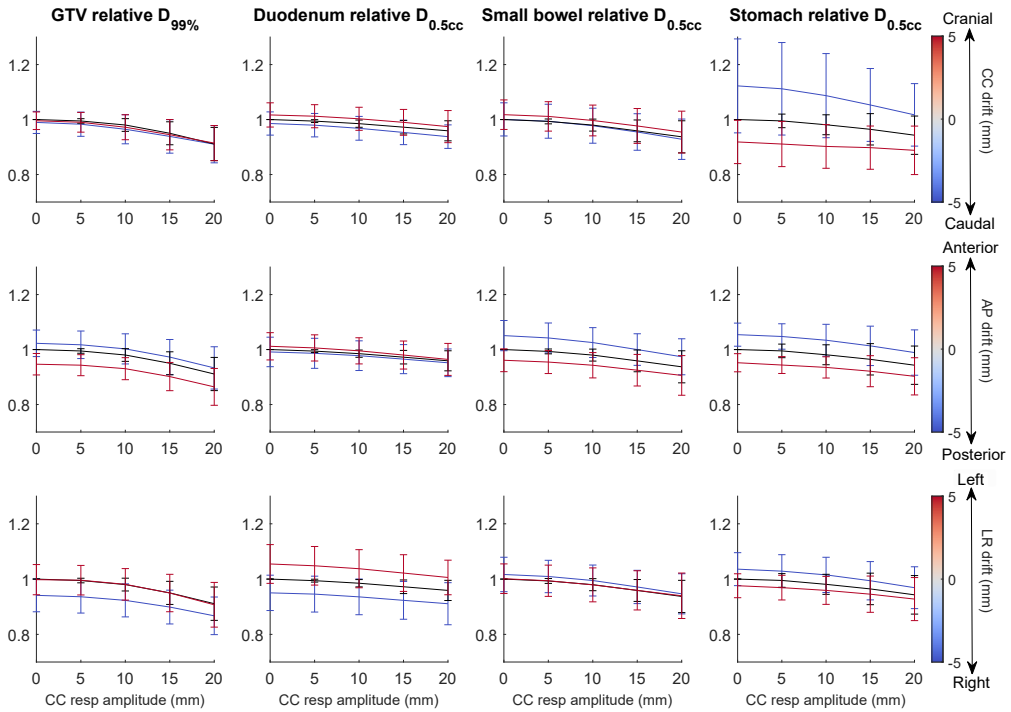


Figure 5.3: The relative DVH parameters in the GTV and OARs, averaged over all fractions, of the simulated intrafraction motion, as a function of respiratory amplitude and drift. The value of the points on the line plot is the average DVH parameter, and the error bars extend one standard deviation above and below the average. Top row: simulations with *CC* drift. Middle row: simulations with *AP* drift. Bottom row: simulations with *LR* drift. The simulations with zero drift are plotted as a black line to aid visualization.

GTV $D_{99\%}$ and OARs $D_{0.5cc}$. This finding was replicated in the simulations: on average, no substantial deviations from the planned dose were observed for respiratory amplitudes below 10 mm *CC*. Since in our cohort respiratory amplitudes larger than 10 mm *CC* were measured in only three fractions, the impact of the respiratory motion on the dose delivery was estimated to be negligible for the vast majority of fractions.

The main deviations from the planned dose were caused by baseline drifts. A larger drift led to with a lower delivered GTV $D_{99\%}$. Dose to the OAR was observed to be higher or lower than the planned dose with an increased drift. The simulations demonstrated that the dosimetric effect of the drift is highly dependent on its direction: for the GTV, simulations with anterior and right drifts lead to systematically lower delivered GTV $D_{99\%}$. For drifts in the other directions, the impact of drift on the delivered $D_{99\%}$ was negligible. For the

OARs, this asymmetric pattern in opposing directions was not observed. Rather, each OAR was sensitive to drift only along one principal axis, and the effect of drift on delivered $D_{0.5cc}$ was of approximately equal magnitude for drifts in opposing directions. For example, the $D_{0.5cc}$ for the duodenum was only influenced by LR drift, where drifts to the right yielded a dose decrease, and drift to the left an increased dose.

These correlations come from the typical anatomical relation of the OARs relative to (peri)pancreatic tumors. The duodenum is typically located on the right side of the GTV, and therefore a tumor drift towards the right will lead to underdosage of the GTV. Drifts to the left will likewise lead to overdosage of the duodenum. Furthermore, the small bowel is often anteriorly positioned to the GTV, whereas the stomach is located cranially of the GTV, leading to an analogous dependence on the drift direction, as depicted in Fig. 5.3. In general, these results reinforced our believe that further motion mitigation strategies should be more directed towards compensating intrafraction drifts than towards further reducing periodic respiratory induced motion patterns.

This finding also held for patient 8, where for fraction 5 the lowest relative GTV $D_{99\%}$ of 0.85 was observed for all analyzed fractions. Subanalysis revealed that substantial right drift of 2.5 mm was observed (Fig. 5.4) which resulted in a lower dose to both the GTV and duodenum.

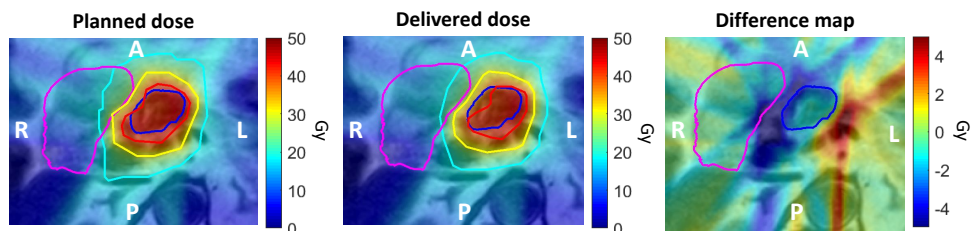


Figure 5.4.: Zoomed maps of planned, delivered, and difference (planned - delivered) dose of the fifth fraction of patient 8, where delivered GTV $D_{99\%} = 85\%$ of planned $D_{99\%}$. The GTV contour is shown in dark blue, and the duodenum contour is shown in pink. The planned and delivered dose contain the isodose contours of 40 Gy (red), 30 Gy (yellow) and 20 Gy (teal). Note that this dose plan is scaled to the complete 5x8 Gy treatment plan.

Recently, Tyagi et al.⁶⁶ also reported on the dosimetric impact of intrafraction motion in pancreatic MRgRT with abdominal compression, by directly comparing the 3D T2w position-verification (PV) and post-scan to the pre-scan. Our findings in terms of delivered GTV coverage are in line with theirs, as the authors reported no significant changes in GTV $V_{100\%}$, and a wider spread in key DVH parameters of the stomach and small bowel in the

PV- and post-scan. This is comparable to the increase in spread in small bowel and stomach relative $D_{0.5cc}$ that we observed for patients with larger drifts.

A limitation of our work is that the dosimetric analysis was based on quasi-rigid motion profiles, i.e. we neglected the impact of possible intrafraction deformations in the dose accumulation process. However, although deformations are well known to be present in the upper abdomen, especially in hollow structures, we believe that impact of this restraint is very limited for two reasons. First, the assessed dose parameters are solely determined by the voxels of the substructures of both the target and the organs at risk that are located at the dose gradients within the high-dose region, which in turn are in the close surrounding of the target volume. Due to the dense cell structure of the tumor, the target volume movement is judged to move rigidly, which was also visually confirmed upon assessment of the cine MRIs. Secondly, we demonstrated that the deviations are mostly determined by small drifts (< 3 mm) often to muscle relaxation, which we believe could well approximated as locally rigid. Finally, while the simulation study allowed a systematic evaluation of the different aspects of intrafraction motion and their effect on delivered dose, the simulated motion remains a simplified model not easily translated to a clinical situation. Especially with larger respiratory amplitudes, the assumption of rigid transformation might no longer hold.

5.5. Conclusion

For the vast majority of fractions and patients, the intrafraction motion observed during treatment delivery with an abdominal corset only modestly impacted the dose to the target and organs at risk. This increases our confidence that MRgRT can be safely executed for patients with abdominal tumors without the use of gating or tracking techniques, potentially allowing dose escalation strategies. The results in this study also add to the supportive evidence for the use of abdominal compression in general, as this can also be applied for radiotherapy on conventional systems. Subanalysis revealed that the impact of the intrafractional drifts on the delivered dose was more prominent than the impact of the respiratory motion. Care should be taken in patients where the tumor and organs at risk are close together, as only small drifts can lead to systematic deviations from the planned dose.

Supplementary materials





CHAPTER 6

Feasibility of delivered dose reconstruction for MR-guided SBRT of pancreatic tumors with fast, real-time 3D cine MRI

G Grimbergen
GG Pötgens
H Eijkelenkamp
BW Raaymakers
MPW Intven
GJ Meijer

Radiotherapy and Oncology (2023), **182**:109506

ABSTRACT

Background and purpose – In MR-guided SBRT of pancreatic cancer, intrafraction motion is typically monitored with (interleaved) 2D cine MRI. However, tumor surroundings are often not fully captured in these images, and motion might be distorted by through-plane movement. In this study, the feasibility of highly accelerated 3D cine MRI to reconstruct the delivered dose during MR-guided SBRT was assessed.

Materials and methods – A 3D cine MRI sequence was developed for fast, time-resolved 4D imaging, featuring a low spatial resolution that allows for rapid volumetric imaging at 430 ms. The 3D cines were acquired during the entire beam-on time of 23 fractions of online adaptive MR-guided SBRT for pancreatic tumors on a 1.5 T MR-Linac. A 3D deformation vector field (DVF) was extracted for every cine dynamic using deformable image registration. Next, these DVFs were used to warp the partial dose delivered in the time interval between consecutive cine acquisitions. The warped dose plans were summed to obtain a total delivered dose. The delivered dose was also calculated under various motion correction strategies. Key DVH parameters of the GTV, duodenum, small bowel and stomach were extracted from the delivered dose and compared to the planned dose. The uncertainty of the calculated DVFs was determined with the inverse consistency error (ICE) in the high-dose regions.

Results – The mean (SD) relative (ratio delivered/planned) $D_{99\%}$ of the GTV was 0.94 (0.06), and the mean (SD) relative $D_{0.5cc}$ of the duodenum, small bowel, and stomach were respectively 0.98 (0.04), 1.00 (0.07), and 0.98 (0.06). In the fractions with the lowest delivered tumor coverage, it was found that significant lateral drifts had occurred. The DVFs used for dose warping had a low uncertainty with a mean (SD) ICE of 0.65 (0.07) mm.

Conclusion – We employed a fast, real-time 3D cine MRI sequence for dose reconstruction in the upper abdomen, and demonstrated that accurate DVFs, acquired directly from these images, can be used for dose warping. The reconstructed delivered dose showed only a modest degradation of tumor coverage, mostly attainable to baseline drifts. This emphasizes the need for motion monitoring and development of intrafraction treatment adaptation solutions, such as baseline drift corrections.

6.1. Introduction

SBRT has been established as a feasible therapy for unresectable tumors in and around the pancreas.^{15, 40, 43, 63, 77, 78} MR-guided radiotherapy^{11, 12} has enabled effective SBRT for this tumor site, with safe delivery of high irradiation doses in hypofractionated regimens, because of its excellent online imaging capabilities compared to its conventional, CT-guided counterparts.⁴²

MR-guided radiotherapy also enables simultaneous imaging during treatment delivery, for e.g. intrafraction motion monitoring and retrospective treatment evaluation. This feature is especially important for SBRT in the upper abdomen, because of the proximity of these tumors to highly radiosensitive OARs and potentially large motion amplitudes. Mitigating respiratory motion with passive motion management, like abdominal compression, is a well-established method in the upper abdomen,^{33, 61, 66, 92–95} but residual motion and small drifts can still have a significant dosimetric impact on target coverage and OAR dose.^{83, 105–107}

Online motion monitoring in the upper abdomen is challenging due to the limitations of contemporary MRI techniques. In order to capture detrimental breathing irregularities and tumor drifts, imaging ideally needs to be conducted in a time-resolved fashion, at a frequency fast enough to capture respiratory motion. In current practice, this is mainly achieved with 2D cine MRI, which was employed in a previous study to perform delivered dose reconstruction in the upper abdomen.¹⁰⁷ However, this technique suffers from limited field-of-view (FOV), being unable to capture tissue motion outside the 2D plane(s), and is unsuitable for assessing out-of-plane motion. Attempts to design time-resolved volumetric acquisitions were often focused on reconstructing 3D motion from 2D cine MRI.^{81, 108–112} However, high-frequency, time-resolved 4D MRI is also possible through direct acquisition when reducing the spatial resolution of the acquired images.¹¹³ This technique results in a lower visual image quality, but modern deformable image registration algorithms can still extract accurate 3D motion information at large voxel sizes.^{114, 115} Moreover, assuming that the motion fields vary slowly in the spatial domain, they can be upsampled and interpolated to different coordinate grids with higher resolutions. This way, low-resolution, real-time 3D cine MRI becomes a potential technique for dose reconstruction in the upper abdomen.

In this study, we aimed to investigate the use of highly accelerated 3D cine MRI for reconstruction of the delivered dose during MR-guided SBRT of pancreatic tumors, and analyze the volumetric motion patterns extracted from these 3D cine MRIs. In addition, the delivered dose was calculated under various simulated motion correction strategies.

6.2. Materials & Methods

6.2.1. Patient and treatment overview

Five patients were included that underwent online adaptive MR-guided SBRT for upper abdominal malignancies between August and September 2022. Patients provided informed consent through the prospective Multi-OutcoMe Evaluation of radiation Therapy Using the MR-linac (MOMENTUM) study (NCT04075305). Patient characteristics are given in Table 6.1.

The patients were treated with a 5x8 Gy SBRT regimen on the Elekta Unity (Elekta AB, Stockholm, Sweden) MR-Linac, a 7 MV flattening filter free (FFF) linear accelerator combined with a 1.5 T wide bore MRI scanner. Treatment was conducted in an online adaptive fashion,¹⁴ in which the treatment plan was adapted to a 3D T_2w MRI sequence acquired at the start of each fraction. Intrafraction tumor motion was mitigated by compression with an abdominal corset.^{33,61} The treatment protocol did not include bowel preparation. An isotropic planning target volume (PTV) margin of 3 mm was used, and treatment was delivered with a 9-14 beam step-and-shoot intensity-modulated radiotherapy (IMRT) technique. Our institutional planning objectives and constraints are given in supplementary Table S1.

Table 6.1.: Patient characteristics. LAPC: locally advanced pancreatic carcinoma. LRPC: locally recurrent pancreatic carcinoma. pNET: pancreatic neuroendocrine tumor.

#	Age	Sex	GTV/PTV volume (cm ³)	Diagnosis	Tumor location
1	71	M	23/38	LAPC	Head
2	73	F	144/202	LAPC	Tail
3	59	M	47/81	LRPC	Tail
4	72	M	2/5	pNET	Tail
5	61	M	5/11	Pancreatic oligometastasis	Head

6.2.2. Imaging overview

A 3D cine MRI sequence was developed for fast, time-resolved 4D imaging. The sequence is an RF-spoiled, T_1 -weighted, gradient echo scan with a low resolution of $5 \times 5 \times 6$ mm³ voxel size. The low resolution allows for high-speed volumetric imaging at 2.3 Hz (430 ms

per volume) when combined with acceleration strategies such as compressed SENSE,^{116,117} partial Fourier, and a large echo train length. The water-fat shift was manually set to a maximum of 0.5 mm, to ensure geometrically accurate images. The sequence was tuned using the standard parameters available in the clinical environment of the MR-Linac, such that this sequence can be readily implemented on similar systems. The 3D cine MRIs were acquired during the entire beam-on time of each fraction. A detailed overview of the sequence parameters is given in Table 6.2.

Table 6.2.: 3D cine MRI sequence parameters

Parameter	Value
Scanning technique	RF-spoiled Fast Field Echo
FOV (mm ³)	400 × 400 × 180
Acquisition/reconstruction voxel size (mm ³)	5 × 5 × 6
TE/TR (ms)	1.1/2.2
FA (°)	10
Compressed SENSE factor	4
Partial Fourier factor	0.7 (<i>x-y</i>), 0.7 (<i>y-z</i>)
Echo train length	185
Readout bandwidth (Hz/pixel)	2170
Scan type per dynamic (s)	0.430

6.2.3. Dose reconstruction

The reconstruction of the delivered dose was conducted in a time-resolved fashion, where the total dose plan was split into partial doses for every cine dynamic. This way, the motion measured in a cine dynamic was only applied to the dose that was delivered during that particular dynamic's acquisition time. This was done by using the machine log files of the linac, which log the current state of the linac (gantry angle, dose rate, and multi-leaf collimator positions) during treatment delivery every 40 ms. Because the entries in these log files are timestamped with the current clock time, they can be segmented into partial logs based on the acquisition times of every cine dynamic. When combined with a pseudo-CT (bulk electron density assignment of the pre MRI: bone = 1.117g/cm³, air = 0.001 g/cm³, all other tissue was assigned as water = 1.000 g/cm³), a partial dose plan can be calculated with GPUMCD¹⁰³ for every cine dynamic.

Motion was extracted from the 3D cine MRIs as deformation vector fields (DVF) using

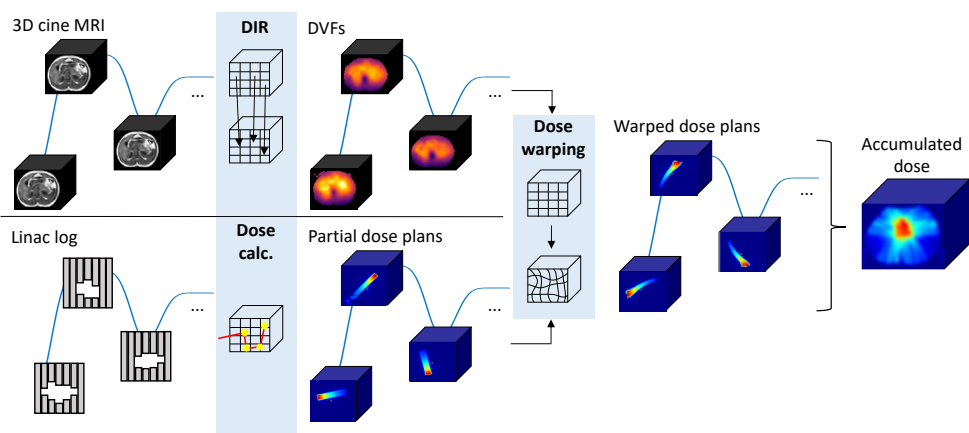


Figure 6.1.: The method pipeline. 3D cines are acquired every 430 ms during beam-on, and for each dynamic the current state of the linac is saved and reconstructed into a partial dose plan. Deformable image registration (DIR) is performed on the cine frames, and the resulting deformation vector field (DVF) is used to warp the corresponding partial dose plan. The warped doses are then summed to obtain the delivered dose.

EVolution⁸⁵ ($\alpha = 0.35$, patch size = $5 \times 5 \times 5$). The cine dynamics were internally registered; therefore, the DVFs relate the motion of each incoming dynamic to a reference state. In order to later apply the DVFs to the partial dose plans, this reference state needs to correspond to the anatomical state for which the dose plan was created, assumed to be the time-weighted average position of the internal anatomy. To create an appropriate reference cine dynamic, a first registration loop was run in which the first 30 seconds of cine MRI data was registered to a dynamic in the exhale state. Then, the average DVF over this period was calculated and used to warp this exhale dynamic to create a new dynamic, corresponding to the time-weighted average position. This dynamic was used as the reference image during the main registration loop.

After every registration of the reference dynamic to an incoming cine dynamic, the resulting 3D DVF was interpolated to the coordinate grid of the partial dose plans (voxel size: $3 \times 3 \times 3 \text{ mm}^3$). A cubic interpolation method was used to preserve large motion gradients between stationary and mobile tissue, for example at the spine interface. After interpolation, the partial dose plan corresponding to the incoming dynamic was warped while preserving energy/mass transfer,¹¹⁸ taking the density changes into account during dose warping. The partial dose plans were summed with and without warping, resulting in the delivered and planned dose, respectively. The method for dose reconstruction is illustrated in Fig. 6.1.

After warping a partial dose plan, the same DVF was used to warp the GTV contour from

the reference state to the incoming dynamic. This was done to create a GTV contour that moved along with the anatomy, of which the center of mass could be tracked to generate a 3D motion trace of the tumor. This motion trace was characterized by its respiratory motion amplitude and maximum drift in the same manner as in our previous studies.^{61,107} The respiratory amplitude was calculated by high-pass filtering the motion trace and calculating the peak-to-peak distance, and the drift magnitude was calculated by low-pass filtering and extracting the maximum absolute value of the drift motion. The overall respiratory amplitude and drift were calculated as the 2-norm of their values in the three cardinal directions: cranio-caudal (*CC*), anterior-posterior (*AP*), and left-right (*LR*).

6.2.4. Motion correction simulation

The above method for dose reconstruction and GTV motion monitoring was also used to simulate various intrafraction motion correction strategies, and calculate their subsequent impact on the delivered dose in terms of tumor coverage.

Three strategies were simulated, using the measured GTV motion trace to apply a beam isocenter shift as a 3D offset to the DVFs before warping the dose. The first strategy was a thresholded baseline shift, where the beam isocenter is set to the moving average tumor position over the last 30 seconds, when this average position exceeds a certain distance threshold from the previous isocenter. Smaller thresholds will lead to better conformity but might require corrections at an unfeasibly high frequency, as each correction would realistically require a minimum processing time. Therefore, six different thresholds were investigated: 0.5, 1.0, 1.5, 2.0, 2.5 and 3.0 mm. The second strategy was tumor trailing,¹¹⁹ where the isocenter is *continuously* updated with the average tumor position. Trailing can be regarded as a thresholded baseline shift with a threshold of 0 mm. The third strategy was tumor tracking, where the applied offset is continuously updated with the actual tumor position.

6.2.5. Evaluation

For delivered dose evaluation, key DVH parameters of the GTV and neighboring OARs (duodenum, small bowel, stomach) were extracted and compared to their respective values of the planned dose, expressed as the ratio between the delivered dose over the planned dose. For the gross tumor volume (GTV), the $D_{99\%}$ was evaluated, and for the OARs the $D_{0.5cc}$.

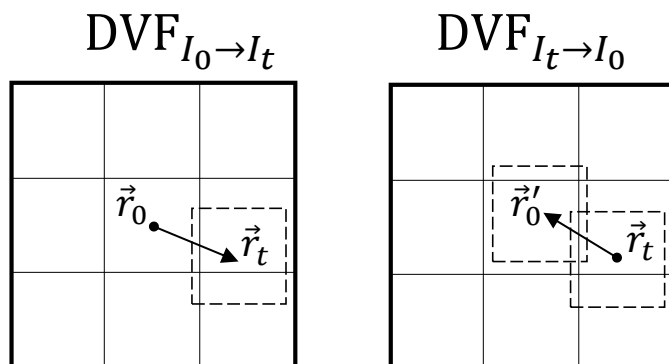


Figure 6.2.: Schematic representation of the inverse consistency error (ICE). After registering reference image I_0 to incoming image I_t , the resulting DVF maps voxel \vec{r}_0 to \vec{r}_t . The inverse DVF, obtained by registering I_t to I_0 , maps \vec{r}_t back to \vec{r}'_0 . If inaccuracies in the registration occur, this location might differ from the starting position. The ICE is defined as the length of the difference vector between \vec{r}'_0 and \vec{r}_0 . Note that \vec{r}_t often does not fall exactly on the image grid, so the inverse DVF needs to be interpolated to obtain the backward vector at that location.

When performing 3D deformable image registration to warp dose maps, it is important to ensure that the obtained motion is realistic up to a dosimetrically relevant level. This is a notoriously complicated problem in the absence of a ground truth. We therefore employed the inverse consistency error (ICE) as a metric to evaluate the quality of the obtained DVFs,^{120,121} and can also be applied to low-resolution DVF evaluation.¹¹³ Moreover, this inverse consistency is a commonly used evaluation metric in dose warping studies, as it measures spatial uncertainty of the warped dose on a voxel-by-voxel basis.^{122–125} A DVF is known to be inverse consistent when a voxel at reference location \vec{r}_0 , mapped to location \vec{r}_t with $\text{DVF}_{I_0 \rightarrow I_t}$, ends up back at \vec{r}_0 when the inverse $\text{DVF}_{I_t \rightarrow I_0}$ is applied to \vec{r}_t . If instead it is mapped at a different location \vec{r}'_0 , the ICE is equal to $\|\vec{r}'_0 - \vec{r}_0\|_2$ (see Fig. 6.2).

The ICE was calculated for the first two minutes of 3D cine MRI data of every fraction, and evaluated in only the dosimetrically relevant area where voxel values in the planned dose were above 20 Gy (scaled to the complete 40 Gy treatment regimen).

6.3. Results

All five patients received complete treatment of five fractions. However, in one fraction the 3D cine acquisition was started too late after beam-on, and in another fraction, the linac log file was missing. Therefore, the data from these fractions was disregarded, and a total

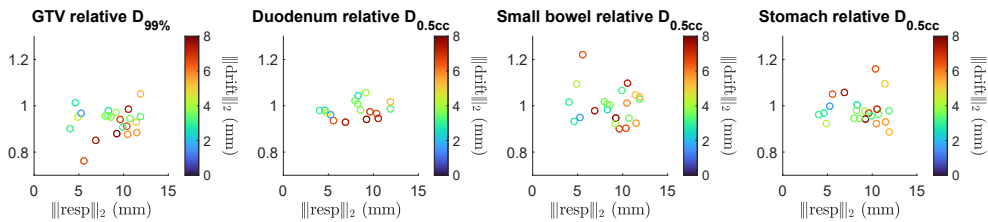


Figure 6.3.: The relative (ratio planned/delivered) DVH parameters in the GTV and OARs of the measured intrafraction motion. Each point represents a fraction, accumulated with the motion measured during that fraction, and characterized by the magnitudes of the respiratory amplitude (x-axis value) and drift of that fraction (point color scale).

of 23 fractions was included in the final analysis.

A 3D cine MRI acquisition demo is given in supplementary video 1 (top row), along with the corresponding motion-compensated dynamics (bottom row). In the latter, the 3D deformable image registration quality can be assessed by the level of residual motion present in the images. Please note that this video is not a real-time representation but sped up for visual purposes to ten dynamics per second, covering 64 seconds of actual cine MRI acquisition. Quantitatively, a high inverse consistency was achieved in the high-dose region, with a mean (SD) ICE of 0.65 (0.07) mm over all fractions. An example of an ICE map is given in supplementary Fig. S1. Upon closer inspection of the obtained motion fields, the motion gradient at the spinal interface turned out less steep than initially inspected, so the cubic interpolation method did not result in different motion fields than with linear interpolation (supplementary Fig. S2).

The relative (ratio delivered/planned) DVH parameters of the GTV, duodenum, small bowel, and stomach are presented in Fig. 6.3, with respect to the measured GTV respiratory amplitude and drift magnitude. The mean (SD) relative $D_{99\%}$ of the GTV was 0.94 (0.06), and the mean (SD) relative $D_{0.5cc}$ of the duodenum, small bowel, and stomach were respectively 0.98 (0.04), 1.00 (0.07), and 0.98 (0.06). Upon closer inspection of the fractions where the largest decline in tumor coverage was measured, it was observed that significant lateral drifts had occurred during these fractions. An example is given in supplementary video 2, where the 3D cine MRI and GTV motion trace can be seen of a fraction where the delivered GTV $D_{99\%}$ was 88% of the planned $D_{99\%}$. The video, played in real-time, features a bulk shift about two-thirds into the treatment as the patient repositioned themselves 6.5 millimeters to their right. One minute and 40 seconds later, the patient shifted back to roughly the baseline position. Another example is the fraction with the lowest relative GTV $D_{99\%}$, which was 76% of the planned $D_{99\%}$. The GTV motion trace is given in supplementary Fig. S3.

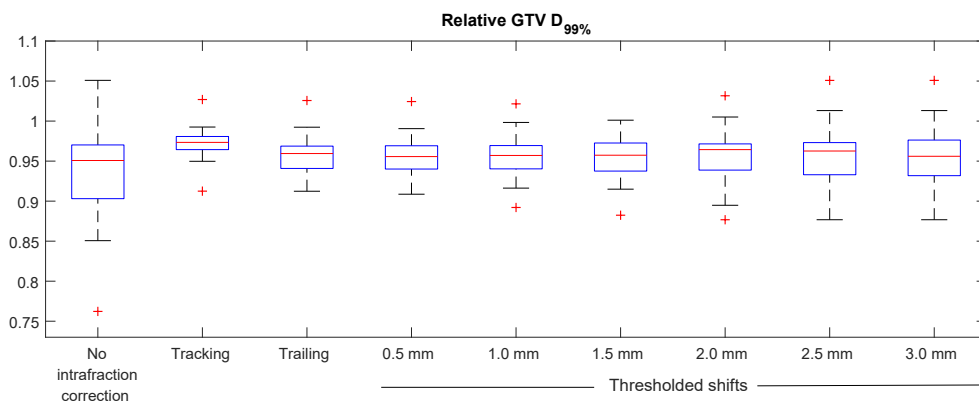


Figure 6.4.: The simulated effect of tracking, trailing and thresholded baseline shifts on the delivered GTV $D_{99\%}$ for the fractions in this study. The whiskers of the boxplot extend to the minimum and maximum of the values not considered outliers (values further than 1.5 times the interquartile range from the box). The outliers are indicated by the red plus signs.

In this fraction, the lateral drift was smaller than in the previous example, but it occurred relatively early into treatment and sustained for almost the entire beam-on time. It had, therefore, a larger detrimental effect on tumor coverage. This same fraction also featured the largest relative OAR dose increase of 122% in small bowel $D_{0.5cc}$.

In the motion correction simulations, it was found that thresholded baseline shifts already greatly mitigate the dosimetric effects of all the intrafraction motion during the beam-on time, similar to the continuous trailing strategy (Fig. 6.4). Tracking strategies further improved the congruence between planned and delivered dose. However, the effects of tracking the respiratory motion turned out to be limited for this cohort. For the different threshold values, the average number of corrections per fraction was: 47 for 0.5 mm, 16 for 1.0 mm, 7 for 1.5 mm, 4 for 2.0 mm, 2 for 2.5 mm and 1 for 3.0 mm. Further improvement in target coverage was limited when using lower thresholds or continuous trailing.

6.4. Discussion

We have employed a fast, real-time 3D cine MRI sequence for delivered dose reconstruction, using deformable image registration to obtain highly accelerated volumetric motion information directly from the acquired images. In this study, we have demonstrated that these motion fields can be used for dose warping to reconstruct the delivered dose for MR-guided

SBRT of upper abdominal tumors.

In its current retrospective setting, we believe that the most useful clinical application of the end-to-end dose reconstruction method would be as a QA tool for offline treatment evaluation, after a fraction has been delivered. Should the delivered dose show that unfavorable deviations have occurred in tumor coverage or OAR dose, the treatment strategy of the upcoming fractions might be adapted to "repair" tumor cold spots and/or mitigate OAR hot spots.

The results from the delivered dose reconstructions showed in most fractions modest dosimetric degradations caused by intrafraction motion. However, in some fractions tumor coverage was clearly impacted by intrafraction drifts during beam-on time. With an average beam-on time of 8+ minutes, there is a realistic probability of these small drifts occurring. The OARs were less impacted by intrafraction motion than the tumor coverage. The largest relative OAR dose increase of 122% in small bowel $D_{0.5cc}$ turned out to be a negligible absolute increase from 11.8 Gy to 14.3 Gy (scaled to the complete 40 Gy treatment regimen). In only two fractions, the delivered dose violated the OAR dose constraints, and in both these cases this violation was already present in the planned dose. One fraction had a violated stomach constraint in the planned dose, but this was as such mitigated by intrafraction motion that the $D_{0.5cc}$ fell below the constraint in the delivered dose. For further clarification, we have included all absolute OAR $D_{0.5cc}$ values in supplementary Table S2.

The simulations demonstrated that the largest degradations in tumor coverage could be sufficiently improved with systematic monitoring of the target in combination with a correction strategy. Since thresholded baseline shifts require a substantially lower number of intrafraction corrections than continuous trailing or tracking, this strategy might be the most accessible candidate for a clinical solution to mitigate detrimental drifts. The chosen threshold value will depend on how long a correction would take to process and execute in practice. Based on the number of corrections that were applied in the simulations, and assuming a maximum correction frequency of once per minute, a threshold of 1.5 mm (resulting in seven intrafraction corrections on average) would have been the recommended value for this cohort.

The 3D cine MRI sequence was developed as plug-and-play, using acquisition and reconstruction options available in the standard clinical environment of the 1.5 T MR-Linac. Therefore, it also has the potential as a motion monitoring tool comparable to the 2D cine sequences used for gating/tracking on MR-Linac systems. However, mainly due to the high compressed SENSE factor, the reconstruction time (approximately one second per dynamic) is currently

too long for online applications. Nonetheless, with future (GPU-based) acceleration of reconstruction, we believe that time-resolved volumetric sequences will become a feasible method for real-time online motion monitoring, overcoming the limitations of 2D acquisitions. Furthermore, with the particular low-resolution sequence employed in this study, the reduced data size also means that images can be streamed and processed with minimal latency.

A critical workflow component in 3D dose warping is the QA of the obtained motion fields. Because of the low resolution of the 3D cine MRIs much detail is lost, which may introduce additional uncertainty in the DVFs. However, we believe that the motion of upper abdominal tumors and the immediate surroundings in the high dose area (such as abutting OARs), are predominantly characterized by rigid transformations, especially when restricted by abdominal compression. This holds both for the respiratory motion and for bulk shifts. Because of their geometric simplicity, these rigid displacements can typically be easily captured by DIR algorithms. There might still be a deformable component present which may be harder to accurately extract under low resolutions, for example the digestive motion of surrounding bowel structures. Bowel motion can be quite subtle and might require imaging with e.g. higher contrast, higher resolution or oral contrast agents.^{126–129} However, this motion in the immediate vicinity of the tumor, as well as the deformable motion component of the tumor itself is much smaller than the rigid component, often periodic and therefore might be less dosimetrically relevant.

While this study only employed a single DVF uncertainty metric and lacks a ground truth for true error quantification, the mean ICE of 0.65 mm in the high-dose region still signifies a low uncertainty in the obtained motion fields. Moreover, this study was confined to a relatively simple problem within the context of dose warping studies; image registration was performed in a highly correlated set of images and produced spatially smooth, low-resolution 3D motion fields reflecting only global anatomical motion. Even though it requires more sophisticated imaging tools, we argue that intrafraction image registration and dose warping is less error-prone than *interfraction* dose accumulation, where motion fields need to reflect much more dramatic anatomy changes, as structures are likely to grow, shrink, appear and disappear between consecutive images.¹³⁰ Nevertheless, uncertainty in the obtained motion fields will still lead to nontrivial uncertainty in the reconstructed dose plans. Quantifying the uncertainty in dose accumulation is a known and open problem in the field,^{131–137} and while considered beyond the scope of this study, it should be a vital part of the clinical implementation of any intrafraction dose accumulation method, if clinical decision making is going to be based on the resulting delivered dose reconstructions.

6.5. Conclusion

This study showed that highly accelerated 3D cine MRI during beam-on can be used for delivered dose reconstruction during MR-guided SBRT of pancreatic tumors. The low-resolution cine dynamics can be deformably registered with substantial inverse consistency. This study's results show that drifts are the most detrimental motion components for adequate tumor coverage in the upper abdomen. However, these errors can be resolved through simple online correction strategies, such as intrafraction baseline shift corrections. Moreover, our method would allow day-to-day treatment evaluation to optimize the treatment strategy of the upcoming fractions.

Supplementary materials





CHAPTER 7

Gating and intrafraction drift correction on a 1.5 T MR-Linac: clinical dosimetric benefits for upper abdominal tumors

G Grimbergen
SL Hackett
F van Ommen
ALHMW van Lier
PTS Borman
LTC Meijers
EN de Groot-van Breugel
JCJ de Boer
BW Raaymakers
MPW Intven
GJ Meijer

Radiotherapy and Oncology (2023), **189**:109932

ABSTRACT

This work reports on the first seven patients treated with gating and baseline drift correction on the high-field MR-Linac system. Dosimetric analysis showed that the active motion management system improved congruence to the planned dose, efficiently mitigating detrimental effects of intrafraction motion in the upper abdomen.

7.1. Introduction

MR-guided stereotactic body radiotherapy (SBRT) has been established as a feasible therapy for unresectable tumors in the upper abdomen, with recent clinical outcomes demonstrating safe delivery of ablative doses with hypofractionated regimens, while maintaining low acute toxicity rates.^{15, 17, 40, 43, 63} The online adaptive workflow of MR-guided SBRT is characterized by the possibility to negate interfraction motion, but further margin reduction and dose escalation is now mainly limited by intrafraction motion.

The ability of MR-Linac systems of simultaneous imaging and treatment delivery means that, potentially, adverse effects of intrafraction motion can be actively alleviated based on real-time image-based tumor tracking. Using image-based tumor tracking, the radiation beam can be gated whenever the tumor moves outside a predetermined window. For low-field MR-Linac systems, gated delivery based on 2D cine MRI has already been implemented,^{36, 138} and has led to improved geometric and dosimetric fidelity to the planned treatment.^{35, 139} Recently, the clinical implementation of active motion management has also been realized on the high-field MR-Linac system. Aside from real-time gating, this motion management system also allows correction for tumor drifts and bulk shifts. This study investigated the achieved dosimetric benefit for the first seven patients treated on abdominal lesions with gating and intrafraction drift correction on a 1.5 T MR-Linac.

7.2. Materials & Methods

7.2.1. Patients and treatment overview

Seven patients (total 31 fractions) that underwent online adaptive MR-guided SBRT for upper abdominal malignancies between April and June 2023 were included. Patients provided informed consent for clinical data collection through the prospective Multi-OutcoMe EvaluationN of radiation Therapy Using the MR-linac (MOMENTUM) study (NCT04075305). The patients were treated with a hypofractionated SBRT regimen on the Elekta Unity (Elekta AB, Stockholm, Sweden) 1.5 T MR-Linac. Treatment was conducted in an online adaptive fashion,¹⁴ in which the treatment plan was adapted to a free breathing 3D T_2w MRI sequence acquired at the start of each fraction (sequence parameters given in supplementary Table S2). Intrafraction tumor motion was passively mitigated by compression with an abdominal corset.^{33, 61} An isotropic PTV margin of 2-3 mm was used, and treatment was delivered with a 9-14 beam step-and-shoot IMRT technique. This protocol for treatment setup and planning was according to the conventional protocol for ungated treatment delivery, using

the same target definition and margin protocols. Patient and treatment characteristics are given in supplementary Table S1.

7.2.2. Motion management

Active motion management was performed using a clinical pre-release of Comprehensive Motion Management (CMM) for the Elekta Unity MR-Linac, a package for automatic beam gating and drift correction through baseline shifting, with online imaging-based target registration. CMM employs a previously developed and validated template-based registration algorithm for real-time motion monitoring on 1.5 T MR-Linac systems.^{140, 141}

The imaging for motion management was continuously acquired using 2D interleaved coronal and sagittal cine MRI, a balanced gradient echo sequence with 170 ms temporal resolution per plane, hence a temporal resolution of 340 ms for the coronal and sagittal planes combined. Further sequence parameters are given in supplementary Table S2. Because of the interleaved coronal and sagittal acquisition, contour tracking was performed in three directions: cranio-caudal (CC), anterior-posterior (AP), and left-right (LR). The exhale position of the tumor at the start of delivery was determined by a 3D-2D registration of the 3D T_2w MRI with a coronal-sagittal image template of exhale anatomy. This template was constructed by averaging exhale-labelled cine images over multiple breathing phases just before beam delivery.^{140, 141} The PTV expansion of the GTV in exhale was set as the gating envelope. During radiation delivery, the beam was automatically gated if the overlapping volume between the target structure (i.e. the GTV) and the gating envelope fell below 95%. The beam was also gated if the registration quality of the tumor tracking was deemed too low by the CMM software, due to e.g. large deformations, large differences in motion between the coronal and sagittal plane, or large out-of-plane motion.

Intrafraction tumor drifts could be corrected through baseline shifts, which adjust the multi-leaf collimator (MLC) apertures to the current time-averaged tumor position, based on the concept of tumor trailing.¹¹⁹ If a baseline shift was initiated by the operator, the beam was manually halted and a suggested CC/AP/LR shift was calculated based on the average drift observed over the last three breathing cycles, with the option for manual adjustments. After approval by the radiation oncologist, the shift was forwarded to the treatment planning system, where it was applied to the original plan as an isocenter shift to calculate a new plan by shifting the plan segments, while keeping the segment weights the same. After plan approval, the treatment delivery was resumed with the updated structure positions, typically within one minute.

7.2.3. Delivered dose reconstruction

The dosimetric benefit of motion management versus no motion management was investigated for all fractions. Logs of the motion management software were retrieved, which included the target position and beam state (on/off) in every separate cine frame, i.e. every 170 ms, as well as the directions and timestamps of any baseline shift. Dose accumulation was performed by applying the target position deviations as isocenter shifts (translations only) to the planned dose in the opposite direction, and afterwards averaging all shifted dose plans to obtain a delivered dose. Because of the online adaptive workflow, each fraction had a unique planned dose and was therefore reconstructed independently. The delivered dose with motion management was calculated using only the target positions when the beam state was on. For the delivered dose without motion management, all target positions were used for dose accumulation regardless of beam state, while also undoing any baseline shifts by adding the shift as an offset to each target position, creating an "uncorrected" motion trace. For this scenario, the total treatment time would have been reduced as the beam would not have been gated. The duty cycle of the gated delivery was used to calculate an ungated beam-on duration, and the uncorrected motion was truncated after this duration. The method pipeline for dose reconstruction is illustrated in Fig. 7.1.

7.2.4. Evaluation

Key dose-volume histogram (DVH) parameters of the GTV, PTV and critical OARs were extracted to compare the delivered dose with and without motion management to the planned (static) dose, as the percentage difference of planned dose. For the GTV the $D_{99\%}$ was calculated, for the PTV the $D_{95\%}$, and for the duodenum, small bowel, stomach, and colon the $D_{0.5cc}$. For each patient, an OAR had to be located within a 2.5 cm margin around the GTV in at least one fraction to be included in the dosimetric evaluation. OARs located more than 2.5 cm away from the GTV in all fractions were deemed not dosimetrically relevant and therefore excluded from consideration for that patient.

7.3. Results

Thirty-one fractions were successfully delivered with online motion management. Four fractions were not included in this study; for patient 1, the last two fractions had to be scheduled on another MR-Linac system without motion management functionality due to staff shortage.

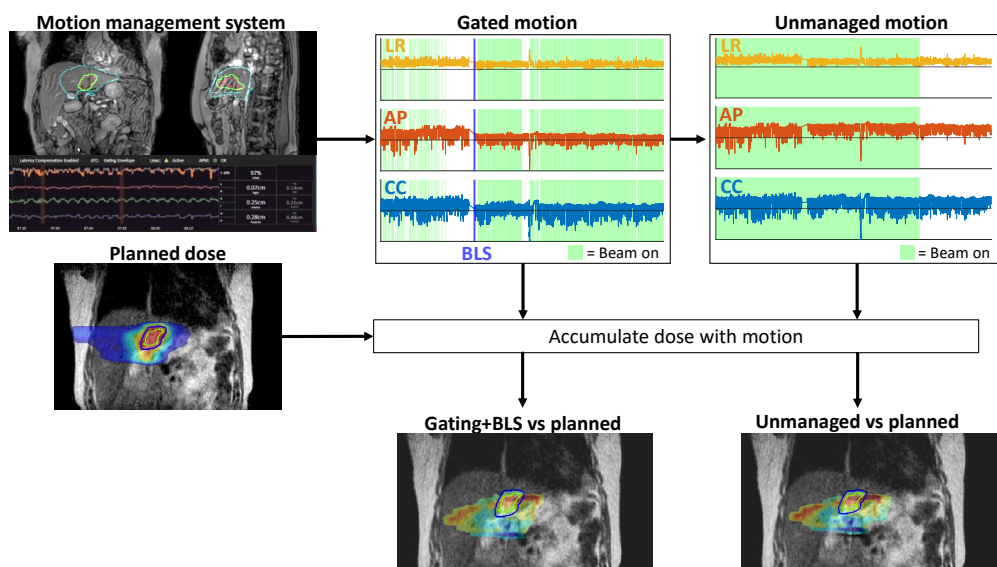


Figure 7.1.: The method pipeline. The logs of the motion management system contain the target positions in left-right (LR), anterior-posterior (AP), and crano-caudal (CC) direction, as well as the beam state (on/off) and any baseline shifts. This particular example shows a poor duty cycle at start of treatment due to a systematic AP and CC offset, which was corrected with a baseline shift. Note that the beam is halted while a shift is being determined and a new plan is calculated. This baseline shift can be reversed to obtain a motion trace for an unmanaged scenario, and the motion trace is also truncated to account for the reduced beam-on time for an ungated delivery. For both motion traces, the planned dose is translated with the target positions when the beam was on, or with all target positions for the unmanaged motion trace. The delivered dose for both scenarios is obtained after averaging over all translated dose maps.

For patient 3, technical issues with the motion management system during fractions 2 and 5 meant that the first part of these fractions was delivered with motion management, while the remainder was delivered without motion management. The incomplete data from these two fractions was therefore left out of consideration.

Overall the mean duty cycle was 68%. Duty cycles varied considerably between patients and fractions (range over all fractions: 41% - 93%). Beam gating decisions were 84% of the time based on the target exceeding the gating envelope, and 16% of the time due to registration quality. The overall number of executed baseline shifts was low. For most fractions (21 out of 31 total), no baseline shifts during beam-on were performed, and only two fractions required more than one shift. Details on the gating and baseline shifting characteristics for each patient are given in supplementary Table S3.

Violin plots of the DVH parameters for the GTV, PTV, and OARs calculated in the dose accumulated with and without motion management, as percentage difference to the planned

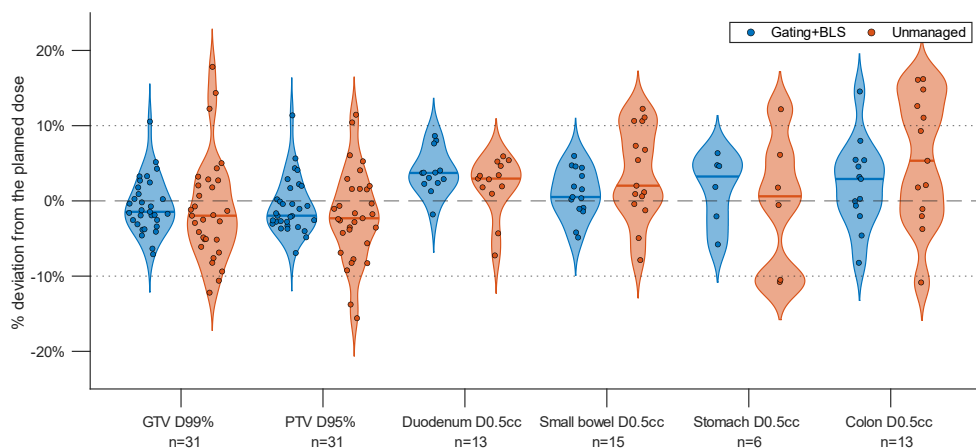


Figure 7.2.: Violin plots of the dosimetric results, with the critical DVH parameters of the GTV, PTV and OARs as their percentual difference to the planned dose. The blue violins represent the dose delivered with gating and baseline shifting (BLS), and the orange plots represent the scenario if no motion management was applied. Each point represents a fraction, with the amount of fractions for which a DVH parameter was evaluated is shown in the bottom row. The median value is indicated by the horizontal line in the violins.

(static) dose, are shown in Fig. 7.2. The median (range) differences to the planned dose were with motion management: GTV $D_{99\%} = -1.5$ (-7.1 — 10.5)%, PTV $D_{95\%} = -2.0$ (-6.9 — 11.4)%, duodenum $D_{0.5cc} = 3.7$ (-1.8 — 8.6)%, small bowel $D_{0.5cc} = 0.5$ (-4.9 — 6.0)%, stomach $D_{0.5cc} = 3.2$ (-5.8 — 6.3)%, and colon $D_{0.5cc} = 2.9$ (-8.2 — 14.5)%. Without motion management, these values were GTV $D_{99\%} = -2.0$ (-12.2 — 17.8)%, PTV $D_{95\%} = -2.3$ (-15.6 — 11.5)%, duodenum $D_{0.5cc} = 3.0$ (-7.2 — 5.9)%, small bowel $D_{0.5cc} = 2.0$ (-7.9 — 12.2)%, stomach $D_{0.5cc} = 0.6$ (-10.8 — 12.2)%, and colon $D_{0.5cc} = 5.3$ (-10.8 — 16.2)%. Here, a negative value indicates a decrease with respect to the planned dose, and a positive value indicates an increase. Generally, gating and baseline shifting led to a better congruence with the planned configuration in terms of both tumor coverage and OAR hotspots, with fewer outliers where the absolute deviation was greater than 10%.

7.4. Discussion

This study reported the dosimetric benefits for the first patients treated with automatic beam gating and intrafraction drift correction on a 1.5 T MR-Linac. The results indicate that gating and baseline shifts improve congruence to the planned dose in a variety of tumor types and sizes in the upper abdomen, in terms of both the intended target coverage and OAR sparing. Moreover, the clinical demonstration of fully MR-based online motion management

is an important step towards real-time adaptive MR-guided radiotherapy.^{138, 142, 143}

The dosimetric analysis shows that also with no motion management, most fractions would have been delivered without large deviations from the planned dose. This corresponds to our previous findings that as long as respiratory motion can be mitigated (through abdominal compression for example, as used in this study), the periodic, respiratory component of intrafraction motion will generally not have a large dosimetric impact for upper abdominal tumors.^{107, 144} In contrast to respiratory motion, shifts or drifts can have a detrimental effect on tumor coverage and OAR dose.¹⁴⁴ In the current motion management workflow, beam gating means that drifts will not automatically lead to problematic deviations from the planned dose, but can lead to reduced duty cycles and therefore to unacceptably long treatment times if not corrected for.

In this study, there was a considerable range of duty cycles (41% - 93%) between patients and fractions. This range is comparable to breath-hold gated delivery in a low-field MR-Linac study.¹³⁹ It should be noted that some fractions with low duty cycles were caused by a persistently low quality factor due to registration issues. This was often resolved in the next fraction by adapting the gating structure to improve tracking performance in the cine MR images. However, breathing irregularities also played a large role in fractions with low duty cycles. Further improvement might be achieved with techniques like visual biofeedback.^{139, 145, 146} Since the beam is also halted during baseline shifts (on average for one minute), duty cycles are reduced if more shifts have to be executed. Still, these drift corrections will by design maintain a high treatment efficiency in a gating delivery, and are therefore an indispensable component of the motion management workflow.

The findings on the dosimetric effects of unmanaged intrafraction motion, as well as the gain in tumor coverage from baseline shifts, correspond to an earlier study on retrospective dose accumulation using 3D cine MRI for volumetric target tracking.¹⁴⁴ This suggests that 2D cine MRI might suffice for image-based tumor tracking for online motion management of upper abdominal tumors, echoing the results from pre-clinical tests of the underlying motion monitoring algorithm of CMM.¹⁴¹ Moreover, aside from the ability to track structures in 3D, the interleaved acquisition of dual orthogonal planes allows for estimation of registration uncertainties that are typical for 2D-based tracking, such as out-of-plane motion, and the CMM software takes these uncertainties into account during beam gating in the form of the quality factor.

The method for delivered dose reconstruction in this study is less sophisticated than ap-

proaches using linac log files^{102,107} or volumetric motion fields (dose warping).¹⁴⁴ However, as mentioned above, the largest deviations from the planned dose are caused by drifts and shifts. We therefore consider this method to still provide a sufficient approximation of the delivered dose for the purpose of comparing motion management versus no motion management; previous work investigating the dosimetric effect of gating versus no gating employed a similar dose reconstruction method, convoluting the planned dose with motion histograms.³⁵

Supplementary materials





CHAPTER 8

Summary

Pancreatic cancer is among the deadliest types of cancer, and effective and safe treatment remains challenging. MR-guided radiotherapy, a noninvasive, low-toxic, local treatment, has recently emerged as a new treatment option for inoperable pancreatic cancer. The aim of this thesis was to explore several technical developments for the planning (**Part I**) and delivery (**Part II**) of radiotherapy for pancreatic cancer on the 1.5 T MR-Linac. These developments are needed to transform contemporary MR-guided radiotherapy into a next-generation treatment for pancreatic cancer, which extensively capitalizes on the capabilities of the 1.5 T MR-Linac.

This penultimate chapter summarizes the main findings of this thesis. We conclude with some take-home messages of this thesis.

The MRI scan that is made at the start of every treatment fraction on the MR-Linac, to which the treatment plan is adapted, is typically based on 3D Cartesian sampling schemes. The main radiotherapeutical advantages of these sequences are a high through-slice resolution and that they can be fully geometrically corrected. The main disadvantage is that they are prone to blurring artifacts as a result of respiratory motion, which can hamper the delineation accuracy of pancreatic tumors. In **Chapter 2**, we investigated two advanced MRI sequences, PROPELLER and 3D Vane. These sequences employ radial sampling schemes that result in a much sharper, motion-robust image. We acquired these scans during MR-Linac treatments of pancreatic cancer patients alongside the standard 3D T_2 -weighted (T_2w) Cartesian scans. The three sequences were then compared quantitatively, with several image quality metrics, and qualitatively, by scoring by three radiation oncologists.

Both the quantitative and qualitative results indicated that PROPELLER scans were at least on par with the 3D T_2w MRI. While the PROPELLER images were indeed sharper in-plane, with less blurry tumor and organ boundaries, the multi-slice 2D acquisition scheme led to substantial variation in anatomy from slice to slice. This was the main reason PROPELLER was not deemed superior to 3D T_2w MRI. It can be expected that if this problem can be resolved, we should seriously consider using PROPELLER sequences as the main delineation scan in the upper abdomen. The 3D Vane images were unequivocally deemed not suitable as main delineation scan because of the exotic T_2/T_1 contrast; T_2 -weighting is often deemed the optimal contrast in the upper abdomen.

The MR-Linac has enabled ablative SBRT treatment planning with relative confidence, because of its superior visualization of the daily position of the target structures and the organs to be avoided. However, creating SBRT treatment plans can be quite complex and depends on a great number of variables, mostly dictated by the institutional protocol for e.g.

prescribed dose and safety margins. Moreover, upper abdominal organs are often so close to the tumor, that it is not uncommon practice to compromise on tumor dose, leading to even more plan complexity for pancreas SBRT. For **Chapter 3**, a consortium was founded of thirteen centers that currently treat pancreatic cancer on the 1.5 T MR-Linac, or centers that are planning to start with this treatment in the near future. Within this consortium, we documented the existing variance in treatment planning protocols and established a consensus protocol to harmonize this variance.

We performed a multi-stage collaborative project, where centers had to create treatment plans for two example cases of pancreatic cancer according to an increasingly stringent protocol. After each phase, the results were compared and discussed, and the instructions for the next phase were determined. After the third stage, the dosimetric variance between the plans was considerably reduced and the final protocol was established. This protocol represents a consensus between thirteen centers on the recommended way to treat pancreatic cancer on the 1.5 T MR-Linac. We hope that with this work, we can not only go towards a higher-quality treatment, but also be able to better compare clinical outcomes between centers. Moreover, this protocol provides a road map for centers that are starting out with this complex treatment modality.

Motion from respiration and drift is one of the major causes for uncertainty during pancreatic tumor radiotherapy. The MR-Linac allows for continuous imaging during irradiation, using cine MRI sequences with a temporal resolution high enough (< 500 ms) to visualize breathing motion. This speed comes at the cost of spatial coverage: cine MRI is typically confined to a single 2D plane. During imaging, the orientation of the 2D plane can be constantly switched between the coronal and sagittal view, allowing for characterization of the 3D motion of the tumor's cross section. This sequence was acquired during the entire beam-on time of patients treated for upper abdominal tumors on the MR-Linac, all wearing a custom-made compression corset, which mitigates respiratory motion in the abdomen. We analyzed the 3D pancreatic tumor motion during irradiation in **Chapter 4**. For every fraction, the tumor motion was extracted from the 2D cine MR images using deformable imaging registration. Using basic signal processing, the motion patterns were separated into the (periodic) respiratory and (non-periodic) drift components.

We found that respiratory amplitudes during treatment were small, and the amplitude of individual patients varied little over their treatment course. Tumor drifts were small as well, with no large systematic displacements observed. These results confirm that the current safety margins that account for intrafraction motion are sufficient for a safe treatment delivery, and that the abdominal corset is a simple but effective method for motion mitigation.

Measurement of the intrafraction motion is only a first-order approximation of the safety and efficiency of a delivered treatment. In **Chapter 5**, we extended the method of the previous chapter by translating the measured motion into the delivered dose. This was done using the linac's delivery logs, which contain the dose being delivered for each time point during treatment. By translating each individual dose with the tumor displacement at the same time point, we can accumulate the dosimetric errors as a result of the intrafraction tumor motion. This results in a delivered dose, which can be compared to the originally planned dose. We performed this method for a new, larger set of patients. Alongside, we simulated a wide range of tumor motion scenarios to investigate the general influence of intrafraction motion on the delivered dose.

The motion measured in this new patient cohort was similar to the previous chapter, and the relatively small average amplitude and absence of large drifts meant that the delivered dose deviated little from the planned dose. The simulation study confirmed that respiratory motion can be quite large (>10 mm) before it starts having a meaningful impact on dose delivery. Tumor drift, on the other hand, can already lead to relevant dose errors when it is in the order of several millimeters.

The previous two chapters measured the tumor motion with standard, 2D cine MRI. The drawback of these images is that only two cross-sectional planes are available, with no 3D spatial information of the entire tumor and its surroundings. For **Chapter 6**, we developed a novel 3D cine MRI sequence that is able to perform volumetric imaging of the upper abdomen, at the same temporal resolution of the standard 2D cine MRI sequence. This 3D cine MRI scan has a much coarser resolution, but deformable image registration algorithms are still able to reliably extract tumor motion from these images. We again acquired these scans during beam-on of pancreatic tumor patients, and performed the same log-based dose accumulation as in the previous chapter. The extracted motion fields were also used in a simulation of various active motion mitigation strategies.

We found once again a modest dosimetric impact from intrafraction motion. A quality assurance check of the volumetric motion extracted from the low-resolution 3D cine images resulted a high degree of consistency within the high-dose region. This indicates that high-frequency, time-resolved 4D imaging and subsequent deformable dose accumulation is feasible on the 1.5 T MR-Linac. The simulation showed that most intrafraction motion, that had resulted in a larger difference between the planned and delivered dose, could have been resolved with simple baseline shifting.

So far, all treatments of pancreatic tumors on the 1.5 T MR-Linac have been ungated deliveries. This means that the radiation beam is continuously on, and while tumor motion can be visualized during treatment, it is not acted upon. In **Chapter 7**, we describe the first treatments on the 1.5 T MR-Linac with gating and baseline drift correction, performed for upper abdominal tumors. Gating means that the radiation beam is turned on or off based on the tumor position. In this case, the beam is only on when the patient has breathed out, and is turned off when the patient starts breathing in again, allowing for a potentially much more precise delivery. With the MR-Linac, we are able to measure this motion and couple this in real-time to whether the beam should be on or off. Any systematic tumor drifts during irradiation can be resolved with a baseline shift, where the remaining planned dose is shifted to match the new tumor position. For these first treatments with active motion management, we calculated the dosimetric advantage over a simulated ungated delivery. It was found that gating and baseline shifting indeed improved the congruence of the delivered dose to the planned dose, compared to the simulated treatment without motion management. This system is a prime demonstration of what the MR-Linac is capable of: real-time treatment intervention, based on the actual anatomical motion, without the need for internal fiducial markers. The baseline shifting functionality is a very welcome addition, as we have demonstrated in the previous chapter that this can resolve most dose-compromising drifts. It is also a critical component to maintain an efficient duty cycle.

To conclude, MR-guided radiotherapy has opened the way for a new, safe, local treatment for inoperable pancreatic cancer. The full potential of the MR-Linac, however, has been far from realized. MRI is an incredibly versatile tool that can be used in every facet of the online adaptive workflow, allowing us to gain more insight into the treatment and ultimately optimizing the planning and delivery. Ablative radiotherapy for pancreatic cancer with the 1.5 T MR-Linac is one of the most intricate procedures in external beam radiotherapy, and the ongoing developments will only further increase complexity. Therefore, the informal dissemination of clinical experiences and treatment techniques, as well as collaboration between MR-Linac centers, remains crucial for further advancement of radiotherapy for pancreatic cancer.



CHAPTER 9

General discussion and
future outlook

The MR-Linac is like a Swiss Army knife for radiotherapy. There is an incredible amount of new tools at our disposal, but it is not always clear how and when to put these to best use. Understandably, the first years after clinical introduction were spent gaining experience and confidence with the primary new tools such as online treatment adaptation with MRI. But just as one would not buy a Swiss Army knife and never use its scissors and nail file, the MR-Linac will only prove its full worth if we continue developing and exploiting both the obvious and subtle functionalities to improve treatment. The treatment of pancreatic cancer, an aggressive disease in a difficult place in the body, will probably benefit the most from these developments, allowing us to further decrease PTV margins and escalate dose.

In this final chapter, we will discuss the individual chapters within the broader context of this thesis. We conclude with some perspectives on how MR-guided radiotherapy for pancreatic cancer will further evolve in the coming years.

9.1. Imaging for online treatment adaptation

MR-guided radiotherapy has very specific requirements for MR imaging that can be quite different than in diagnostic radiology. If a scan is used for online delineation of the target and OAR, geometric fidelity (which is not always a given in the world of MRI) is the prime priority. After that, the most important quality is that the radiation oncologist can recognize and delineate the boundaries of the structures with ease, confidence, and speed. After all, this is the first step of the online adaptive process, and accurate delineations with low (inter and intra) observer variability are key to the effectiveness of the further technical developments like those presented in this thesis. Therefore, improving image quality for online treatment adaptation, and tailoring sequences to the specific tumor site of interest should be a continuous area of research in MR-guided radiotherapy.^{147–149}

The PROPELLER sequence from **Chapter 2** remains the prime candidate to be the next-generation MRI sequence for online adaptive planning. Its superior visual quality is obvious, it can be acquired out-of-the-box, and upcoming software updates will ensure geometric correction in 3D for this M2D scan. As for the large interslice variability problem, the best solution is probably acquiring this scan in exhale with a respiratory trigger, ensuring all slices are acquired in the same respiratory phase. While this will prolong acquisition time, the scan can be used in combination with the gating software described in Chapter 7, which can determine the transformation between the 3D scan and the desired gating envelope position in the 2D cine MRI. This way, the 3D scan can be acquired in any respiratory

state. As currently most pieces of the puzzle are either already in place, or are concretely planned for clinical implementation, this method can probably be adapted within the shortest time frame. An alternative solution involves respiratory correlated 4D-MRI, which can estimate a midposition anatomy based on internal registration of the individual respiratory phases.^{108,150} In CT-based radiotherapy planning, this is already an established method to create a midposition CT from 4D-CT.⁵⁷ A PROPELLER scan in exhale can then be warped to the midposition, and the treatment can be delivered without the requirement for gating. 4D-MRI typically has long acquisition times, but advanced sequences like MR-RIDDLE can make efficient use of the idle time by starting image reconstruction while acquisition is still in progress.¹⁵¹ Here, an expanding window in the undersampled k -space produces low-resolution 4D images in under a minute, which are already sufficient to reconstruct midposition motion fields. As acquisition continues, higher resolution images become available may be used to further upsample the warped midposition image.

9.2. Treatment planning

The MR-Linac has enabled ablative SBRT treatment planning with relative confidence, because of its superior visualization of the daily position of the target structures and the organs to be avoided. However, the final treatment plan is fully dictated by the institutional protocol for prescribed dose, safety margins, and - especially for pancreatic tumors - how one deals with organs so close to the tumor that dose coverage must be compromised. This latter consideration directly correlates with the amount of tumor coverage in case of dose-limiting anatomies, but is almost never reported in literature. This can lead to a situation where two institutions use the same protocol on the surface, but would create two very different treatment plans for a patient with unfavorable anatomy.

The global consensus protocol **Chapter 3** extends beyond the basic dosimetric parameters for prescribed dose, OAR constraints, and PTV margins. Technical planning details such as the number of segments and use of PRVs are also taken into account. Because pancreas SBRT involves steep dose gradients and complex anatomies, these parameters can be highly influential for the final treatment plan and must therefore be discussed and, where possible, harmonized. Granted, the consensus protocol was less strong on these parameters, but were generally accepted under the explicit condition that active motion management, as described in Chapter 7, would be in place. It is not surprising that the ability to "see what you treat, as you treat", with automatic beam gating in the event of unexpected motion, will increase one's confidence that these aggressive plans can be delivered without risking

serious adverse events. Future clinical outcomes from centers that employ this protocol can easily be collected from the prospective Multi-OutcoMe EvaluationN of radiation Therapy Using the MR-linac (MOMENTUM) study (NCT04075305).⁷⁴

Regardless of the protocol that is employed, future clinical studies on MR-guided pancreas SBRT should include the dosimetric characteristics of their treatments. This would provide an impression of the number of fractions with unfavorable anatomies, in which case the planned tumor coverage might be much lower than the prescribed dose according to the protocol. To be clear, clinical outcomes like local control are not *purely* dictated by the tumor coverage over the treatment course, but knowing whether the included patients received an average 30% or 99% of the prescribed dose is still very valuable information to judge to treatment efficiency. Moreover, because the treatment is online adaptive, the dosimetric characteristics are different every fraction. This information is lost if a trial only reports the intended dose, which is now almost exclusively the case. In contrast, the recent SMART trial¹⁷ reported, amongst other parameters, the GTV V_{50Gy} on a per-fraction basis for its patient population. The inclusion of such results is an admirable development and one would hope that future, large clinical trials follow suit.

9.3. Intrafraction motion: from monitoring to managing

Chapters 4 to 7 revolved around pancreatic tumor motion during irradiation as measured in real-time cine MRI. All patients in these chapters were wearing an abdominal corset to passively mitigate the respiratory motion in the upper abdomen.

In **Chapter 4**, we extracted the tumor motion from 2D interleaved coronal/sagittal cine MR images, which were continuously acquired during the entire beam-on time of each fraction. This allowed for better understanding and characterization of tumor motion compared to the conventional workflows, where motion is only assessed during the pretreatment phase in cine MRI⁸⁰ (with a limited time span) or in 4D-CT, which is known to underestimate motion^{152,153} and does not capture breathing irregularities.

This method was repeated for a new, larger set of patients in **Chapter 5**, and extended to translate the measured tumor motion into the delivered dose. This was done using linac machine log files, which can be converted into linac states that represent the dose being delivered in a certain time frame. This way, the tumor displacement measured during a single cine MRI frame (~ 350 ms) could be applied to the dose that was delivered when that displacement took place, a more realistic approach than convoluting (or "shaking") the

complete planned dose with all measured motion.^{139,154}

The 3D cine MRI developed in **Chapter 6** allowed for arguably the most physiologically realistic dose accumulation model in this thesis, incorporating volumetric deformations to the time-resolved approach of Chapter 5. However, it can be questioned whether sophisticated imaging like 3D cine MRI is necessary for tumor tracking and dose accumulation. It introduces additional uncertainties and the low-resolution approach means visual assessment is much more difficult. Meanwhile, the dosimetric results from Chapter 6 correspond once again to the previous chapters, indicating that 2D cine MRI might suffice for both tumor tracking and dose accumulation. Indeed, a major assumption of the dose accumulation as performed in this study is that the anatomy within the area of interest moves rigidly and in bulk, which would mean that 2D cine MRI-derived isocenter shifts would suffice for accumulating dose. Still, this demonstration of an out-of-the-box, highly accelerated, time-resolved 4D MRI sequence is both an example of both how far we can push beam-on imaging, and of how imaging should be tailored to its purpose. To elaborate, *intrafraction* deformable dose accumulation does not require high-resolution, high-contrast imaging (in fact, because interpolation is not required, deformable image registration might even benefit from a natively isotropic sequence!) and one can work under the assumption that motion fields are spatially smooth. This latter assumption means that intrafraction motion fields can be validly upsampled¹¹³ without loss of physiological realisticness. As examples of other practical applications, this 3D cine MRI sequence might be used as a quick, secondary check for pre-beam respiratory-correlated 4D-MRI motion fields used for deriving a high-resolution mid-position. First-order quality assurance like this will be important to validate 3D motion fields in clinical use, as there is no ground truth for in-vivo deformable image registration.

The beam gating system described in **Chapter 7**, based purely on real-time MRI tracking without the need for fiducial markers or other surrogates, is a prime demonstration of the promises of MR-guided radiotherapy. The baseline shifting functionality is a very welcome addition, as we have demonstrated in Chapter 6 that this can resolve most dose-compromising drifts. It is also a critical component to maintain an efficient duty cycle. The previous chapters have demonstrated that for tumors with small amplitudes, respiratory motion will generally not lead to large dosimetric errors. It can therefore be argued that these treatments could be delivered without gating and only baseline shifting to resolve drifts, maintaining a 100% duty cycle. However, even in these treatment automatic gating (with large envelopes) might still be desired as a safety fallback in case of unexpected motion (e.g. coughing or repositioning).

Finally, one might ask oneself: can we lose the abdominal corset, now that we can mitigate respiratory motion with gating? A personal recommendation would be: no. We have seen that abdominal compression can reduce the respiratory amplitude enough that the tumor stays within the gating envelope for most of the time, whereas no compression would lead to the beam being gated almost every respiratory cycle. Abdominal compression is therefore a simple and well-tolerated strategy to increase the duty cycle. Aside from aiding treatment delivery, it is also beneficial for delineation MRI image quality by reducing motion artifacts. Other approaches like visual biofeedback^{139, 145, 146, 155} might be attractive alternatives, because they also permit breath holding for a longer, and more reproducible gating window. Once biofeedback systems are in place on the MR-Linac, a comparison with abdominal compression will therefore be quite interesting, especially with regards to patient tolerability.

9.4. Future outlook

The full potential of MR-guided radiotherapy for the treatment of pancreatic cancer has been far from realized, but armed with the knowledge of this thesis, we have a clear view of the directions we will and should take. In this final section, we will delve into the most interesting and promising developments for next-generation MR-guided radiotherapy. Some of these advancements will not just improve the treatment of pancreatic cancer specifically, but also radiotherapy in general. Fig. 9.1 provides a graphical summary of this section.

9.4.1. The clinical perspective

In a recent review, Daamen et al.¹⁹ collected both retrospective and prospective clinical outcomes of sixteen studies on MR-guided radiotherapy for pancreatic cancer. Various dose levels were used, but almost all studies contained at least one cohort that received ablative levels with BED₁₀ of at least 100 Gy. The minimal acute toxicity rates establish MR-guided SBRT as a well-tolerated and safe treatment modality. As for treatment efficiency, the nine studies reporting one-year local control after treatment demonstrate promising rates of 79% to 98%.^{43, 67, 156–162} However, the clinical evidence supporting these figures is lacking. Most of these studies were retrospective, described very heterogeneous populations, and combined radiotherapy with various combinations of chemotherapy and surgery. Strong, definite evidence for local control will be provided in (ongoing) randomized clinical trials, with a standardized follow-up. Nevertheless, we can definitely speculate about a future where the results of these trials are comparable to the clinical evidence currently available.

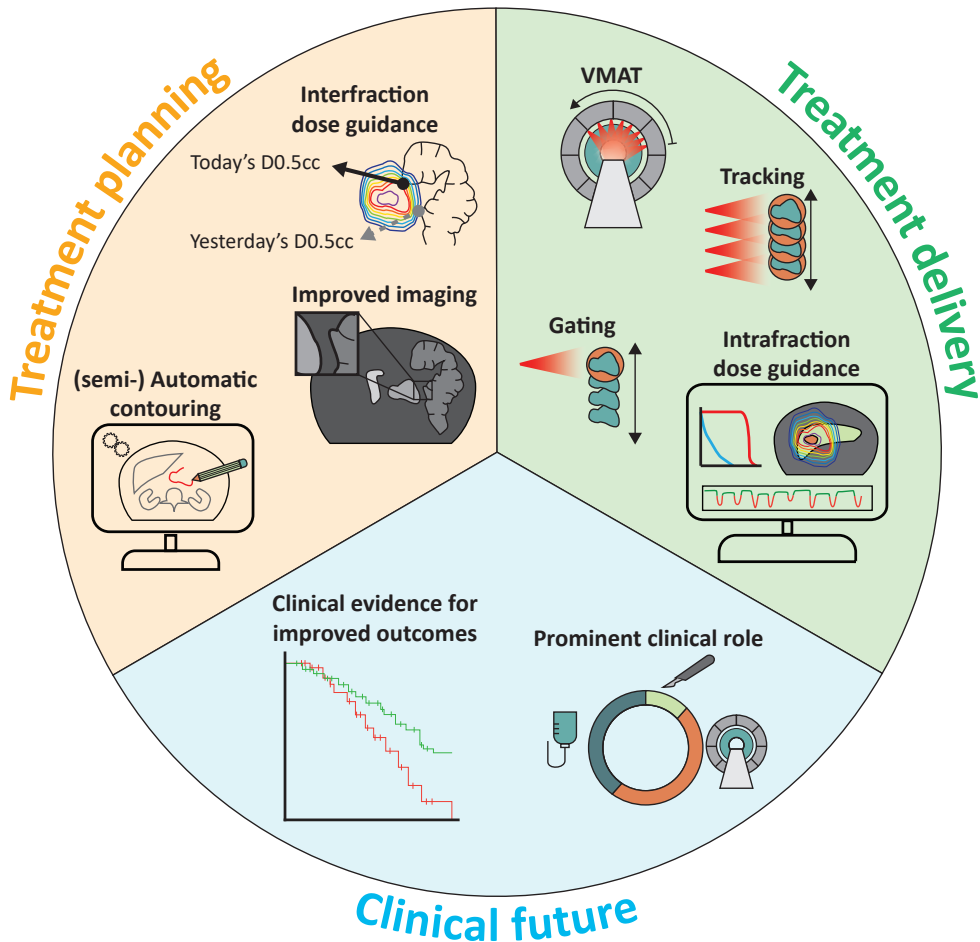


Figure 9.1.: MR-guided radiotherapy for pancreatic cancer in 2028: an overview of some of the future developments that are discussed in this last section.

In such a scenario, there is no doubt that MR-guided SBRT will join the standard treatment arsenal for pancreatic cancer, and other tumors in and around the pancreas. For operable pancreatic adenocarcinoma, surgery will most likely remain the primary treatment because it still offers a chance of disease cure. However, given the fact that disease recurrence occurs in almost all patients after surgery,⁷⁵ and the procedure carries a high mortality and complication rate,^{163,164} MR-guided SBRT may very well become the standard second-line treatment for early-stage pancreatic cancer. Elderly or frail patients could greatly benefit

from MR-guided SBRT as a palliative treatment, prescribed with the intent to prolong life expectancy and reduce symptoms of local tumor destruction. Looking further ahead, MR-guided SBRT might even be given upfront for resectable cases, followed by a watch-and-wait strategy, with the option for salvage surgery in case of progression. Functional, quantitative MRI metrics like ADC, which we can measure "for free" during MR-guided treatments, might aid here in assessing response to radiotherapy. However, motion distortion and the inferior MRI hardware means that reliable biological imaging on the MR-Linac remains challenging. These challenges need to be addressed thoroughly and critically before we can look into a possible predictive relationship.¹⁶⁵

There are also other pancreatic tumor types, of a less aggressive nature than adenocarcinoma, for which MR-guided SBRT might much sooner be considered a serious alternative to (immediate) surgery. Two examples are pancreatic neuroendocrine tumors (pNETs) and pancreatic oligometastases of renal cell carcinoma. Both tumor types, especially pNETs, are relatively slow growing tumors, but currently the only treatment options are pancreatic resection or chemotherapy. For these settings, there are ongoing investigations to determine whether MR-guided SBRT can delay surgery or systemic therapy.^{166,167}

MR-guided radiotherapy will have the largest impact on patients that are no longer operable, which is by far the largest part of all pancreatic cancer diagnoses.² The standard treatment for this patient group is systemic therapy (even for localized cases), which comes with a substantial toxicity burden. Considering the importance of maintaining quality of life in this patient group, who generally have a very poor life expectancy, there is a very viable argument to give upfront low-toxic, local, and effective MR-guided SBRT. Early studies on patient-reported outcomes indicate a stable quality of life after MR-guided SBRT.^{18,159,162} This last point brings us to the role that CBCT-guided radiotherapy might still play in future treatment of pancreatic cancer, which might not be confined to MR-guided systems after all. Cone-beam guided adaptive radiotherapy has only just begun to emerge,^{168,169} and clinicians may be hesitant to prescribe the ablative dose levels on these systems. However, short-course, non-ablative radiotherapy can effectively relieve pancreatic cancer-related pain, as demonstrated by a recent trial.¹⁷⁰ This would be a relatively cheap and accessible palliative treatment, deliverable with conventional linacs, and which may benefit a large part of the pancreatic cancer population.

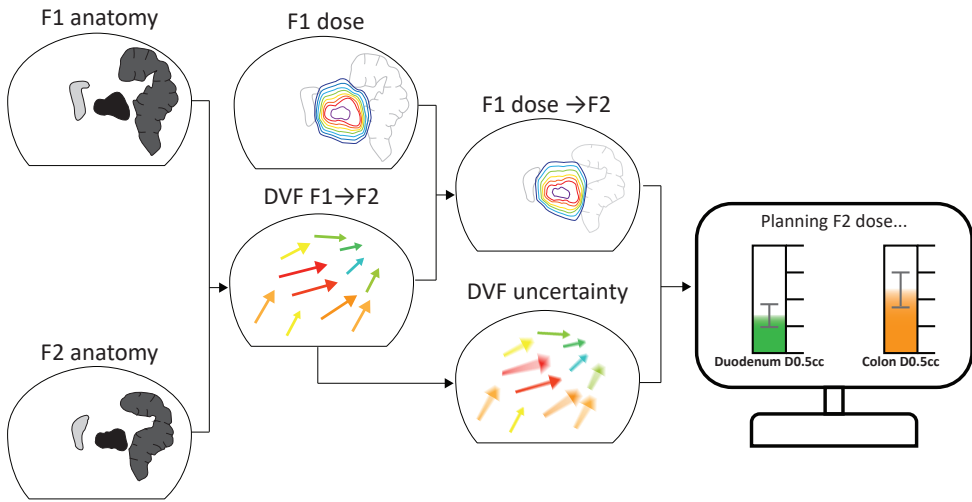


Figure 9.2.: A proposed workflow for interfraction dose warping for prospective treatment guidance. Imaging acquired at the start of each fraction is deformably registered to the imaging of the previous fraction. The resulting deformation vector field (DVF) is used to warp the planned (or delivered!) dose of the previous fraction onto the anatomy of the current fraction. Along with some underlying local uncertainty of the DVF, this can be taken into account when planning of the current fraction's dose. Here, this is envisioned as a user interface where the dose of the previous fraction is displayed as the usual DVH parameters of some OARs.

9.4.2. Deformable image registration and dose accumulation

Before the era of MR-guided radiotherapy, many considered dose accumulation infeasible due to lack of accurate and validated image registration algorithms.¹³⁰ Considering the growing body of literature, focus groups, and vendor involvement, the MR-Linac has clearly rekindled this interest.³²

The work in this thesis mainly revolved around retrospective intrafraction dose accumulation. Prospective intrafraction dose accumulation will be discussed in the final section of this chapter on real-time adaptive radiotherapy. For now, we will mainly focus on the thus far not touched upon *interfraction* dose accumulation, and its future applicability and considerations within the context of pancreatic cancer.

Interfraction dose accumulation is where the dose of previously delivered fractions is deformably projected onto the anatomy of the next fraction. This can be done in a prospective sense, to "guide" dose calculation of upcoming fractions, but also retrospectively, to evaluate the delivered dose over a complete treatment course, taking into account anatomical deformations between fractions. Since the link between the *delivered* dose and clinical outcome is

the foundation of radiotherapy, the information that can be inferred from interfraction dose accumulation is potentially extremely valuable. The holy grail would be a direct correlation between accumulated tumor coverage and local control time, and between accumulated OAR dose and toxicity rate.

Online adaptive MR-guided radiotherapy means that a new treatment plan is created for every fraction, and we are no longer forced to assume the worst-case scenario that the OAR hotspot or GTV coldspot is located in the same anatomical position every day. As always, it is important to determine to which degree a complex calculation like deformable dose accumulation can have a clinically relevant advantage over a simpler method like DVH summation. For example, the position of the duodenum is typically closely coupled to the tumor, due to ingrowth or presence of fibrotic tissue. Therefore, the duodenal hotspot is unlikely to change position over the treatment course either, and deformable dose accumulation will result in the same value as DVH summation. On the other hand, organs like the small bowel are much more motile and might benefit more from deformable dose accumulation.

How should we incorporate interfraction dose accumulation into the clinical workflow? The accumulated dose from previous fractions might be automatically incorporated as a bias dose for the optimizer, to locally increase the dose to underdosed areas or decrease the dose to overdosed areas ("dose repair"). A more pragmatic, less black-box, and informative approach might be simply displaying the remaining dosimetric "bandwidth" of the target and OARs as DVH parameters to the operator. If, say, the warped dose would indicate that the OAR hotspots are in a very different anatomical location for the upcoming fraction, a more permissive treatment plan could be created. This would allow more dosimetric freedom, potentially increasing the total possible tumor dose in unfavorable anatomies or dose-escalated treatments. An envisioned workflow for this process is illustrated in Fig. 9.2.

This all assumes that we can confidently perform dose accumulation, but these complex techniques will always have an underlying uncertainty. Quantification of this uncertainty will be a crucial part of any dose accumulation algorithm before clinical implementation, but this is still very much an open problem in the field.¹³¹⁻¹³⁷ Most uncertainty metrics are dominated by the spatial uncertainty of the underlying deformation vector field, which makes sense: the sharp gradients in pancreas MRgRT treatment plans can turn a misregistration of only a few millimeters into a dosimetric error of several Gray. In contrast to image gray values, dose is a physical quantity and how it is transformed by deformation vectors is not a trivial matter. Especially in interfraction dose accumulation, this becomes not just a geometrical but also a radiobiological problem. How do deal with growing, shrinking, appearing, or disappearing

tissue? For this reason is intrafraction dose accumulation a more accessible feat, because the anatomical changes on these timescales are much less drastic. Prof Dr Wolfgang A. Tomé made precisely this argument in a 2012 debate on deformable dose accumulation: "*[I]deally one would acquire anatomical image information and record the machine state and dose delivery status at time points during the delivery. This information could then be used, employing deformable dose accumulation across image sets that are highly correlated, to arrive at a more accurate estimate of dose received for both the target and organs at risk for a given fraction.*".¹³⁰ Indeed, this is exactly what is now possible on the MR-Linac as demonstrated in Chapter 6 and other studies on intrafraction dose accumulation.^{102,171} Going back to interfraction dose accumulation and uncertainty quantification, we should once again ask ourselves how to incorporate this in clinical practice. Because dose is a local phenomenon, uncertainty should be quantified on a voxel-by-voxel basis as well. However, we should probably not bother clinical staff with maps of Jacobian determinants or vector curls. Simpler approaches like a standard deviation on top of the well-known DVH parameters come to mind.

Lastly, we should be critical of the imaging from which we extract the interfraction motion. A good creed is that one should tailor the imaging to its specific purpose, a freedom we can permit ourselves due to the versatility of MRI. Instead of just registering the 3D T_2w scans used for delineation, we could also acquire a separate sequence that is optimized for obtaining the deformation field with respect to a reference fraction. Going back to interfraction dose warping, Fig. 9.3 illustrates an attempt to develop a sequence that would allow gradient-based DIR algorithms like EVolution to track bowel displacement between fractions. The resulting deformations could be used to warp the dose and keep track the small bowel hotspot in every fraction. A sequence like this would probably result in a much lower uncertainty in accumulated bowel dose than if the standard 3D T_2w sequence was used for this purpose.

9.4.3. Accelerating treatment

The plethora of innovations postulated in this thesis and this future outlook have pushed or will push us further towards what is becoming the one of the most problematic bottlenecks of treatments on the MR-Linac: time. Compared to surgery and chemotherapy, MR-guided radiotherapy is by far the least burdensome treatment of pancreatic cancer, but unfortunately there are still patients unable to complete treatment due to discomfort. A rule of thumb for the maximum on-table time is one hour, which can be already difficult to sustain for

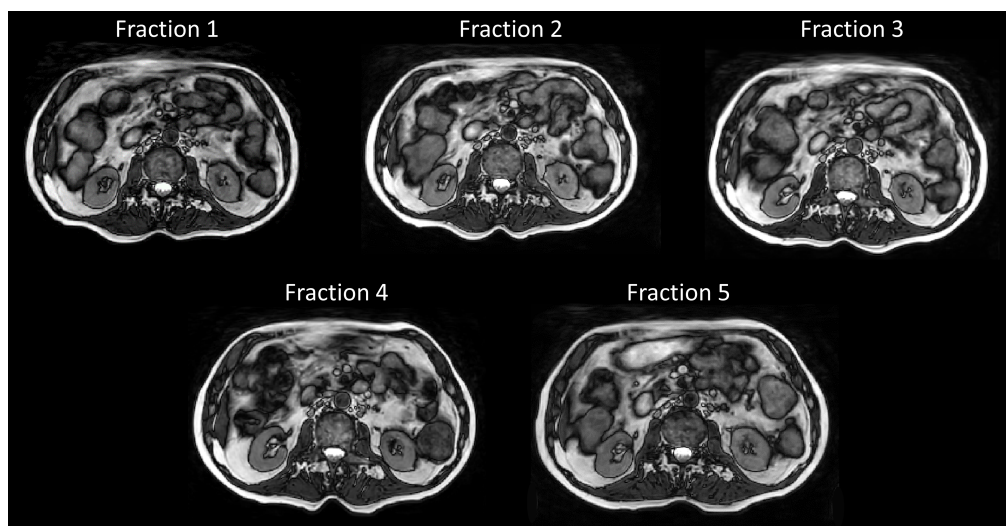


Figure 9.3.: A balanced gradient echo sequence designed specifically for tracking bowel structures and edges, for the purpose of interfraction dose warping. This sequence heavily exploits the phase cancellation artifact, where voxels containing an equal amount of water and fat results in a dark outline at organ boundaries. The interfraction bowel motility is well visible in these images.

relatively healthy individuals*. In our clinic, completing a fraction within 45 minutes is currently a feasible goal, with an extra 15 minutes for unforeseen delays like a second recontouring or technical issues during irradiation. However, such time frames are mainly achieved through experience and patient volume; clinics starting out with pancreas MRgRT may often exceed the hour mark per fraction. Furthermore, many of the expected future developments discussed here will only further prolong treatment time, most notably gating (due to decreased duty cycle during delivery) and dose escalation (due to an increased number of MUs for a treatment plan). It is therefore essential that we investigate how we can accelerate every part of the workflow.

As said before, the most time consuming step is online contour adaptation. A highly investigated solution is automatic contouring with deep learning,¹⁷² improving speed and quality over contours warped with deformable image registration. A challenge with autocontouring in general is the trust needed in the generated contours. The experience that if these contours are produced by a black box, "computer says so" algorithm, they are often subject to extensive manual fine tuning even if these adjustments are dosimetrically irrelevant. This would negate the achieved time advantage. One could imagine an autocontouring algorithm

*The author is speaking from personal experience.

that only allows adjustment of the high-dose area; there is already a lot of potential to save time if the large, out of field organs can confidently be contoured completely automatically. For the more important target and OAR contours, which require a higher degree of precision and stricter visual verification by the clinical staff, the automatically generated contours could come with some kind of local uncertainty metric like in the abovementioned interfraction dose accumulation workflow.

A higher confidence in automatically generated contours will also decrease existing interobserver variation, which is known to be substantial for online adaptive pancreas MRgRT.^{71,72} It is important to consider this interobserver variation within the context of Chapter 3, as it will probably degrade the achieved harmonization for treatment planning. Keeping this in mind, one can imagine that autocontouring could improve plan quality in many ways, some more subtle than others.

Finally, as we continue to escalate doses, we must also look into ways to accelerate treatment delivery. The dose rate of the 1.5 T MR-Linac is inherently limited due to its construction. Because the 7 MV linac is located outside the magnet, its source-axis distance is much larger than CBCT-linacs, and the beam must also pass through the cryostat. Perhaps the next-generation of MR-Linacs can be equipped with a higher photon energy. For now, we could also look towards volumetric modulated arc therapy (VMAT) which is currently being developed on the 1.5 T MR-Linac.^{173,174} VMAT has shorter delivery times than IMRT on conventional linacs, but the MR-Linac's gantry rotation and leaf travel are fast enough that there is not much time gain in practice. This does not mean that we should not strive for MR-guided VMAT in clinical practice, as it will still lead to more conformal dose distributions while maintaining target coverage, which is especially important for the case of pancreatic cancer.

9.4.4. Real-time adaptive MR-guided radiotherapy: *sic itur ad astra?*

One of the most anticipated long-term goals of the MR-Linac is the ability to adapt the treatment beam based on real-time online imaging.^{138,142,143} Here, "real-time" means that an MLC shift or reshape, triggered by an anatomical event (respiratory motion, drift, bulk shift) is applied so quickly that when the adaptation is completed, the anatomical state is still sufficiently close to the moment the adaptation was triggered. The biggest challenge here is that the motion has to be tracked with MRI, a notoriously slow imaging modality. Beyond that, it has to be ensured that the tracked motion is accurate, and the MLC has to be adapted

in the right way. An often cited rule of thumb is that to compensate for respiratory motion, the maximum time budget for this entire image-track-adapt cycle is 500 ms. Over the last years, many promising attempts have been made to unify MRI with real-time adaptation.¹⁷⁵ Here, we see again an interesting role for deep learning, as trained neural networks are one of the fastest known methods able to accurately infer a very large amount of information like volumetric motion fields¹⁷⁶ and accompanying uncertainties¹⁷⁷ from very minimal MRI data.

This thesis already introduced gating, which could be classified as real-time adaptive RT, since the gating decision is based on real-time cine MRI and is built upon a constant feedback loop between the linac and the imaging system. However, gating does not change the beam shape or position, so one can argue that it cannot be considered *adaptive*. This is different with tumor tracking or trailing. In tumor tracking, the beam is continuously following the latest tumor position as detected in real-time imaging.^{174,178} Tumor trailing is a low-pass filtered version of tracking, where the beam only follows the average position over the last few respiratory cycles.¹¹⁹ The theory of trailing is that it is dosimetrically not that important to track the tumor through the entire respiratory cycle, but irradiating the average position would negate the much more detrimental effects of drift or shifts. This is supported by the analyses in the second part of this thesis. It is important to realize that tracking and trailing have a 100% duty cycle, overcoming the time disadvantage of a gated delivery, and are therefore more probable long-term solutions to intrafraction motion than gating. More importantly, with perfect MLC tracking the positional uncertainty of the target at *any* point during treatment is zero (even in this hypothetical scenario, a small margin would still be needed to account for the beam penumbra), making real-time tracking the most probable path towards further margin reduction.

Finally, let us revisit dose accumulation, but now in the intrafractional setting. If this is performed in a prospective sense, treatment is adapted during irradiation in such a way that it will result in the optimal delivered dose, rather than the optimal geometric position like in tracking or trailing. Aside from continuous monitoring of tumor motion, we now also need to calculate its dosimetric impact on the fly, as well as estimate the beam adaptation that would result in the remaining dose being delivered as close as possible to what was planned. Now, the delivery sequence is not just updated prior to, but also *during* treatment. This concept is called intrafraction dose-guided radiotherapy.

Shortly before clinical introduction of the 1.5 T MR-Linac, the technical feasibility of such a system was already presented.⁸² A new treatment planning system called Adaptive Sequencer (ASEQ) that can handle intrafraction plan adaptation was developed in the

years before.^{179,180} In the proof-of-concept, inter-beam IMRT replanning was performed during simulated kidney SBRT, taking into account the 3D anatomical deformations and accumulated dose. Intrafraction dose-guidance has also been demonstrated in silico on conventional linacs during liver SBRT¹⁸¹ and prostate VMAT.¹⁸² In its ultimate form, the treatment is adapted not just between beams but in real-time: a continuous feedback loop that captures the complete 3D deformation, calculates its dosimetric impact, reoptimizes the treatment plan for the remaining dose and updates the current MLC shape and weight accordingly. By far the biggest challenge here would be the extremely short time window for dose calculation and optimizing. But one can wonder whether dose-guidance would actually need to be in real-time. With tracking, even a slight latency would risk severe dosimetric errors. This is less so with trailing or baseline shifting, but these strategies only result in a *geometrically* optimal MLC update. Dose-guidance, on the other hand, takes into account the accumulated dose before any adaptation and would therefore aim to "repair" underdosed areas, if a tumor drift has occurred that has not immediately been acted upon. Developments like these should be followed with great interest, as their central goal reflects the foundation of radiotherapy: getting the right dose in the right place.

Appendix

Nederlandse samenvatting

Alveesklierkanker is een van de dodelijkste kankersoorten, en effectieve en veilige behandeling blijft een uitdaging. Vanwege het agressieve ziektebeloop komt slechts een klein deel van de patiënten in aanmerking voor tumorresectie, een complexe en risicovolle operatie. Patiënten die niet meer geopereerd kunnen worden — de overgrote meerderheid van de alveesklierkankerpatiënten — worden behandeld met systeemtherapie, ook in de gevallen waarbij de ziekte nog gelokaliseerd is. Radiotherapie, een niet-invasieve, lokale behandeling met een veel lagere toxiciteit dan chemotherapie, is recent opgekomen als een complementaire of alternatieve behandeloptie voor inoperabele alveesklierkanker.

Radiotherapie wordt van oudsher gezien als een ineffektieve behandeling voor alveesklierkanker. Conventionele radiotherapietoestellen zijn uitgerust met kegelbundelcomputertomografie (*cone-beam computed tomography*, CBCT), een type beeldvorming met zeer slecht contrast in de bovenbuik. Op CBCT-scans kan de precieze locatie van de tumor en het omliggende gezonde weefsel niet goed worden bepaald op het moment van de behandeling. De bestralingsdosis wordt daarom op zeer conservatieve wijze afgegeven, verspreid over vele behandel fracties, zodat de dosis beperkt kan blijven in de vele stralingsgevoelige darm- en vaatstructuren in de bovenbuik. Helaas betekent dit dat de tumor zelf ook een beperkte stralingsdosis krijgt, met als gevolg weinig tot geen therapeutisch effect.

Een veel preciezere behandeling is mogelijk met de MR-Linac. De MR-Linac combineert een radiotherapieversneller (*linear accelerator*, linac) met kernspintomografie (*magnetic resonance imaging*, MRI). Op MRI-scans zijn alveeskliertumoren en de omliggende, gezonde organen bijzonder goed zichtbaar, veel beter dan op CBCT. Met de MR-Linac kan een nieuwe MRI-scan gemaakt aan het begin van iedere behandel fractie, zodat de behandeling kan worden aangepast aan de anatomie van dat moment. Deze zogenoemde MRI-geleide, online adaptieve methode neemt de onzekerheid weg over de locatie van de gezonde organen, waardoor alveesklierkanker behandeld kan worden met stereotactische radiotherapie (*stereotactic body radiotherapy*, SBRT). SBRT wordt gekenmerkt door complexe dosisplannen, met steile dosisgradiënten en een veel hogere tumordosis, die wordt afgegeven in veel minder fracties. De eerste klinische resultaten suggereren dat MRI-geleide SBRT de tumor langer

onder controle houdt dan conventionele radiotherapie, en daarmee de klinische uitkomsten op betekenisvolle wijze verbetert.

De MR-Linac kan niet alleen vlak voor, maar ook *tijdens* de bestraling beelden maken. We kunnen dit gebruiken om orgaan- en tumorbeweging door bijvoorbeeld ademhaling en afzakking in kaart te brengen. Deze intrafractiebeweging verstoort de dosis die oorspronkelijk gepland was, en door het te meten kunnen we nadien afschatten wat voor dosis er uiteindelijk is afgegeven.

Het doel van dit proefschrift was om de nieuwe mogelijkheden van de MR-Linac verder te benutten om de behandeling van alvleesklierkanker te verbeteren. Dit proefschrift bevat technische ontwikkelingen voor het plannen (**Deel I**) en de uitvoering (**Deel II**) van radiotherapie voor alvleesklierkanker op de 1.5 T MR-Linac.

De MRI scan die aan het begin van iedere behandel fractie wordt gemaakt, en waarop de behandeling wordt aangepast, gebruiken meestal sequenties met driedimensionale cartesische bemonstering van de k -ruimte. De voornaamste voordelen voor radiotherapie zijn dat dit soort scans een kleine plakdikte hebben, en dat ze geometrisch volledig gecorrigeerd kunnen worden. Het grootste nadeel is dat ze gevoelig zijn voor vervagingsartefacten door ademhalingsbeweging, waardoor het intekenen van alvleeskiertumoren minder precies wordt. In **Hoofdstuk 2** onderzochten we twee geavanceerde MRI sequenties, PROPELLER en 3D Vane. Deze sequenties gebruiken radiële bemonstering, waardoor de beelden veel scherper zijn en minder gevoelig voor beweging. Voor dit onderzoek werden deze scans opgenomen tijdens alvleesklierkankerbehandelingen op de MR-Linac, samen met de standaard, 3D cartesische T_2 -gewogen (T_2w) scan. De drie sequenties werden zowel kwantitatief vergeleken, met verschillende maten voor beeldkwaliteit, als kwalitatief, door ze te laten scoren door drie radiotherapeut-oncologen.

Zowel de kwantitatieve als de kwalitatieve resultaten lieten zien dat de PROPELLER scans minstens net zo goed zijn als de 3D T_2w scans. De PROPELLER scans waren binnen het axiale vlak inderdaad scherper, met minder vage grenzen tussen tumor en organen, maar de multi-slice 2D opnamemethode resulteerde in grote anatomische verspringingen van plak naar plak. Dit was de voornaamste reden dat PROPELLER niet als beter werd beschouwd dan 3D T_2w MRI. Als dit probleem opgelost wordt, moeten we serieus overwegen om PROPELLER scans te gebruiken voor het online intekenen van de bovenbuik. De 3D Vane scans werden unaniem beschouwd als niet geschikt voor online intekenen, vanwege het exotische T_2/T_1 -contrast; T_2 -weging wordt meestal beschouwd als het beste contrast voor de bovenbuik.

De MR-Linac heeft ervoor gezorgd dat we SBRT-behandelingen met relatief veel zelfvertrouwen kunnen plannen, dankzij de verbeterde beeldvorming van de dagelijkse positie van het doelgebied en de organen die we moeten vermijden. Het plannen van SBRT-behandelingen kan echter vrij complex zijn, en hangt af van veel variabelen die voornamelijk bepaald worden door het institutionele protocol, voor bijvoorbeeld de voorgeschreven dosis en veiligheidsmarge. Bovendien liggen de organen in de bovenbuik vaak zo dicht tegen de tumor aan, dat het niet ongebruikelijk is om een deel van de tumordosis op te offeren. Dit leidt tot nog complexere plannen bij SBRT voor alveesklierkanker. Voor **Hoofdstuk 3** werd een consortium gevormd van dertien centra over de hele wereld, die momenteel of in de nabije toekomst alveesklierkanker behandelen met de 1.5 T MR-Linac. De behandelplanvariatie binnen dit consortium werd vastgelegd, en een consensusprotocol werd vastgesteld om deze variatie te harmoniseren.

Een project met meerdere fasen werd opgezet, waarin ieder centrum een behandelplan moest maken voor twee voorbeeldcasussen van alveesklierkanker, volgens een steeds meer omvattende instructies. Na iedere fase werden de resultaten vergeleken en besproken, en werden de instructies voor de volgende fase vastgesteld. Na de derde fase was de dosimetrische variatie tussen alle plannen dusdanig klein dat het consensusprotocol kon worden vastgesteld. Dit protocol representeert een overeenkomst tussen de dertien centra over de aanbevolen manier om alveesklierkanker te behandelen met de 1.5 T MR-Linac. We hopen dat we met dit werk de behandelkwaliteit verbeteren, maar ook dat we beter de klinische uitkomsten kunnen vergelijken. Bovendien kan dit protocol centra wegwijs maken die willen beginnen met deze complexe behandeling.

Beweging door ademhaling en afzakking is een van de grootste oorzaken van onzekerheid bij radiotherapie van alveeskliertumoren. De MR-Linac kan continu beelden maken tijdens bestraling, dankzij zogenaamde cine MRI sequenties met een temporele resolutie die hoog genoeg is (< 500 ms) om ademhaling te visualiseren. Deze snelheid gaat ten koste van het ruimtelijke bereik: cine MRI is meestal beperkt tot een enkel 2D vlak. Tijdens scannen kan dit constant gewisseld worden tussen het coronale en sagittale vlak, waardoor we de 3D beweging van de tumordoorsnede in kaart kunnen brengen. Deze sequentie werd gemaakt tijdens de gehele tijd dat de bundel aan stond bij de behandeling van patiënten met bovenbuiktumoren op de MR-Linac. Deze patiënten droegen allen een op maat gemaakt compressiekorset, waarmee de ademhaling in de buik beperkt blijft. We analyseerden de 3D beweging van de alveeskliertumor in **Hoofdstuk 4**. Van iedere fractie werd de tumorbeweging uit de 2D cine MRI scans gehaald door middel van deformable beeldregistratie. Met behulp van

simpele signaalverwerkingstechnieken konden we de beweging scheiden in de (periodieke) ademhalingscomponent en de (niet-periodieke) afzakingscomponent.

We zagen dat ademhalingsamplitudes klein waren, en dat per patiënt zijn of haar ademhaling niet veel varieerde over de verschillende fracties. Tumorafzakking was ook redelijk beperkt, en we zagen geen grote systematische verplaatsingen. Deze resultaten tonen aan de huidige veiligheidsmarges, om voor deze intrafractiebeweging te compenseren, genoeg zijn voor een veilige behandeling. Het abdominale korset is een simpele maar effectieve manier om beweging te beperken.

Het meten van intrafractiebeweging is slechts een eerste-ordebenadering van de veiligheid en effectiviteit van een afgegeven behandeling. In **Hoofdstuk 5** hebben we de methode van het vorige hoofdstuk uitgebreid door de gemeten beweging te vertalen in de afgegeven dosis. Dit werd gedaan met de logbestanden van de linac, die bijhouden welke dosis werd afgegeven op ieder tijdstip van de behandeling. Door iedere losse dosis te verplaatsen met de beweging die op datzelfde tijdstip is gemeten, kunnen we de onnauwkeurigheden als gevolg van de intrafractietumorbeweging accumuleren. Dit resulteert in een afgegeven dosis, die vergeleken kan worden met de oorspronkelijk geplande dosis. We voerden deze methode uit voor een nieuwe, grotere patiëntengroep. Tegelijkertijd simuleerden we een veelvoud aan tumorbewegingen om de algemene invloed van intrafractiebeweging op de afgegeven dosis te kwantificeren.

De beweging die gemeten is in dit nieuwe patiëntencohort was vergelijkbaar met het vorige hoofdstuk. De relatief kleine ademhaling, en het wegblijven van grote afzakkingen, betekende dat de afgegeven dosis niet veel verschilde van de geplande dosis. De simulaties bevestigden dat ademhalingsbeweging vrij groot kan zijn (> 10 mm) voordat het een problematisch effect gaat hebben op de afgegeven dosis. Aan de andere kant kunnen enkele millimeters afzakking van de tumor al leiden tot grotere dosimetrische fouten.

In de vorige twee hoofdstukken hebben we tumorbeweging gemeten met standaard, 2D cine MRI. Het nadeel van deze beelden is dat het slechts twee doorsnedes zijn, en er geen driedimensionale informatie is van de gehele tumor en omgeving. Voor **Hoofdstuk 6** ontwikkelden we een 3D cine MRI sequentie die volumetrisch de bovenbuik kan scannen, met een vergelijkbare temporele resolutie met de standaard 2D cine MRI. Deze 3D cine MRI scan heeft wel een veel grovere resolutie, maar algoritmes voor deformable beeldregistratie kunnen hier nog steeds betrouwbare tumorbeweging uit halen. We namen deze scans wederom op tijdens de behandeling van alvleesklierkankerpatiënten, en voerden dezelfde dosisaccumulatie uit als het vorige hoofdstuk, op basis van de logbestanden. De bewegingsvelden werden ook

gebruikt voor het simuleren van verschillende methoden om beweging actief te compenseren. We zagen wederom een beperkte invloed van intrafractiebeweging op de afgegeven dosis. Een kwaliteitcheck van de volumetrische beweging, die gemeten is in de lage resolutie 3D cine MRI beelden, toonden een hoge mate van consistentie aan in het hoge-dosisgebied. Dit laat zien dat hoogfrequente, tijdsgetrouwe 4D beeldvorming, en daaropvolgende deformabele dosisaccumulatie mogelijk zijn op de 1.5 T MR-Linac. De simulaties toonden aan dat de meeste intrafractiebeweging, die had geleid tot grotere verschillen tussen geplande en afgegeven dosis, opgelost hadden kunnen worden met eenvoudige baselinecorrecties.

Tot dusver zijn alle behandelingen van alveeskiertumoren op de 1.5 T MR-Linac niet-gegate behandelingen. Dit betekent dat de stralingsbundel constant aan staat, en ook al kunnen we tumorbeweging in kaart brengen tijdens de behandeling, er wordt niet op geacteerd. In **Hoofdstuk 7** beschrijven we de eerste behandelingen op de 1.5 T MR-Linac met *gating* en afzakkingscorrectie, uitgevoerd voor bovenbuiktumoren. *Gating* betekent dat de stralingsbundel aan en uit wordt gezet afhankelijk van de tumorpositie. In dit geval wordt de bundel alleen aangezet als de patiënt uitgeademd heeft, en wordt weer uitgezet zodra de patiënt begint met inademen. Hierdoor kunnen we mogelijk een stuk preciezer bestralen. Deze beweging kan met de MR-Linac gemeten worden, en gelijk worden teruggekoppeld aan de linac om te bepalen of de bundel aan of uit moet staan. Ook kunnen systematische afwijkingen van de tumor tijdens het bestralen gecorrigeerd worden met een afzakkingscorrectie, waarbij de resterende dosis verschoven wordt naar de nieuwe tumorpositie. Voor deze eerste behandelingen met actieve bewegingscorrectie hebben wij het dosimetrische voordeel berekend ten opzichte van een gesimuleerde, niet-gegate behandeling.

Gating en afzakkingscorrectie zorgden er inderdaad voor dat de afgegeven dosis beter overeenkomt met de geplande dosis, wanneer vergeleken met de simulatie van een behandeling zonder deze actieve bewegingscorrectie. Dit systeem is een goed voorbeeld van wat mogelijk is met de MR-Linac: directe terugkoppeling tijdens de behandeling, op basis van de daadwerkelijke anatomische beweging, zonder gebruik te maken van implantaten. De afzakkingscorrectie is een welkome functionaliteit, omdat dit de grootste dosimetrische fouten door beweging kan corrigeren, zoals aangetoond in het vorige hoofdstuk. Het is ook een onmisbaar component om efficiënt te kunnen gaten.

Al met al heeft MRI-geleide radiotherapie de weg vrijgemaakt voor een nieuwe, veilige, lokale behandeling van inoperabele alveesklierkanker. De volledige mogelijkheden de MR-Linac zijn echter nog lang niet gerealiseerd. MRI is een ongelooflijk veelzijdig gereedschap dat ingezet kan worden bij iedere tussenstap van online adaptieve behandeling. Het stelt ons

in staat om meer inzicht te krijgen in de behandeling, en uiteindelijk het plannen en de uitvoeren daarvan te optimaliseren. Ablatieve radiotherapie voor alveesklierkanker met de 1.5 T MR-Linac is een van de meest ingewikkelde behandelingen in de radiotherapie, en de lopende ontwikkelingen zullen de complexiteit alleen maar doen toenemen. Het informeel uitwisselen van klinische ervaringen en behandeltechnieken, alsmede de samenwerkingen tussen centra met MR-Linacs, zijn daarom van het grootste belang voor de vooruitgang van radiotherapie voor alveesklierkanker.



Bibliography

- [1] Schrag, D. Optimizing treatment for locally advanced pancreas cancer: progress but no precision. *JAMA*, **315**(17):1837–1838, 2016. doi:10.1001/jama.2016.4284.
- [2] Latenstein, A. E., van der Geest, L. G., Bonsing, B. A., Koerkamp, B. G., Mohammad, N. H., de Hingh, I. H., de Meijer, V. E., Molenaar, I. Q., van Santvoort, H. C., van Tienhoven, G., et al. Nationwide trends in incidence, treatment and survival of pancreatic ductal adenocarcinoma. *Eur. J. Cancer*, **125**:83–93, 2020. doi:10.1016/j.ejca.2019.11.002.
- [3] Mizrahi, J. D., Surana, R., Valle, J. W., and Shroff, R. T. Pancreatic cancer. *Lancet*, **395**(10242):2008–2020, 2020. doi:10.1016/S0140-6736(20)30974-0.
- [4] Vincent, A., Herman, J., Schulick, R., Hruban, R. H., and Goggins, M. Pancreatic cancer. *Lancet*, **378**(9791):607–620, 2011. doi:10.1016/S0140-6736(10)62307-0.
- [5] Brahme, A. Optimization of stationary and moving beam radiation therapy techniques. *Radiother. Oncol.*, **12**(2):129–140, 1988. doi:10.1016/0167-8140(88)90167-3.
- [6] Bortfeld, T., Bürkelbach, J., Boesecke, R., and Schlegel, W. Methods of image reconstruction from projections applied to conformation radiotherapy. *Phys. Med. Biol.*, **35**(10):1423, 1990. doi:10.1088/0031-9155/35/10/007.
- [7] Liu, F., Erickson, B., Peng, C., and Li, X. A. Characterization and management of interfractional anatomic changes for pancreatic cancer radiotherapy. *Int. J. Radiat. Oncol. Biol. Phys.*, **83**(3):e423–e429, 2012. doi:10.1016/j.ijrobp.2011.12.073.
- [8] Krishnan, S., Chadha, A. S., Suh, Y., Chen, H.-C., Rao, A., Das, P., Minsky, B. D., Mahmood, U., Delclos, M. E., Sawakuchi, G. O., et al. Focal radiation therapy dose escalation improves overall survival in locally advanced pancreatic cancer patients receiving induction chemotherapy and consolidative chemoradiation. *Int. J. Radiat. Oncol. Biol. Phys.*, **94**(4):755–765, 2016. doi:10.1016/j.ijrobp.2015.12.003.
- [9] Reyngold, M., O'Reilly, E. M., Varghese, A. M., Fiasconaro, M., Zinovoy, M., Romesser, P. B., Wu, A., Hajj, C., Cuaron, J. J., Tuli, R., et al. Association of ablative radiation therapy with survival among patients with inoperable pancreatic cancer. *JAMA Oncol.*, **7**(5):735–738, 2021. doi:10.1001/jamaoncol.2021.0057.
- [10] Legendijk, J. J. W., Raaymakers, B. W., and Van Vulpen, M. The magnetic resonance imaging–linac system. *Semin. Radiat. Oncol.*, **24**(3):207–209, 2014. doi:10.1016/j.semradonc.2014.02.009.
- [11] Mucic, S. and Dempsey, J. F. The ViewRay system: magnetic resonance–guided and controlled radiotherapy. *Semin. Radiat. Oncol.*, **24**(3):196–199, 2014. doi:10.1016/j.semradonc.2014.02.008.
- [12] Raaymakers, B. W., Jürgenliemk-Schulz, I. M., Bol, G. H., Glitzner, M., Kotte, A. N. T. J., Van Asselen, B., De Boer, J. C. J., Bluemink, J. J., Hackett, S. L., Moerland, M. A., et al. First patients treated with a 1.5 T MRI-Linac: clinical proof of concept of a high-precision, high-field MRI guided radiotherapy treatment. *Phys. Med. Biol.*, **62**(23):L41, 2017. doi:10.1088/1361-6560/aa9517.

- [13] Winkel, D., Bol, G. H., Kroon, P. S., van Asselen, B., Hackett, S. S., Werensteijn-Honingh, A. M., Intven, M. P., Eppinga, W. S. C., Tijssen, R. H. N., Kerkmeijer, L. G. W., et al. Adaptive radiotherapy: the Elekta Unity MR-linac concept. *Clin. Transl. Radiat. Oncol.*, **18**:54–59, 2019. doi:10.1016/j.ctro.2019.04.001.
- [14] Daamen, L. A., de Mol van Otterloo, S. R., van Goor, I. W., Eijkelenkamp, H., Erickson, B. A., Hall, W. A., Heerkens, H. D., Meijer, G. J., Molenaar, I. Q., van Santvoort, H. C., et al. Online adaptive MR-guided stereotactic radiotherapy for unresectable malignancies in the upper abdomen using a 1.5 T MR-linac. *Acta Oncol.*, **61**(1):111–115, 2022. doi:10.1080/0284186X.2021.2012593.
- [15] Rudra, S., Jiang, N., Rosenberg, S. A., Olsen, J. R., Roach, M. C., Wan, L., Portelance, L., Mellon, E. A., Bruynzeel, A., Lagerwaard, F., et al. Using adaptive magnetic resonance image-guided radiation therapy for treatment of inoperable pancreatic cancer. *Cancer Med.*, **8**(5):2123–2132, 2019. doi:10.1002/cam4.2100.
- [16] Hassanzadeh, C., Rudra, S., Bommireddy, A., Hawkins, W. G., Wang-Gillam, A., Fields, R. C., Cai, B., Park, J., Green, O., Roach, M., et al. Ablative five-fraction stereotactic body radiation therapy for inoperable pancreatic cancer using online MR-guided adaptation. *Adv. Radiat. Oncol.*, **6**(1):100506, 2021. doi:10.1016/j.adro.2020.06.010.
- [17] Parikh, P. J., Lee, P., Low, D. A., Kim, J., Mittauer, K. E., Bassetti, M. F., Glide-Hurst, C. K., Raldow, A. C., Yang, Y., Portelance, L., et al. A multi-institutional phase II trial of ablative 5-fraction stereotactic MR-guided on-table adaptive radiation therapy for borderline resectable and locally advanced pancreatic cancer. *Int. J. Radiat. Oncol. Biol. Phys.*, **117**(4):799–808, 2023. doi:10.1016/j.ijrobp.2023.05.023.
- [18] Eijkelenkamp, H., Grimbergen, G., Daamen, L. A., Heerkens, H. D., Van de Ven, S., Mook, S., Meijer, G. J., Molenaar, I. Q., van Santvoort, H., Erickson, B. A., et al. Clinical outcomes after online adaptive MR-guided stereotactic body radiotherapy for pancreatic tumors on a 1.5 T MR-linac. *Front. Oncol.*, **13**:1040673, 2023. doi:10.3389/fonc.2023.1040673.
- [19] Daamen, L. A., Parikh, P. J., and Hall, W. A. The use of MR-guided radiation therapy for pancreatic cancer. *Semin. Radiat. Oncol.*, **34**(1):23–35, 2024. doi:10.1016/j.semradonc.2023.10.002.
- [20] Boldrini, L., Cusumano, D., Cellini, F., Azario, L., Mattiucci, G. C., and Valentini, V. Online adaptive magnetic resonance guided radiotherapy for pancreatic cancer: state of the art, pearls and pitfalls. *Radiat. Oncol.*, **14**(1):1–6, 2019. doi:10.1186/s13014-019-1275-3.
- [21] Hall, W. A., Small, C., Paulson, E., Koay, E. J., Crane, C., Intven, M., Daamen, L. A., Meijer, G. J., Heerkens, H. D., Bassetti, M., et al. Magnetic resonance guided radiation therapy for pancreatic adenocarcinoma, advantages, challenges, current approaches, and future directions. *Front. Oncol.*, **11**:628155, 2021. doi:10.3389/fonc.2021.628155.
- [22] Bohoudi, O., Bruynzeel, A. M. E., Meijerink, M. R., Senan, S., Slotman, B. J., Palacios, M. A., and Lagerwaard, F. J. Identification of patients with locally advanced pancreatic cancer benefiting from plan adaptation in MR-guided radiation therapy. *Radiother. Oncol.*, **132**:16–22, 2019. doi:10.1016/j.radonc.2018.11.019.
- [23] Nasief, H. G., Parchur, A. K., Omari, E., Zhang, Y., Chen, X., Paulson, E., Hall, W. A., Erickson, B., and Li, X. A. Predicting necessity of daily online adaptive replanning based on wavelet image features for MRI guided adaptive radiation therapy. *Radiother. Oncol.*, **176**:165–171, 2022. doi:10.1016/j.radonc.2022.10.001.

- [24] Paulson, E. S., Ahunbay, E., Chen, X., Mickevicius, N. J., Chen, G.-P., Schultz, C., Erickson, B., Straza, M., Hall, W. A., and Li, X. A. 4D-MRI driven MR-guided online adaptive radiotherapy for abdominal stereotactic body radiation therapy on a high field MR-Linac: Implementation and initial clinical experience. *Clin. Transl. Radiat. Oncol.*, **23**:72–79, 2020. doi:10.1016/j.ctro.2020.05.002.
- [25] Stanescu, T., Shessel, A., Carpino-Rocca, C., Taylor, E., Semeniuk, O., Li, W., Barry, A., Lukovic, J., Dawson, L., and Hosni, A. MRI-guided online adaptive stereotactic body radiation therapy of liver and pancreas tumors on an MR-Linac system. *Cancers*, **14**(3):716, 2022. doi:10.3390/cancers14030716.
- [26] de Leon, J., Crawford, D., Moutrie, Z., Alvares, S., Hogan, L., Pagulayan, C., Jelen, U., Loo, C., Aylward, J. D., Condon, K., et al. Early experience with MR-guided adaptive radiotherapy using a 1.5 T MR-Linac: First 6 months of operation using adapt to shape workflow. *J. Med. Imaging Radiat. Oncol.*, **66**(1):138–145, 2022. doi:10.1111/1754-9485.13336.
- [27] Bussels, B., Goethals, L., Feron, M., Bielen, D., Dymarkowski, S., Suetens, P., and Haustermans, K. Respiration-induced movement of the upper abdominal organs: a pitfall for the three-dimensional conformal radiation treatment of pancreatic cancer. *Radiother. Oncol.*, **68**(1):69–74, 2003. doi:10.1016/s0167-8140(03)00133-6.
- [28] Feng, M., Balter, J. M., Normolle, D., Adusumilli, S., Cao, Y., Chenevert, T. L., and Ben-Josef, E. Characterization of pancreatic tumor motion using cine MRI: surrogates for tumor position should be used with caution. *Int. J. Radiat. Oncol. Biol. Phys.*, **74**(3):884–891, 2009. doi:10.1016/j.ijrobp.2009.02.003.
- [29] Van Herk, M., Remeijer, P., Rasch, C., and Lebesque, J. V. The probability of correct target dosage: dose-population histograms for deriving treatment margins in radiotherapy. *Int. J. Radiat. Oncol. Biol. Phys.*, **47**(4):1121–1135, 2000. doi:10.1016/S0360-3016(00)00518-6.
- [30] Van Herk, M. Errors and margins in radiotherapy. *Semin. Radiat. Oncol.*, **14**(1):52–64, 2004. doi:10.1053/j.semradonc.2003.10.003.
- [31] McDonald, B. A., Zachiu, C., Christodouleas, J., Naser, M. A., Ruschin, M., Sonke, J.-J., Thorwarth, D., Létourneau, D., Tyagi, N., Tadic, T., et al. Dose accumulation for MR-guided adaptive radiotherapy: From practical considerations to state-of-the-art clinical implementation. *Front. Oncol.*, **12**:7471, 2023. doi:10.3389/fonc.2022.1086258.
- [32] Murr, M., Brock, K. K., Fusella, M., Hardcastle, N., Hussein, M., Jameson, M. G., Wahlstedt, I., Yuen, J., McClelland, J. R., and Osorio, E. V. Applicability and usage of dose mapping/accumulation in radiotherapy. *Radiother. Oncol.*, **182**:109527, 2023. doi:10.1016/j.radonc.2023.109527.
- [33] Heerkens, H. D., Reerink, O., Intven, M. P. W., Hiensch, R. R., Van Den Berg, C. A. T., Crijns, S. P. M., van Vulpen, M., and Meijer, G. J. Pancreatic tumor motion reduction by use of a custom abdominal corset. *Phys. Imaging Radiat. Oncol.*, **2**:7–10, 2017. doi:10.1016/j.phro.2017.02.003.
- [34] Papalazarou, C., Klop, G. J., Milder, M. T. W., Marijnissen, J. P. A., Gupta, V., Heijmen, B. J. M., Nuyttens, J. J. M. E., and Hoogeman, M. S. CyberKnife with integrated CT-on-rails: system description and first clinical application for pancreas SBRT. *Med. Phys.*, **44**(9):4816–4827, 2017. doi:10.1002/mp.12432.
- [35] Ehrbar, S., Käser, S. B., Chamberlain, M., Kraysenbühl, J., Wilke, L., Mayinger, M., Schüler, H. G., Guckenberger, M., Andratschke, N., and Tanadini-Lang, S. MR-guided beam gating: Residual motion, gating efficiency and dose reconstruction for stereotactic treatments of the liver and lung. *Radiother. Oncol.*, **174**:101–108, 2022. doi:10.1016/j.radonc.2022.07.007.

- [36] Green, O. L., Rankine, L. J., Cai, B., Curcuru, A., Kashani, R., Rodriguez, V., Li, H. H., Parikh, P. J., Robinson, C. G., Olsen, J. R., et al. First clinical implementation of real-time, real anatomy tracking and radiation beam control. *Med. Phys.*, **45**(8):3728–3740, 2018. doi:10.1002/mp.13002.
- [37] Grimbergen, G., Hackett, S. L., van Ommen, F., van Lier, A. L. H. M. W. v. L., Borman, P. T. S., Meijers, L. T. C., de Groot-van Breugel, E. N., de Boer, J. C. J., Raaymakers, B. W., Intven, M. P. W., et al. Gating and intrafraction drift correction on a 1.5 T MR-Linac: clinical dosimetric benefits for upper abdominal tumors. *Radiother. Oncol.*, **189**:109932, 2023. doi:10.1016/j.radonc.2023.109932.
- [38] Glitznier, M., Woodhead, P. L., Borman, P. T. S., Lagendijk, J. J. W., and Raaymakers, B. W. MLC-tracking performance on the Elekta unity MRI-linac. *Phys. Med. Biol.*, **64**(15):15NT02, 2019. doi:10.1088/1361-6560/ab2667.
- [39] Raaymakers, B. W., Lagendijk, J. J. W., Overweg, J., Kok, J. G. M., Raaijmakers, A. J. E., Kerkhof, E. M., Van Der Put, R. W., Meijnsing, I., Crijns, S. P. M., Benedosso, F., et al. Integrating a 1.5 T MRI scanner with a 6 MV accelerator: proof of concept. *Phys. Med. Biol.*, **54**(12):N229, 2009. doi:10.1088/0031-9155/54/12/N01.
- [40] Heerkens, H. D., Van Vulpen, M., Erickson, B., Reerink, O., Intven, M. P. W., van den Berg, C. A. T., Molenaar, I. Q., Vleggaar, F. P., and Meijer, G. J. MRI guided stereotactic radiotherapy for locally advanced pancreatic cancer. *Br. J. Radiol.*, **91**(1091):20170563, 2018. doi:10.1259/bjr.20170563.
- [41] Bohoudi, O., Bruynzeel, A. M. E., Senan, S., Cuijpers, J. P., Slotman, B. J., Lagerwaard, F. J., and Palacios, M. A. Fast and robust online adaptive planning in stereotactic MR-guided adaptive radiation therapy (SMART) for pancreatic cancer. *Radiother. Oncol.*, **125**(3):439–444, 2017. doi:10.1016/j.radonc.2017.07.028.
- [42] Placidi, L., Romano, A., Chiloiro, G., Cusumano, D., Boldrini, L., Cellini, F., Mattiucci, G. C., and Valentini, V. On-line adaptive MR guided radiotherapy for locally advanced pancreatic cancer: Clinical and dosimetric considerations. *Tech. Innov. Patient Support Radiat. Oncol.*, **15**:15–21, 2020. doi:10.1016/j.tipsro.2020.06.001.
- [43] Tringale, K. R., Tyagi, N., Reyngold, M., Romesser, P. B., Wu, A., O'Reilly, E. M., Varghese, A. M., Sripes, P. G., Khalil, D. N., Park, W., et al. Stereotactic ablative radiation for pancreatic cancer on a 1.5 tesla magnetic resonance-linac system. *Phys. Imaging Radiat. Oncol.*, **24**:88–94, 2022. doi:10.1016/j.phro.2022.10.003.
- [44] Ehman, R., McNamara, M., Brasch, R., Felmlee, J., Gray, J., and Higgins, C. Influence of physiologic motion on the appearance of tissue in MR images. *Radiol.*, **159**(3):777–782, 1986. doi:10.1148/radiology.159.3.3704156.
- [45] Pipe, J. G. Motion correction with PROPELLER MRI: application to head motion and free-breathing cardiac imaging. *Magn. Reson. Med.*, **42**(5):963–969, 1999. doi:10.1002/(sici)1522-2594(199911)42:5%3C963::aid-mrm17%3E3.0.co;2-l.
- [46] Michaely, H. J., Kramer, H., Weckbach, S., Dietrich, O., Reiser, M. F., and Schoenberg, S. O. Renal T2-weighted turbo-spin-echo imaging with BLADE at 3.0 tesla: initial experience. *J. Magn. Reson. Imaging*, **27**(1):148–153, 2008. doi:10.1002/jmri.21240.
- [47] Nanko, S., Oshima, H., Watanabe, T., Sasaki, S., Hara, M., and Shibamoto, Y. Usefulness of the application of the BLADE technique to reduce motion artifacts on navigation-triggered prospective acquisition correction (PACE) T2-weighted MRI (T2WI) of the liver. *J. Magn. Reson. Imaging*, **30**(2):321–326, 2009. doi:10.1002/jmri.21855.

- [48] Hirokawa, Y., Isoda, H., Okada, T., Arizono, S., Shimada, K., Yamamoto, A., Shibata, T., and Togashi, K. Improved detection of hepatic metastases from pancreatic cancer using periodically rotated overlapping parallel lines with enhanced reconstruction (PROPELLER) technique after SPIO administration. *Investig. Radiol.*, **45**(3):158–164, 2010. doi:10.1097/RLI.0b013e3181d32139.
- [49] Rosenkrantz, A., Mannelli, L., Mossa, D., and Babb, J. Breath-hold T2-weighted MRI of the liver at 3 T using the BLADE technique: impact upon image quality and lesion detection. *Clin. Radiol.*, **66**(5):426–433, 2011. doi:10.1016/j.crad.2010.10.018.
- [50] Nyberg, E., Sandhu, G., Jesberger, J., Blackham, K., Hsu, D., Griswold, M., and Sunshine, J. Comparison of brain MR images at 1.5 T using BLADE and rectilinear techniques for patients who move during data acquisition. *Am. J. Neuroradiol.*, **33**(1):77–82, 2012. doi:10.3174/ajnr.A2737.
- [51] Lavdas, E., Mavroidis, P., Kostopoulos, S., Glotsos, D., Roka, V., Topalzikis, T., Bakas, A., Oikonomou, G., Papanikolaou, N., Batsikas, G., et al. Improvement of image quality using BLADE sequences in brain MR imaging. *Magn. Reson. Imaging*, **31**(2):189–200, 2013. doi:10.1016/j.mri.2012.08.001.
- [52] Mavroidis, P., Giankou, E., Tsirikla, A., Kapsalaki, E., Chatzigeorgiou, V., Batsikas, G., Zaimis, G., Kostopoulos, S., Glotsos, D., Ninos, K., et al. Brain imaging: comparison of T1W FLAIR BLADE with conventional T1W SE. *Magn. Reson. Imaging*, **37**:234–242, 2017. doi:10.1016/j.mri.2016.12.007.
- [53] Sartoretti, E., Wyss, M., Eichenberger, B., van Smoorenburg, L., Binkert, C., Sartoretti-Schefer, S., and Sartoretti, T. Rapid T2-weighted turbo spin echo MultiVane brain MRI using compressed SENSE: a qualitative analysis. *Clin. Radiol.*, **76**(10):786–e15, 2021. doi:10.1016/j.crad.2021.06.017.
- [54] Kim, H. G., Choi, J. W., Yoon, S. H., and Lee, S. Image quality assessment of silent T2 PROPELLER sequence for brain imaging in infants. *Br. J. Radiol.*, **91**(1083):20170680, 2018. doi:10.1259/bjr.20170680.
- [55] Kraus, M. S., Coblentz, A. C., Deshpande, V. S., Peeters, J. M., Itriago-Leon, P. M., and Chavhan, G. B. State-of-the-art magnetic resonance imaging sequences for pediatric body imaging. *Pediatr. Radiol.*, 2022. doi:10.1007/s00247-022-05528-y.
- [56] McGee, K. P., Manduca, A., Felmlee, J. P., Riederer, S. J., and Ehman, R. L. Image metric-based correction (autocorrection) of motion effects: analysis of image metrics. *J. Magn. Reson. Imaging*, **11**(2):174–181, 2000. doi:10.1002/(SICI)1522-2586(200002)11:2%3C174::AID-JMRI15%3E3.0.CO;2-3.
- [57] Wolthaus, J. W., Sonke, J.-J., van Herk, M., Belderbos, J. S., Rossi, M. M., Lebesque, J. V., and Damen, E. M. Comparison of different strategies to use four-dimensional computed tomography in treatment planning for lung cancer patients. *Int. J. Radiat. Oncol. Biol. Phys.*, **70**(4):1229–1238, 2008. doi:10.1016/j.ijrobp.2007.11.042.
- [58] Bertelsen, A., Bernchou, U., Schytte, T., Brink, C., and Mahmood, F. The effect of respiration-induced target motion in 3D magnetic resonance images. *Phys. Imaging Radiat. Oncol.*, **24**:167–172, 2022. doi:10.1016/j.phro.2022.11.010.
- [59] Bernstein, M. A., King, K. F., and Zou, X. J. *Handbook of MRI pulse sequences*. Elsevier, 2004.
- [60] Brown, R. W., Cheng, Y.-C. N., Haacke, E. M., Thompson, M. R., and Venkatesan, R. *Magnetic Resonance Imaging: Physical Principles and Sequence Design*. John Wiley & Sons, Inc., 2014.
- [61] Grimbergen, G., Eijkelenkamp, H., Heerkens, H. D., Raaymakers, B. W., Intven, M. P. W., and Meijer, G. J. Intrafraction pancreatic tumor motion patterns during ungated magnetic resonance

- guided radiotherapy with an abdominal corset. *Phys. Imaging Radiat. Oncol.*, **21**:1–5, 2022. doi:10.1016/j.phro.2021.12.001.
- [62] Keesman, R., van de Lindt, T. N., Juan-Cruz, C., van den Wollenberg, W., van der Bijl, E., Nowee, M. E., Sonke, J.-J., van der Heide, U. A., and Fast, M. F. Correcting geometric image distortions in slice-based 4D-MRI on the MR-linac. *Med. Phys.*, **46**(7):3044–3054, 2019. doi:10.1002/mp.13602.
- [63] Reyngold, M., Parikh, P., and Crane, C. H. Ablative radiation therapy for locally advanced pancreatic cancer: techniques and results. *Radiat. Oncol.*, **14**(1):1–8, 2019. doi:10.1186/s13014-019-1309-x.
- [64] Henke, L., Kashani, R., Robinson, C., Curcuru, A., DeWees, T., Bradley, J., Green, O., Michalski, J., Mutic, S., Parikh, P., et al. Phase I trial of stereotactic MR-guided online adaptive radiation therapy (SMART) for the treatment of oligometastatic or unresectable primary malignancies of the abdomen. *Radiother. Oncol.*, **126**(3):519–526, 2018. doi:10.1016/j.radonc.2017.11.032.
- [65] Koay, E. J., Hanania, A. N., Hall, W. A., Taniguchi, C. M., Rebueno, N., Myrehaug, S., Aitken, K. L., Dawson, L. A., Crane, C. H., Herman, J. M., et al. Dose-escalated radiation therapy for pancreatic cancer: a simultaneous integrated boost approach. *Pract. Radiat. Oncol.*, **10**(6):e495–e507, 2020. doi:10.1016/j.prro.2020.01.012.
- [66] Tyagi, N., Liang, J., Burselson, S., Subashi, E., Sripes, P. G., Tringale, K. R., Romesser, P. B., Reyngold, M., and Crane, C. H. Feasibility of ablative stereotactic body radiation therapy of pancreas cancer patients on a 1.5 Tesla magnetic resonance-linac system using abdominal compression. *Phys. Imaging Radiat. Oncol.*, **19**:53–59, 2021. doi:10.1016/j.phro.2021.07.006.
- [67] Chuong, M. D., Bryant, J., Mittauer, K. E., Hall, M., Kotecha, R., Alvarez, D., Romaguera, T., Rubens, M., Adamson, S., Godley, A., et al. Ablative 5-fraction stereotactic magnetic resonance-guided radiation therapy with on-table adaptive replanning and elective nodal irradiation for inoperable pancreas cancer. *Pract. Radiat. Oncol.*, **11**(2):134–147, 2021. doi:10.1016/j.prro.2020.09.005.
- [68] Yoon, S. M., Luterstein, E., Chu, F.-I., Cao, M., Lamb, J., Agazaryan, N., Low, D., Raldow, A., Steinberg, M. L., and Lee, P. Clinical outcomes of stereotactic magnetic resonance image-guided adaptive radiotherapy for primary and metastatic tumors in the abdomen and pelvis. *Cancer Med.*, **10**(17):5897–5906, 2021. doi:10.1002/cam4.4139.
- [69] Barrord, M., Ahmad, S., Patel, S., Olowokure, O., Sussman, J., Smith, M., Poreddy, S., Esslinger, H., Latif, T., Choe, K., et al. Patterns of failure after neoadjuvant stereotactic body radiation therapy or fractionated chemoradiation in resectable and borderline resectable pancreatic cancer. *Pancreas*, **49**(7):941–946, 2020. doi:10.1097/MPA.0000000000001602.
- [70] UK SABR Consortium. Stereotactic ablative radiation therapy (SABR) - a resource. Version 6.1. <https://www.sabr.org.uk/wp-content/uploads/2019/04/SABRconsortium-guidelines-2019-v6.1.0.pdf>, 2019. Accessed 18 Feb 2021.
- [71] Gurney-Champion, O. J., Versteijne, E., van der Horst, A., Lens, E., Rütten, H., Heerkens, H. D., Paardekooper, G. M. R. M., Berbee, M., Rasch, C. R. N., Stoker, J., et al. Addition of MRI for CT-based pancreatic tumor delineation: a feasibility study. *Acta Oncol.*, **56**(7):923–930, 2017. doi:10.1080/0284186X.2017.1304654.
- [72] Hall, W. A., Heerkens, H. D., Paulson, E. S., Meijer, G. J., Kotte, A. N., Knechtges, P., Parikh, P. J., Bassetti, M. F., Lee, P., Aitken, K. L., et al. Pancreatic gross tumor volume contouring on computed tomography (CT) compared with magnetic resonance imaging (MRI): Results of an international contouring conference. *Pract. Radiat. Oncol.*, **8**(2):107–115, 2018. doi:10.1016/j.prro.2017.11.005.

- [73] Colbert, L. E., Rebueno, N., Moningi, S., Beddar, S., Sawakuchi, G. O., Herman, J. M., Koong, A. C., Das, P., Holliday, E. B., Koay, E. J., et al. Dose escalation for locally advanced pancreatic cancer: How high can we go? *Adv. Radiat. Oncol.*, **3**(4):693–700, 2018. doi:10.1016/j.adro.2018.07.008.
- [74] de Mol van Otterloo, S. R., Christodouleas, J. P., Blezer, E. L., Akhiat, H., Brown, K., Choudhury, A., Eggert, D., Erickson, B. A., Faivre-Finn, C., Fuller, C. D., et al. The MOMENTUM study: an international registry for the evidence-based introduction of MR-guided adaptive therapy. *Front. Oncol.*, **10**:1328, 2020. doi:10.3389/fonc.2020.01328.
- [75] Daamen, L. A., Groot, V. P., Besselink, M. G., Bosscha, K., Busch, O. R., Cirkel, G. A., van Dam, R. M., Festen, S., Koerkamp, B. G., Mohammad, N. H., et al. Detection, treatment, and survival of pancreatic cancer recurrence in the Netherlands: A nationwide analysis. *Annals Surg.*, 2021.
- [76] Brada, L. J. H., Walma, M. S., Daamen, L. A., van Roessel, S., van Dam, R. M., de Hingh, I. H., Liem, M. L. S., de Meijer, V. E., Patijn, G. A., Festen, S., et al. Predicting overall survival and resection in patients with locally advanced pancreatic cancer treated with FOLFIRINOX: Development and internal validation of two nomograms. *J. Surg. Oncol.*, **124**(4):589–597, 2021. doi:10.1002/jso.26567.
- [77] Chang, D. T., Schellenberg, D., Shen, J., Kim, J., Goodman, K. A., Fisher, G. A., Ford, J. M., Desser, T., Quon, A., and Koong, A. C. Stereotactic radiotherapy for unresectable adenocarcinoma of the pancreas. *Cancer*, **115**(3):665–672, 2009. doi:10.1002/cncr.24059.
- [78] Mahadevan, A., Jain, S., Goldstein, M., Miksad, R., Pleskow, D., Sawhney, M., Brennan, D., Callery, M., and Vollmer, C. Stereotactic body radiotherapy and gemcitabine for locally advanced pancreatic cancer. *Int. J. Radiat. Oncol. Biol. Phys.*, **78**(3):735–742, 2010. doi:10.1016/j.ijrobp.2009.08.046.
- [79] Yovino, S., Poppe, M., Jabbour, S., David, V., Garofalo, M., Pandya, N., Alexander, R., Hanna, N., and Regine, W. F. Intensity-modulated radiation therapy significantly improves acute gastrointestinal toxicity in pancreatic and ampullary cancers. *Int. J. Radiat. Oncol. Biol. Phys.*, **79**(1):158–162, 2011. doi:10.1016/j.ijrobp.2009.10.043.
- [80] Heerkens, H. D., van Vulpen, M., van den Berg, C. A. T., Tijssen, R. H. N., Crijns, S. P. M., Molenaar, I. Q., van Santvoort, H. C., Reerink, O., and Meijer, G. J. MRI-based tumor motion characterization and gating schemes for radiation therapy of pancreatic cancer. *Radiother. Oncol.*, **111**(2):252–257, 2014. doi:10.1016/j.radonc.2014.03.002.
- [81] Stemkens, B., Tijssen, R. H. N., de Senneville, B. D., Heerkens, H. D., Van Vulpen, M., Lagendijk, J. J. W., and van den Berg, C. A. T. Optimizing 4-dimensional magnetic resonance imaging data sampling for respiratory motion analysis of pancreatic tumors. *Int. J. Radiat. Oncol. Biol. Phys.*, **91**(3):571–578, 2015. doi:10.1016/j.ijrobp.2014.10.050.
- [82] Kontaxis, C., Bol, G. H., Stemkens, B., Glitzner, M., Prins, F. M., Kerkmeijer, L. G. W., Lagendijk, J. J. W., and Raaymakers, B. W. Towards fast online intrafraction replanning for free-breathing stereotactic body radiation therapy with the MR-linac. *Phys. Med. Biol.*, **62**(18):7233, 2017. doi:10.1088/1361-6560/aa82ae.
- [83] Cusumano, D., Dhont, J., Boldrini, L., Chiloiro, G., Teodoli, S., Massaccesi, M., Fionda, B., Cellini, F., Azario, L., Vandemeulebroucke, J., et al. Predicting tumour motion during the whole radiotherapy treatment: a systematic approach for thoracic and abdominal lesions based on real time MR. *Radiother. Oncol.*, **129**(3):456–462, 2018. doi:10.1016/j.radonc.2018.07.025.
- [84] Prins, F. M., Stemkens, B., Kerkmeijer, L. G. W., Barendrecht, M. M., de Boer, H. J., Vonken, E.-J. P. A., Lagendijk, J. J. W., and Tijssen, R. H. N. Intrafraction motion management of renal cell

- carcinoma with magnetic resonance imaging-guided stereotactic body radiation therapy. *Pract. Radiat. Oncol.*, **9**(1):e55–e61, 2019.
- [85] de Senneville, B. D., Zachiu, C., Ries, M., and Moonen, C. EVolution: an edge-based variational method for non-rigid multi-modal image registration. *Phys. Med. Biol.*, **61**(20):7377, 2016. doi:10.1088/0031-9155/61/20/7377.
- [86] Poulsen, P. R., Worm, E. S., Hansen, R., Larsen, L. P., Grau, C., and Høyer, M. Respiratory gating based on internal electromagnetic motion monitoring during stereotactic liver radiation therapy: first results. *Acta Oncol.*, **54**(9):1445–1452, 2015. doi:10.3109/0284186X.2015.1062134.
- [87] Worm, E. S., Høyer, M., Hansen, R., Larsen, L. P., Weber, B., Grau, C., and Poulsen, P. R. A prospective cohort study of gated stereotactic liver radiation therapy using continuous internal electromagnetic motion monitoring. *Int. J. Radiat. Oncol. Biol. Phys.*, **101**(2):366–375, 2018. doi:10.1016/j.ijrobp.2018.02.010.
- [88] Vinogradskiy, Y., Goodman, K. A., Schefter, T., Miften, M., and Jones, B. L. The clinical and dosimetric impact of real-time target tracking in pancreatic SBRT. *Int. J. Radiat. Oncol. Biol. Phys.*, **103**(1):268–275, 2019. doi:10.1016/j.ijrobp.2018.08.021.
- [89] Kaučić, H., Kosmina, D., Schwarz, D., Čehobašić, A., Leipold, V., Pedišić, I., Mlinarić, M., Lekić, M., Šobat, H., and Mack, A. An evaluation of total internal motions of locally advanced pancreatic cancer during SABR using calypso® extracranial tracking, and its possible clinical impact on motion management. *Curr. Oncol.*, **28**(6):4597–4610, 2021. doi:10.3390/curroncol28060389.
- [90] Zeng, C., Xiong, W., Li, X., Reyngold, M., Gewanter, R. M., Cuaron, J. J., Yorke, E. D., and Li, T. Intrafraction tumor motion during deep inspiration breath hold pancreatic cancer treatment. *J. Appl. Clin. Med. Phys.*, **20**(5):37–43, 2019. doi:10.1002/acm2.12577.
- [91] Placidi, L., Cusumano, D., Boldrini, L., Votta, C., Pollutri, V., Antonelli, M. V., Chiloiro, G., Romano, A., De Luca, V., Catucci, F., et al. Quantitative analysis of MRI-guided radiotherapy treatment process time for tumor real-time gating efficiency. *J. Appl. Clin. Med. Phys.*, **21**(11):70–79, 2020. doi:10.1002/acm2.13030.
- [92] Lovelock, D. M., Zatzky, J., Goodman, K., and Yamada, Y. The effectiveness of a pneumatic compression belt in reducing respiratory motion of abdominal tumors in patients undergoing stereotactic body radiotherapy. *Technol. Cancer Res. Treat.*, **13**(3):259–267, 2014. doi:10.7785/tcrt.2012.500379.
- [93] Campbell, W. G., Jones, B. L., Schefter, T., Goodman, K. A., and Miften, M. An evaluation of motion mitigation techniques for pancreatic SBRT. *Radiother. Oncol.*, **124**(1):168–173, 2017. doi:10.1016/j.radonc.2017.05.013.
- [94] Dolde, K., Schneider, S., Stefanowicz, S., Alimusaj, M., Flügel, B., Saito, N., Troost, E. G., Pfaffenberger, A., and Hoffmann, A. L. Comparison of pancreatic respiratory motion management with three abdominal corsets for particle radiation therapy: case study. *J. Appl. Clin. Med. Phys.*, **20**(6):111–119, 2019. doi:10.1002/acm2.12613.
- [95] Fujimoto, K., Shiinoki, T., Yuasa, Y., Onizuka, R., and Yamane, M. Evaluation of the effects of motion mitigation strategies on respiration-induced motion in each pancreatic region using cine-magnetic resonance imaging. *J. Appl. Clin. Med. Phys.*, **20**(9):42–50, 2019. doi:10.1002/acm2.12693.
- [96] Heinzerling, J. H., Anderson, J. F., Papiez, L., Boike, T., Chien, S., Zhang, G., Abdulrahman, R., and Timmerman, R. Four-dimensional computed tomography scan analysis of tumor and organ motion at

- varying levels of abdominal compression during stereotactic treatment of lung and liver. *Int. J. Radiat. Oncol. Biol. Phys.*, **70**(5):1571–1578, 2008. doi:10.1016/j.ijrobp.2007.12.023.
- [97] Eccles, C. L., Patel, R., Simeonov, A. K., Lockwood, G., Haider, M., and Dawson, L. A. Comparison of liver tumor motion with and without abdominal compression using cine-magnetic resonance imaging. *Int. J. Radiat. Oncol. Biol. Phys.*, **79**(2):602–608, 2011. doi:10.1016/j.ijrobp.2010.04.028.
- [98] Liang, Z., Liu, H., Xue, J., Hu, B., Zhu, B., Li, Q., Zhang, S., and Wu, G. Evaluation of the intra- and interfractional tumor motion and variability by fiducial-based real-time tracking in liver stereotactic body radiation therapy. *J. Appl. Clin. Med. Phys.*, **19**(3):94–100, 2018. doi:10.1002/acm2.12292.
- [99] Lee, M., Simeonov, A., Stanescu, T., Dawson, L. A., Brock, K. K., and Velec, M. MRI evaluation of normal tissue deformation and breathing motion under an abdominal compression device. *J. Appl. Clin. Med. Phys.*, **22**(2):90–97, 2021. doi:10.1002/acm2.13165.
- [100] Zachiu, C., Papadakis, N., Ries, M., Moonen, C., and De Senneville, B. D. An improved optical flow tracking technique for real-time MR-guided beam therapies in moving organs. *Phys. Med. Biol.*, **60**(23):9003, 2015. doi:10.1088/0031-9155/60/23/9003.
- [101] Klein, S., Staring, M., Murphy, K., Viergever, M. A., and Pluim, J. P. Elastix: a toolbox for intensity-based medical image registration. *IEEE Trans. Med. Imaging*, **29**(1):196–205, 2009. doi:10.1109/TMI.2009.2035616.
- [102] Kontaxis, C., de Muinck Keizer, D. M., Kerkmeijer, L. G. W., Willigenburg, T., den Hartogh, M. D., de Groot-van Breugel, E. N., Hes, J., Raaymakers, B. W., Lagendijk, J. J. W., de Boer, H. C. J., et al. Delivered dose quantification in prostate radiotherapy using online 3D cine imaging and treatment log files on a combined 1.5 T magnetic resonance imaging and linear accelerator system. *Phys. Imaging Radiat. Oncol.*, **15**:23–29, 2020. doi:10.1016/j.phro.2020.06.005.
- [103] Hissoiny, S., Raaijmakers, A. J. E., Ozell, B., Després, P., and Raaymakers, B. W. Fast dose calculation in magnetic fields with GPUMCD. *Phys. Med. Biol.*, **56**(16):5119, 2011. doi:10.1088/0031-9155/56/16/003.
- [104] Lujan, A. E., Larsen, E. W., Balter, J. M., and Ten Haken, R. K. A method for incorporating organ motion due to breathing into 3D dose calculations. *Med. Phys.*, **26**(5):715–720, 1999. doi:10.1118/1.598577.
- [105] Dhont, J., Vandemeulebroucke, J., Burghelena, M., Poels, K., Depuydt, T., Van Den Begin, R., Jaudet, C., Collen, C., Engels, B., Reynders, T., et al. The long- and short-term variability of breathing induced tumor motion in lung and liver over the course of a radiotherapy treatment. *Radiother. Oncol.*, **126**(2):339–346, 2018. doi:10.1016/j.radonc.2017.09.001.
- [106] Cusumano, D., Dhont, J., Boldrini, L., Chiloiro, G., Romano, A., Votta, C., Longo, S., Placidi, L., Azario, L., De Spirito, M., et al. Reliability of ITV approach to varying treatment fraction time: a retrospective analysis based on 2D cine MR images. *Radiat. Oncol.*, **15**(1):1–9, 2020. doi:10.1186/s13014-020-01530-6.
- [107] Grimbergen, G., Eijkelenkamp, H., Heerkens, H. D., Raaymakers, B. W., Intven, M. P., and Meijer, G. J. Dosimetric impact of intrafraction motion under abdominal compression during MR-guided SBRT for (peri-) pancreatic tumors. *Phys. Med. Biol.*, **67**(18):185016, 2022. doi:10.1088/1361-6560/ac8ddd.
- [108] Stemkens, B., Paulson, E. S., and Tijssen, R. H. N. Nuts and bolts of 4D-MRI for radiotherapy. *Phys. Med. Biol.*, **63**(21):21TR01, 2018. doi:10.1088/1361-6560/aae56d.

- [109] Paganelli, C., Portoso, S., Garau, N., Meschini, G., Via, R., Buizza, G., Keall, P., Riboldi, M., and Baroni, G. Time-resolved volumetric MRI in MRI-guided radiotherapy: an in silico comparative analysis. *Phys. Med. Biol.*, **64**(18):185013, 2019. doi:10.1088/1361-6560/ab33e5.
- [110] Li, G., Liu, Y., and Nie, X. Respiratory-correlated (RC) vs. time-resolved (TR) four-dimensional magnetic resonance imaging (4DMRI) for radiotherapy of thoracic and abdominal cancer. *Front. Oncol.*, **9**:1024, 2019. doi:10.3389/fonc.2019.01024.
- [111] Borman, P. T. S., Bos, C., Stemkens, B., Moonen, C. T. W., Raaymakers, B. W., and Tijssen, R. H. N. Assessment of 3D motion modeling performance for dose accumulation mapping on the MR-linac by simultaneous multislice MRI. *Phys. Med. Biol.*, **64**(9):095004, 2019. doi:10.1088/1361-6560/ab13e3.
- [112] Dasnoy-Sumell, D., Aspeel, A., Souris, K., and Macq, B. Locally tuned deformation fields combination for 2D cine-MRI-based driving of 3D motion models. *Phys. Medica*, **94**:8–16, 2022. doi:10.1016/j.ejmp.2021.12.010.
- [113] Li, G., Wei, J., Kadbi, M., Moody, J., Sun, A., Zhang, S., Markova, S., Zakian, K., Hunt, M., and Deasy, J. O. Novel super-resolution approach to time-resolved volumetric 4-dimensional magnetic resonance imaging with high spatiotemporal resolution for multi-breathing cycle motion assessment. *Int. J. Radiat. Oncol. Biol. Phys.*, **98**(2):454–462, 2017. doi:10.1016/j.ijrobp.2017.02.016.
- [114] Glitznert, M., De Senneville, B. D., Lagendijk, J. J. W., Raaymakers, B. W., and Crijs, S. P. M. On-line 3D motion estimation using low resolution MRI. *Phys. Med. Biol.*, **60**(16):N301, 2015. doi:10.1088/0031-9155/60/16/N301.
- [115] Bosma, L., Zachiu, C., Ries, M., de Senneville, B. D., and Raaymakers, B. Quantitative investigation of dose accumulation errors from intra-fraction motion in MRgRT for prostate cancer. *Phys. Med. Biol.*, **66**(6):065002, 2021. doi:10.1088/1361-6560/abe02a.
- [116] Lustig, M., Donoho, D., and Pauly, J. M. Sparse MRI: The application of compressed sensing for rapid MR imaging. *Magn. Reson. Med.*, **58**(6):1182–1195, 2007. doi:10.1002/mrm.21391.
- [117] Lustig, M., Donoho, D. L., Santos, J. M., and Pauly, J. M. Compressed sensing MRI. *IEEE Signal Process. Mag.*, **25**(2):72–82, 2008. doi:10.1109/MSP.2007.914728.
- [118] Li, H. S., Zhong, H., Kim, J., Glide-Hurst, C., Gulam, M., Nurushev, T. S., and Chetty, I. J. Direct dose mapping versus energy/mass transfer mapping for 4D dose accumulation: fundamental differences and dosimetric consequences. *Phys. Med. Biol.*, **59**(1):173, 2013. doi:10.1088/0031-9155/59/1/173.
- [119] Fast, M., van de Schoot, A., van de Lindt, T., Carbaat, C., van der Heide, U., and Sonke, J.-J. Tumor trailing for liver SBRT on the MR-linac. *Int. J. Radiat. Oncol. Biol. Phys.*, **103**(2):468–478, 2019. doi:10.1016/j.ijrobp.2018.09.011.
- [120] Christensen, G. E. and Johnson, H. J. Consistent image registration. *IEEE Trans. Med. Imaging*, **20**(7):568–582, 2001. doi:10.1109/42.932742.
- [121] Bender, E. T. and Tomé, W. A. The utilization of consistency metrics for error analysis in deformable image registration. *Phys. Med. Biol.*, **54**(18):5561, 2009. doi:10.1088/0031-9155/54/18/014.
- [122] Bender, E. T., Hardcastle, N., and Tomé, W. A. On the dosimetric effect and reduction of inverse consistency and transitivity errors in deformable image registration for dose accumulation. *Med. Phys.*, **39**(1):272–280, 2012. doi:10.1118/1.3666948.
- [123] Varadhan, R., Karangelis, G., Krishnan, K., and Hui, S. A framework for deformable image registration validation in radiotherapy clinical applications. *J. Appl. Clin. Med. Phys.*, **14**(1):192–213, 2013. doi:10.1120/jacmp.v14i1.4066.

- [124] Veiga, C., Lourenço, A. M., Mouinuddin, S., Van Herk, M., Modat, M., Ourselin, S., Royle, G., and McClelland, J. R. Toward adaptive radiotherapy for head and neck patients: uncertainties in dose warping due to the choice of deformable registration algorithm. *Med. Phys.*, **42**(2):760–769, 2015. doi:10.1118/1.4905050.
- [125] Lowther, N. J., Marsh, S. H., and Louwe, R. J. Quantifying the dose accumulation uncertainty after deformable image registration in head-and-neck radiotherapy. *Radiother. Oncol.*, **143**:117–125, 2020. 10.1016/j.radonc.2019.12.009.
- [126] Sprengers, A. M. J., van der Paardt, M. P., Zijta, F. M., Caan, M. W. A., Lamerichs, R. M., Nederveen, A. J., and Stoker, J. Use of continuously MR tagged imaging for automated motion assessment in the abdomen: a feasibility study. *J. Magn. Reson. Imaging*, **36**(2):492–497, 2012. doi:10.1002/jmri.23637.
- [127] De Jonge, C. S., Smout, A. J., Nederveen, A. J., and Stoker, J. Evaluation of gastrointestinal motility with MRI: Advances, challenges and opportunities. *Neurogastroenterol. Motil.*, **30**(1):e13257, 2018. doi:10.1111/nmo.13257.
- [128] de Jonge, C. S., Gollifer, R. M., Nederveen, A. J., Atkinson, D., Taylor, S. A., Stoker, J., and Menys, A. Dynamic MRI for bowel motility imaging—how fast and how long? *Br. J. Radiol.*, **91**(1088):20170845, 2018. doi:10.1259/bjr.20170845.
- [129] Barten, D. L., Laan, J. J., Nelissen, K. J., Visser, J., Westerveld, H., Bel, A., de Jonge, C. S., Stoker, J., and van Kesteren, Z. A 3D cine-MRI acquisition technique and image analysis framework to quantify bowel motion demonstrated in gynecological cancer patients. *Med. Phys.*, **48**(6):3109–3119, 2021. doi:10.1002/mp.14851.
- [130] Schultheiss, T. E., Tomé, W. A., and Orton, C. G. It is not appropriate to “deform” dose along with deformable image registration in adaptive radiotherapy. *Med. Phys.*, **39**(11):6531–6533, 2012. doi:10.1118/1.4722968.
- [131] Murphy, M. J., Salguero, F. J., Siebers, J. V., Staub, D., and Vaman, C. A method to estimate the effect of deformable image registration uncertainties on daily dose mapping. *Med. Phys.*, **39**(2):573–580, 2012. doi:10.1118/1.3673772.
- [132] Saleh, Z. H., Apte, A. P., Sharp, G. C., Shusharina, N. P., Wang, Y., Veeraraghavan, H., Thor, M., Muren, L. P., Rao, S. S., Lee, N. Y., et al. The distance discordance metric—a novel approach to quantifying spatial uncertainties in intra-and inter-patient deformable image registration. *Phys. Med. Biol.*, **59**(3):733, 2014. doi:10.1088/0031-9155/59/3/733.
- [133] Rigaud, B., Simon, A., Castelli, J., Gobeli, M., Ospina Arango, J.-D., Cazoulat, G., Henry, O., Haigron, P., and De Crevoisier, R. Evaluation of deformable image registration methods for dose monitoring in head and neck radiotherapy. *Biomed Res. Int.*, **2015**, 2015. doi:10.1155/2015/726268.
- [134] García-Mollá, R., de Marco-Blancas, N., Bonaque, J., Vidueira, L., López-Tarjuelo, J., and Perez-Calatayud, J. Validation of a deformable image registration produced by a commercial treatment planning system in head and neck. *Phys. Medica*, **31**(3):219–223, 2015. doi:10.1016/j.ejmp.2015.01.007.
- [135] Nassef, M., Simon, A., Cazoulat, G., Duménil, A., Blay, C., Lafond, C., Acosta, O., Balosso, J., Haigron, P., and De Crevoisier, R. Quantification of dose uncertainties in cumulated dose estimation compared to planned dose in prostate IMRT. *Radiother. Oncol.*, **119**(1):129–136, 2016. doi:10.1016/j.radonc.2016.03.007.

- [136] Takemura, A., Nagano, A., Kojima, H., Ikeda, T., Yokoyama, N., Tsukamoto, K., Noto, K., Isomura, N., Ueda, S., and Kawashima, H. An uncertainty metric to evaluate deformation vector fields for dose accumulation in radiotherapy. *Phys. Imaging Radiat. Oncol.*, **6**:77–82, 2018. doi:10.1016/j.phro.2018.05.005.
- [137] Bohoudi, O., Lagerwaard, F. J., Bruynzeel, A. M., Niebuhr, N. I., Johnen, W., Senan, S., Slotman, B. J., Pfaffenberger, A., and Palacios, M. A. End-to-end empirical validation of dose accumulation in MRI-guided adaptive radiotherapy for prostate cancer using an anthropomorphic deformable pelvis phantom. *Radiother. Oncol.*, **141**:200–207, 2019. doi:10.1016/j.radonc.2019.09.014.
- [138] Hunt, A., Hansen, V. N., Oelfke, U., Nill, S., and Hafeez, S. Adaptive radiotherapy enabled by MRI guidance. *Clin. Oncol.*, **30**(11):711–719, 2018. doi:10.1016/j.clon.2018.08.001.
- [139] van Sörnsen de Koste, J. R., Palacios, M. A., Bruynzeel, A. M., Slotman, B. J., Senan, S., and Lagerwaard, F. J. MR-guided gated stereotactic radiation therapy delivery for lung, adrenal, and pancreatic tumors: a geometric analysis. *Int. J. Radiat. Oncol. Biol. Phys.*, **102**(4):858–866, 2018. doi:10.1016/j.ijrobp.2018.05.048.
- [140] Keiper, T. D., Tai, A., Chen, X., Paulson, E., Lathuilière, F., Bériault, S., Hébert, F., Cooper, D. T., Lachaine, M., and Li, X. A. Feasibility of real-time motion tracking using cine MRI during MR-guided radiation therapy for abdominal targets. *Med. Phys.*, **47**(8):3554–3566, 2020. doi:10.1002/mp.14230.
- [141] Jassar, H., Tai, A., Chen, X., Keiper, T. D., Paulson, E., Lathuilière, F., Bériault, S., Hébert, F., Savard, L., Cooper, D. T., et al. Real-time motion monitoring using orthogonal cine MRI during MR-guided adaptive radiation therapy for abdominal tumors on 1.5 T MR-Linac. *Med. Phys.*, **50**(5):3103–3116, 2023. doi:10.1002/mp.16342.
- [142] Corradini, S., Alongi, F., Andratschke, N., Belka, C., Boldrini, L., Cellini, F., Debus, J., Guckenberger, M., Hörner-Rieber, J., Lagerwaard, F., et al. MR-guidance in clinical reality: current treatment challenges and future perspectives. *Radiat. Oncol.*, **14**(1):1–12, 2019. doi:10.1186/s13014-019-1308-y.
- [143] Thorwarth, D. and Low, D. A. Technical challenges of real-time adaptive MR-guided radiotherapy. *Front. Oncol.*, **11**:634507, 2021. doi:10.3389/fonc.2021.634507.
- [144] Grimbergen, G., Pötgens, G. G., Eijkelenkamp, H., Raaymakers, B. W., Intven, M. P. W., and Meijer, G. J. Feasibility of delivered dose reconstruction for MR-guided SBRT of pancreatic tumors with fast, real-time 3D cine MRI. *Radiother. Oncol.*, **182**:109506, 2023. doi:10.1016/j.radonc.2023.109506.
- [145] Kim, T., Lewis, B. C., Price, A., Mazur, T., Gach, H. M., Park, J. C., Cai, B., Wittland, E., Henke, L., Kim, H., et al. Direct tumor visual feedback during free breathing in 0.35 T MRgRT. *J. Appl. Clin. Med. Phys.*, **21**(10):241–247, 2020. doi:10.1002/acm2.13016.
- [146] Borman, P. T. S., Raaymakers, B. W., and Fast, M. F. First demonstration of visual biofeedback with Elekta Unity's comprehensive motion management gating solution. In *AAPM 65th Annual Meeting*, 2023.
- [147] Groot Koerkamp, M. L., Vasmel, J. E., Russell, N. S., Shaitelman, S. F., Anandadas, C. N., Currey, A., Vesprini, D., Keller, B. M., De-Colle, C., Han, K., et al. Optimizing MR-guided radiotherapy for breast cancer patients. *Front. Oncol.*, **10**:1107, 2020. doi:10.3389/fonc.2020.01107.
- [148] Nowee, M. E., van Pelt, V. W. J., Walraven, I., Simões, R., Liskamp, C. P., Lambregts, D. M. J., Heijmink, S., Schaake, E., van der Heide, U. A., and Janssen, T. M. The impact of image acquisition time on registration, delineation and image quality for magnetic resonance guided radiotherapy of prostate cancer patients. *Phys. Imaging Radiat. Oncol.*, **19**:85–89, 2021. doi:10.1016/j.phro.2021.07.002.

- [149] Chick, J., Alexander, S., Herbert, T., Huddart, R., Ingle, M., Mitchell, A., Nill, S., Oelfke, U., Dunlop, A., and Hafeez, S. Evaluation of non-vendor magnetic resonance imaging sequences for use in bladder cancer magnetic resonance image guided radiotherapy. *Phys. Imaging Radiat. Oncol.*, **27**:100481, 2023. doi:10.1016/j.phro.2023.100481.
- [150] Van de Lindt, T. N., Fast, M., Van Kranen, S. R., Nowee, M. E., Jansen, E. P. M., Van der Heide, U. A., and Sonke, J. J. MRI-guided mid-position liver radiotherapy: validation of image processing and registration steps. *Radiother. Oncol.*, **138**:132–140, 2019. doi:10.1016/j.radonc.2019.06.007.
- [151] Bruijnen, T., Stemkens, B., Lagendijk, J. J. W., Van Den Berg, C. A. T., and Tijssen, R. H. N. Multiresolution radial MRI to reduce IDLE time in pre-beam imaging on an MR-Linac (MR-RIDDLE). *Phys. Med. Biol.*, **64**(5):055011, 2019. doi:10.1088/1361-6560/aafd6b.
- [152] Biederer, J., Dinkel, J., Remmert, G., Jetter, S., Nill, S., Moser, T., Bendl, R., Thierfelder, C., Fabel, M., Oelfke, U., et al. 4D-Imaging of the lung: reproducibility of lesion size and displacement on helical CT, MRI, and cone beam CT in a ventilated ex vivo system. *Int. J. Radiat. Oncol. Biol. Phys.*, **73**(3):919–926, 2009. doi:10.1016/j.ijrobp.2008.09.014.
- [153] Li, H., Noel, C., Garcia-Ramirez, J., Low, D., Bradley, J., Robinson, C., Mutic, S., and Parikh, P. Clinical evaluations of an amplitude-based binning algorithm for 4DCT reconstruction in radiation therapy. *Med. Phys.*, **39**(2):922–932, 2012. doi:10.1118/1.3679015.
- [154] Bernchou, U., Schytte, T., Bertelsen, A., Lorenzen, E. L., Brink, C., and Mahmood, F. Impact of abdominal compression on intra-fractional motion and delivered dose in magnetic resonance image-guided adaptive radiation ablation of adrenal gland metastases. *Phys. Medica*, **114**:102682, 2023. doi:10.1016/j.ejmp.2023.102682.
- [155] Keijnemans, K., Borman, P. T. S., Raaymakers, B. W., and Fast, M. F. Effectiveness of visual biofeedback-guided respiratory-correlated 4D-MRI for radiotherapy guidance on the MR-linac. *Magn. Reson. Med.*, **91**(1):297–311, 2024. doi:10.1002/mrm.29857.
- [156] Bryant, J. M., Palm, R. F., Herrera, R., Rubens, M., Hoffe, S. E., Kim, D. W., Kaiser, A., Ucar, A., Fleming, J., De Zarraga, F., et al. Multi-institutional outcomes of patients aged 75 years and older with pancreatic ductal adenocarcinoma treated with 5-fraction ablative stereotactic magnetic resonance image-guided adaptive radiation therapy (A-SMART). *Cancer Control.*, **30**, 2023. doi:10.1177/10732748221150228.
- [157] Bordeau, K., Michalet, M., Keskes, A., Valdenaire, S., Debuire, P., Cantaloube, M., Cabail e, M., Portales, F., Draghici, R., Ychou, M., et al. Stereotactic MR-guided adaptive radiotherapy for pancreatic tumors: Updated results of the montpellier prospective registry study. *Cancers*, **15**(1):7, 2023. doi:10.3390/cancers15010007.
- [158] Bryant, J. M., Palm, R. F., Liveringhouse, C., Boyer, E., Hodul, P., Malafa, M., Denbo, J., Kim, D., Carballido, E., Fleming, J. B., et al. Surgical and pathologic outcomes of pancreatic adenocarcinoma (PA) after preoperative ablative stereotactic magnetic resonance image guided adaptive radiation therapy (A-SMART). *Adv. Radiat. Oncol.*, **7**(6):101045, 2022. doi:10.1016/j.adro.2022.101045.
- [159] Kim, H., Olsen, J. R., Green, O. L., Chin, R.-I., Hawkins, W. G., Fields, R. C., Hammill, C., Doyle, M. B., Chapman, W., Suresh, R., et al. MR-guided radiation therapy with concurrent gemcitabine/nab-paclitaxel chemotherapy in inoperable pancreatic cancer: A TITE-CRM phase I trial. *Int. J. Radiat. Oncol. Biol. Phys.*, **115**(1):214–223, 2023. doi:10.1016/j.ijrobp.2022.07.015.

- [160] Chuong, M. D., Herrera, R., Kaiser, A., Rubens, M., Romaguera, T., Alvarez, D., Kotecha, R., Hall, M. D., McCulloch, J., Ucar, A., et al. Induction chemotherapy and ablative stereotactic magnetic resonance image-guided adaptive radiation therapy for inoperable pancreas cancer. *Front. Oncol.*, **12**:888462, 2022. doi:10.3389/fonc.2022.888462.
- [161] Michalet, M., Bordeau, K., Cantaloube, M., Valdenaire, S., Debuire, P., Simeon, S., Portales, F., Draghici, R., Ychou, M., Assenat, E., et al. Stereotactic MR-guided radiotherapy for pancreatic tumors: Dosimetric benefit of adaptation and first clinical results in a prospective registry study. *Front. Oncol.*, **12**:563, 2022. doi:10.3389/fonc.2022.842402.
- [162] Chuong, M. D., Bryant, J. M., Herrera, R., McCulloch, J., Contreras, J., Kotecha, R., Romaguera, T., Alvarez, D., Hall, M. D., Rubens, M., et al. Dose-escalated magnetic resonance image-guided abdominopelvic reirradiation with continuous intrafraction visualization, soft tissue tracking, and automatic beam gating. *Adv. Radiat. Oncol.*, **7**(2):100840, 2022. doi:10.1016/j.adro.2021.100840.
- [163] Pugalenthi, A., Protic, M., Gonen, M., Kingham, T. P., Angelica, M. I. D., Dematteo, R. P., Fong, Y., Jarnagin, W. R., and Allen, P. J. Postoperative complications and overall survival after pancreaticoduodenectomy for pancreatic ductal adenocarcinoma. *J. Surg. Oncol.*, **113**(2):188–193, 2016. doi:10.1002/jso.24125.
- [164] Smits, F. J., Verweij, M. E., Daamen, L. A., van Werkhoven, C. H., Goense, L., Besselink, M. G., Bonsing, B. A., Busch, O. R., Van Dam, R. M., Van Eijck, C. H. J., et al. Impact of complications after pancreatoduodenectomy on mortality, organ failure, hospital stay, and readmission: analysis of a nationwide audit. *Annals Surg.*, **275**(1):e222–e228, 2022. doi:10.1097/SLA.0000000000003835.
- [165] van Houdt, P. J., Li, S., Yang, Y., and van der Heide, U. A. Quantitative MRI on MR-Linacs: Towards Biological Image-Guided Adaptive Radiotherapy. *Semin. Radiat. Oncol.*, **34**(1):107–119, 2024. doi:10.1016/j.semradonc.2023.10.010.
- [166] van Vliembergen, E. N. M., Eijkelenkamp, H., Valk, G. D., Vriens, M. R., Meijer, G. J., Intven, M. P. W., and de Laat, J. M. Precision radiotherapy using MR-linac for pancreatic neuroendocrine tumors in MEN1 patients (PRIME): a protocol for a phase I-II trial, and systematic review on available evidence for radiotherapy of pNETs. *Front. Endocrinol.*, **14**:994370, 2023. doi:10.3389/fendo.2023.994370.
- [167] van Vulpen, J. K., Eijkelenkamp, H., Wessels, F., Mulder, S., Meijer, G. J., and Intven, M. P. W. MR-guided stereotactic ablative body radiotherapy for pancreatic oligometastases from renal cell carcinoma. *Int. J. Radiat. Oncol. Biol. Phys.*, **117**(2):e112, 2023. doi:10.1016/j.ijrobp.2023.06.892.
- [168] Schiff, J. P., Price, A. T., Stowe, H. B., Laugeman, E., Chin, R.-I., Hatscher, C., Pryser, E., Cai, B., Hugo, G. D., Kim, H., et al. Simulated computed tomography-guided stereotactic adaptive radiotherapy (CT-STAR) for the treatment of locally advanced pancreatic cancer. *Radiother. Oncol.*, **175**:144–151, 2022. doi:10.1016/j.radonc.2022.08.026.
- [169] Liu, H., Schaal, D., Curry, H., Clark, R., Magliari, A., Kupelian, P., Khuntia, D., and Beriwal, S. Review of cone beam computed tomography based online adaptive radiotherapy: Current trend and future direction. *Radiat. Oncol.*, **18**(1):144, 2023. doi:10.1186/s13014-023-02340-2.
- [170] Valverde, C. P. T., Ebrahimi, G., Sprangers, M. A., Pateras, K., Bruynzeel, A. M., Jacobs, M., Wilmlink, J. W., Besselink, M. G., Crezee, H., van Tienhoven, G., et al. Impact of short-course palliative radiation therapy on pancreatic cancer-related pain: Prospective phase 2 nonrandomized PAINPANC trial. *Int. J. Radiat. Oncol. Biol. Phys.*, 2023. doi:10.1016/j.ijrobp.2023.08.055.

- [171] Menten, M. J., Mohajer, J. K., Nilawar, R., Bertholet, J., Dunlop, A., Pathmanathan, A. U., Moreau, M., Marshall, S., Wetscherek, A., Nill, S., et al. Automatic reconstruction of the delivered dose of the day using MR-linac treatment log files and online MR imaging. *Radiother. Oncol.*, **145**:88–94, 2020. doi:10.1016/j.radonc.2019.12.010.
- [172] Cusumano, D., Boldrini, L., Dhont, J., Fiorino, C., Green, O., Güngör, G., Jornet, N., Klüter, S., Landry, G., Mattiucci, G. C., et al. Artificial intelligence in magnetic resonance guided radiotherapy: Medical and physical considerations on state of art and future perspectives. *Phys. Medica*, **85**:175–191, 2021. doi:10.1016/j.ejmp.2021.05.010.
- [173] Kontaxis, C., Woodhead, P. L., Bol, G. H., Lagendijk, J. J. W., and Raaymakers, B. W. Proof-of-concept delivery of intensity modulated arc therapy on the Elekta Unity 1.5 T MR-linac. *Phys. Med. Biol.*, **66**(4):04LT01, 2021. doi:10.1088/1361-6560/abd66d.
- [174] Uijtewaal, P., Borman, P. T. S., Woodhead, P. L., Kontaxis, C., Hackett, S. L., Verhoeff, J., Raaymakers, B. W., and Fast, M. F. First experimental demonstration of VMAT combined with MLC tracking for single and multi fraction lung SBRT on an MR-linac. *Radiother. Oncol.*, **174**:149–157, 2022. doi:10.1016/j.radonc.2022.07.004.
- [175] Lombardo, E., Dhont, J., Page, D., Garibaldi, C., Künzel, L. A., Hurkmans, C., Tijssen, R. H., Paganelli, C., Liu, P. Z., Keall, P. J., Riboldi, M., Kurz, C., Landry, G., Cusumano, D., Fusella, M., and Placidi, L. Real-time motion management in MRI-guided radiotherapy: Current status and AI-enabled prospects. *Radiother. Oncol.*, **190**:109970, 2023. doi:10.1016/j.radonc.2023.109970.
- [176] Terpstra, M. L., Maspero, M., Bruijnen, T., Verhoeff, J. J. C., Lagendijk, J. J. W., and van den Berg, C. A. T. Real-time 3D motion estimation from undersampled MRI using multi-resolution neural networks. *Med. Phys.*, **48**(11):6597–6613, 2021. doi:10.1002/mp.15217.
- [177] Smolders, A. J., Lomax, A. J., Weber, D. C., and Albertini, F. Deep learning based uncertainty prediction of deformable image registration for contour propagation and dose accumulation in online adaptive radiotherapy. *Phys. Med. Biol.*, **68**(24):245027, 2023. doi:10.1088/1361-6560/ad0282.
- [178] Uijtewaal, P., Borman, P. T. S., Woodhead, P. L., Hackett, S. L., Raaymakers, B. W., and Fast, M. F. Dosimetric evaluation of MRI-guided multi-leaf collimator tracking and trailing for lung stereotactic body radiation therapy. *Med. Phys.*, **48**(4):1520–1532, 2021. doi:10.1002/mp.14772.
- [179] Kontaxis, C., Bol, G. H., Lagendijk, J. J. W., and Raaymakers, B. W. Towards adaptive IMRT sequencing for the MR-linac. *Phys. Med. Biol.*, **60**(6):2493, 2015. doi:10.1088/0031-9155/60/6/2493.
- [180] Kontaxis, C., Bol, G. H., Lagendijk, J. J. W., and Raaymakers, B. W. A new methodology for inter-and intrafraction plan adaptation for the mr-linac. *Phys. Med. Biol.*, **60**(19):7485, 2015. doi:10.1088/0031-9155/60/19/7485.
- [181] Muurholm, C. G., Ravkilde, T., Skouboe, S., Worm, E., Hansen, R., Høyer, M., Keall, P. J., and Poulsen, P. R. Real-time dose-guidance in radiotherapy: Proof of principle. *Radiother. Oncol.*, **164**:175–182, 2021. doi:10.1016/j.radonc.2021.09.024.
- [182] Mejnertsen, L., Hewson, E., Nguyen, D. T., Booth, J., and Keall, P. Dose-based optimisation for multi-leaf collimator tracking during radiation therapy. *Phys. Med. Biol.*, **66**(6):065027, 2021. doi:10.1088/1361-6560/abe836.



List of publications

Journal articles

G Grimbergen, H Eijkelenkamp, LMW Snoeren, R Bahij, U Bernchou, E van der Bijl, HD Heerkens, S Binda, SSW Ng, C Bouchart, Z Paquier, K Brown, R Khor, R Chuter, L Freear, A Dunlop, RA Mitchell, BA Erickson, WA Hall, P Godoy Sripes, N Tyagi, J de Leon, C Tran, S Oh, P Renz, A Shessel, E Taylor, MPW Intven, and GJ Meijer. Treatment planning for MR-guided SBRT of pancreatic tumors on a 1.5 T MR-Linac: a global consensus protocol. Submitted (2023).

G Grimbergen, SL Hackett, F van Ommen, ALHMW van Lier, PTS Borman, LTC Meijers, EN de Groot-van Breugel, JCJ de Boer, BW Raaymakers, MPW Intven, and GJ Meijer. Gating and intrafraction drift correction on a 1.5 T MR-Linac: clinical dosimetric benefits for upper abdominal tumors. *Radiotherapy and Oncology* (2023), 189:109932.

H Eijkelenkamp, **G Grimbergen**, LA Daamen, HD Heerkens, S van de Ven, S Mook, GJ Meijer, IQ Molenaar, HC van Santvoort, ES Paulson, BA Erickson, HM Verkooijen, WA Hall, and MPW Intven. Clinical outcomes after online adaptive MR-guided stereotactic body radiotherapy for pancreatic tumors on a 1.5 T MR-linac. *Frontiers in Oncology* (2023), 13:1040673.

G Grimbergen, H Eijkelenkamp, JK van Vulpen, S van de Ven, BW Raaymakers, MPW Intven, and GJ Meijer. Feasibility of online radial magnetic resonance imaging for adaptive radiotherapy of pancreatic tumors. *Physics and Imaging in Radiation Oncology* (2023), 26:100434.

G Grimbergen, GG Pötgens, H Eijkelenkamp, BW Raaymakers, MPW Intven, and GJ Meijer. Feasibility of delivered dose reconstruction for MR-guided SBRT of pancreatic tumors with fast, real-time 3D cine MRI. *Radiotherapy and Oncology* (2023), 182:109506.

G Grimbergen, H Eijkelenkamp, HD Heerkens, BW Raaymakers, MPW Intven, and GJ

Meijer. Dosimetric impact of intrafraction motion under abdominal compression during MR-guided SBRT for (peri-) pancreatic tumors. *Physics in Medicine & Biology* (2022), 67(18):185016.

G Grimbergen, H Eijkelenkamp, HD Heerkens, BW Raaymakers, MPW Intven, and GJ Meijer. Intrafraction pancreatic tumor motion patterns during ungated magnetic resonance guided radiotherapy with an abdominal corset. *Physics and Imaging in Radiation Oncology* (2022), 21:1–5.

MH Vu, **G Grimbergen**, T Nyholm, and T Löfstedt. Evaluation of multi-slice inputs to convolutional neural networks for medical image segmentation. *Medical Physics* (2020), 47(12):6216–6231.

Conference proceedings (first author)

G Grimbergen, H Eijkelenkamp, LMW Snoeren, U Bernchou, S Binda, C Bouchart, K Brown, R Chuter, P Godoy Sripes, WA Hall, HD Heerkens, J de Leon, RA Mitchell, P Renz, A Shessel, MPW Intven, and GJ Meijer. Treatment planning for MR-guided pancreas SBRT on a 1.5 T MR-Linac: a global consensus protocol. *ESTRO 2024*, poster.

G Grimbergen, H Eijkelenkamp, U Bernchou, C Bouchart, K Brown, R Chuter, A Dunlop, P Godoy Sripes, HD Heerkens, J de Leon, SSW Ng, P Renz, A Shessel, MPW Intven, and GJ Meijer. Towards global consensus for MR-guided treatment planning for pancreatic tumors on a 1.5 T MR-Linac. *Elekta MR-Linac Consortium meeting 2023*, oral presentation.

G Grimbergen, H Eijkelenkamp, U Bernchou, C Bouchart, K Brown, R Chuter, A Dunlop, P Godoy Sripes, HD Heerkens, J de Leon, SSW Ng, P Renz, A Shessel, MPW Intven, and GJ Meijer. Towards global consensus for MR-guided treatment planning for pancreatic tumors on a 1.5 T MR-Linac. *ASTRO 2023*, poster.

G Grimbergen, GG Pötgens, H Eijkelenkamp, BW Raaymakers, MPW Intven, and GJ Meijer. Delivered dose reconstruction for MR-guided SBRT of pancreatic tumors with fast 3D cine MRI. *ESTRO 2023*, oral presentation.

G Grimbergen, H Eijkelenkamp, HD Heerkens, BW Raaymakers, MPW Intven, and GJ

Meijer. Dosimetric impact of intrafraction motion during MR-guided SBRT for upper abdominal tumors. *Elekta MR-Linac Consortium meeting 2022*, poster.

G Grimbergen, H Eijkelenkamp, HD Heerkens, BW Raaymakers, MPW Intven, and GJ Meijer. Dosimetric impact of intrafraction upper abdominal tumor motion during MR-guided SBRT. *ESTRO 2022*, oral presentation, Young Investigator Award.

G Grimbergen, H Eijkelenkamp, HD Heerkens, BW Raaymakers, MPW Intven, and GJ Meijer. Intrafraction pancreatic tumor motion patterns during ungated MR-guided SBRT with abdominal corset. *ESTRO 2021*, poster.

G Grimbergen, H Eijkelenkamp, HD Heerkens, BW Raaymakers, MPW Intven, and GJ Meijer. Intrafraction pancreatic tumor motion patterns during ungated MR-guided SBRT with abdominal corset. *Elekta MR-Linac Consortium meeting 2021*, poster.

G Grimbergen, H Eijkelenkamp, HD Heerkens, BW Raaymakers, MPW Intven, and GJ Meijer. Tumor motion analysis of pancreatic cancer patients during ungated MRgRT with abdominal corset. *MR in RT 2021*, oral presentation.



Dankwoord

Er wordt wel eens gezegd het dankwoord vaak het eerste (en soms het enige) is wat men leest van een proefschrift. Mijns inziens is dat geheel terecht, aangezien de personen hieronder het fundament zijn van het werk dat nu voor u ligt. Dankzij hen heb ik geen moment spijt gehad van mijn promotie. Ik ben ontzettend dankbaar dat ik in een omgeving ben gekomen met zoveel leuke mensen die zoveel belangrijk werk doen. Buiten het ziekenhuis zijn er ook vele mensen die een indirecte, maar niet minder belangrijke bijdrage hebben geleverd aan dit proefschrift.

Dr. G.J. Meijer, beste Gert, ik kan oprecht zeggen dat jij van mijn promotietijd een feestje hebt gemaakt. Sinds de eerste keer dat ik jouw kantoor in ben gelopen om te praten over de vacature voor deze promotieplek, heb ik je deur vele malen platgelopen. En iedere keer als ik dan weer vertrok, soms na een iets te lange whiteboard-sessie, werkte er eigenlijk weinig motiverender dan een "Goed bezig, Guus!". Ik heb enorm veel te danken aan je grenzeloze inzet die niet alleen voor dit proefschrift onmisbaar was, maar ook voor mijn persoonlijke ontwikkeling als onderzoeker en professional. Je enthousiasme en pragmatische instelling ("The proof of the pudding is in the eating!") zijn bijzonder aanstekelijk en hebben mij bovenal geleerd dat je er gewoon voor moet gaan. Ik ben trots dat ik je vakgenoot mag worden, en hoop dat we nog veel mooie dingen gaan doen op de afdeling.

Prof. dr. M.P.W. Intven, beste Martijn. Je bent een onuitputtelijke bron van nieuwe ideeën en gevatte opmerkingen tijdens het donderdagoverleg. Er zijn weinig mensen die zo benaderbaar zijn én zo'n grote speler zijn binnen de radiotherapiewereld. De hoeveelheid taken die je op je neemt, van hoogleraarschap en management op ziekenhuis-, nationaal, en internationaal niveau, tot het rondbrengen van bitterballen in de koffiekamer, zijn niets minder dan bewonderenswaardig. Je vormt met Gert het perfecte team. Dank voor alles wat je me hebt bijgebracht.

Prof. dr. B.W. Raaymakers, beste Bas, ik ben blij dat ik je in de loop van mijn promotietraject beter heb leren kennen. Je inzichten waren af en toe hoognodig tijdens de voortgangsgesprekken om de boel weer de juiste kant op te sturen ("Als ik eerlijk ben, lijkt

me een review schrijven ongelofelijk saai.”). Ik herken een beetje van jouw no-nonsense mentaliteit in alle fysicapromovendi van de afdeling: als je een leuk idee hebt, gewoon de MRL boeken en uitproberen. Het was een voorrecht om je als promotor te hebben.

Geachte leden van de beoordelingscommissie, dr. M.F. Fast, prof. dr. M.S. Hoogeman, prof. dr. ir. J.J.W. Lagendijk, prof. dr. J.H.W. Leusen, prof. dr. H.C. van Santvoort, hartelijk dank voor de tijd en moeite die jullie gestoken hebben in het lezen en beoordelen van dit proefschrift.

Dank aan mijn paranimfen, Hidde Eijkelenkamp en Lando Bosma. Hidde, amice, confrère, we zijn samen op de pancreas-MRL-trein gestapt en komen nu ook weer samen aan bij het eindstation. We hebben elkaar veel bijgebracht over elkaars vakgebieden en over het leven; je kan er waarschijnlijk een tweede proefschrift mee vullen. Ik beloof te blijven werken aan mijn empathie. Een mooiere afsluiter van deze jaren kan ik me niet voorstellen! Lando, je stelt nooit teleur om de lat net wat hoger te leggen dan de rest, zowel qua onderzoek als tijdens congressen (overdag én 's avonds). Ooit zullen we met ons dosisaccumulatieproject beginnen. MIM it to win it!

Mijn (oud-)Qamergenoten: Anouk, Arthur, Celeste, Eline, Ethan, Fia, Floris, Hidde, Hilde, Jikke, Julius, Katrinus, Koen, Maaïke, Maxime, Robin, Osman, Veerle, dank voor alle lunches, wandelingen, koffie's, scansessies, RT-ledereen-anekdotes, en het aanhoren van mijn vele klaagzangen. Katrinus, van alle collega's ken ik jou verreweg het langst. We moeten elkaar niet veel later ontmoet hebben dan de derde week van onze BMT-bachelor. Wie had toen gedacht dat we nu, bijna 10 jaar later, nog steeds samen zouden werken? En ook zijn we geen kamergenoten meer, we gaan beide gewoon door in het UMCU dus we zijn nog lang niet van elkaar af! Osman, ik geloof dat je het volledige menu van De Brink wel hebt uitgespeeld. Ben benieuwd of ze daar in het AvL aan kunnen tippen! Robin, je vertrek uit *hierdie klomp vriende* is een groot gemis. Dank dat je ons hebt laten zien dat je bovenal gewoon moet doen wat je leuk vindt in het leven (ik zal het maar niet over MIM workflows hebben).

Aan mijn verdere (oud-)collegapromovendi: Bas, David, Dieuwke, Eva, Frédérique, Georgios, Iris, Jacobien, Jamila, Jasmijn, Leon, Luuk, Lois, Maarten, Madelon, Manon, Maureen, Max, Mike, Paris, Prescilla, Rodrigo, Saskia, Stijn, Thomas, Thomas, Tom, Tom. Het is inmiddels niet meer origineel om het beroemde motto van prof. dr. J. Westerdijk aan te halen, maar hoe zou ik het ook beter kunnen samenvatten dan "*Werken en feesten vormt schoone*

geesten". Ik heb genoten van de vrijmiborrels, ESTRO-feestjes, tafelvoetbalwedstrijdjes, Spag-diners, PhD-weekendjes, en het warme bad dat jullie vormen. Frédérique, dinsdag is het nieuwe vrijdag! Dank voor je Illustrator/InDesign/Photoshoptips die essentieel waren voor de totstandkoming van de creatieve onderdelen van dit proefschrift.

De stafleden van de radiotherapie met wie ik in meer of mindere mate heb samengewerkt: Alexis, Anette, Astrid, Bram, Cornel, Fasco, Gijs, Hans, Jonna, Maarten, Matteo, Mariëlle, Niels, Peter, Pim, Saskia, Sara, Simon, Tim. Van co-auteurschap tot een enkele "korte vraag" (lees: een uur lang sparren), dank voor jullie kennis en bijdragen.

Ik wil ook alle MRL/MRI laboranten van de radiotherapie bedanken, in het bijzonder Eline, Lieke, Louk, Reijer, Roel, Tuan. Dank voor jullie vrolijkheid, hulp, en kennis. Zonder jullie geduld voor mijn veel te luide, veel te lange MRI-scans was dit proefschrift er niet geweest.

Heren van het HRD, vroeger was alles beter, maar dat hoeft niet te betekenen dat men zich niet kan verheugen op de toekomst. De erkenning komt sluipenderwijs dichterbij. Richard en Pieter, dank voor jullie lange vriendschap en de vele brakke Wii Golf uren. Rich, onze nestor universalis, het einde lonkt nu aan de horizon. Piet, ook ons het heeft wat jaartjes gekost maar straks zijn we beiden eindelijk in opleiding!

David en Bernd, het is maar goed dat we de boel bij Viking een beetje hebben opgeschud. Ik hoop dat we onze Pimanov verder zullen perfectioneren, en laten vooral doorgaan met de URV naar een hoger niveau tillen!

Mam en pap, ik kan alleen maar dankbaar zijn voor jullie grenzeloze steun en interesse. Bij jullie voelt het nog steeds als thuiskomen in plaats van langskomen. Mam, eigenlijk treft jou meer dank dan ieder ander, aangezien jij was degene die de vacature voor deze PhD het eerst zag staan, toen nog op de interne website van het UMCU. Pap, laten we er snel weer eens samen op uit gaan. Misschien dat laatste stuk van de Thames maar eens afmaken? Oma, fijn dat je er ook bij kan zijn op de grote dag!

Eva en Marieke, lieve zussen, in het dagelijks leven zijn jullie mijn paranimfen: altijd aan mijn zijde en bereid om in te grijpen als het mis dreigt te gaan. Eva, ooit zullen we de eerste studie door *Grimbergen, Grimbergen, et al.* publiceren. Marieke, buurvrouw, super leuk dat we nu zo makkelijk bij elkaar langs kunnen komen. Ngā mihi voor al je tips voor mijn Nieuw Zeelandreis!

Mieke, het laatste is voor jou. In de vier jaar dat we samen zijn is er ongelooflijk veel veranderd voor ons beiden, en hebben we ondertussen al ontelbare mooie herinneringen (en foto's van Moki) gemaakt. Ik ben dankbaar voor al deze grote en kleine avonturen die we samen hebben beleefd en ontzettend blij dat jij mijn vriendin bent. Dank voor je steun en liefde. Ik kijk uit naar wat de toekomst ons gaat brengen. Ik zou het voor geen goud willen missen!



Curriculum vitae auctoris

Guus Grimbergen was born on August 27th, 1997 in Nieuwegein, the Netherlands, and grew up in the neighboring city of IJsselstein. After obtaining his high school diploma in 2015, he relocated to the south of the Netherlands, where he attended the Eindhoven University of Technology. He obtained a Bachelor of Science degree in Biomedical Engineering in 2018.



Next, he joined the Medical Engineering graduate program, which focuses on medical imaging and physics in the clinic. In the first year of his Master's, he spent three months in Umeå, Sweden, where he worked as a research intern on deep learning for medical image segmentation under the supervision of dr. Tommy Löfstedt and prof. dr. Tufve Nyholm. Returning to the Netherlands to conduct his Master thesis project, he began as a graduate intern in the Computational Imaging group of prof. dr. ir. Nico van den Berg at the University Medical Center Utrecht. This group had developed a quantitative MRI framework called MR-STAT, and Guus investigated extending MR-STAT beyond the brain to imaging of the pelvis and abdomen. He obtained his Master of Science degree in 2020.

After graduating, he got the opportunity to remain as a PhD student at the department of radiotherapy of the UMC Utrecht, under the supervision of dr. Gert Meijer, prof. dr. Martijn Intven, and prof. dr. Bas Raaymakers. His PhD research was on technical developments for MR-guided radiotherapy of pancreatic cancer, resulting in this thesis.

Following completion of his doctorate in 2024, he will continue his career at the radiotherapy department of the UMC Utrecht with a residency in medical physics.

Guus currently lives in Utrecht with his girlfriend Mieke and their cat Moki.

